University of Colorado, Boulder
CU Scholar

Civil Engineering Graduate Theses & Dissertations Civil, Environmental, and Architectural Engineering

Spring 1-1-2011

Small Strain Shear Modulus of Unsaturated, Compacted Soils During Hydraulic Hysteresis

Ali Khosravi
University of Colorado at Boulder, khosravi@colorado.edu

Follow this and additional works at: https://scholar.colorado.edu/cven_gradetds

 Part of the Civil Engineering Commons

Recommended Citation
Khosravi, Ali, "Small Strain Shear Modulus of Unsaturated, Compacted Soils During Hydraulic Hysteresis" (2011). *Civil Engineering Graduate Theses & Dissertations*. 203.
https://scholar.colorado.edu/cven_gradetds/203

This Dissertation is brought to you for free and open access by Civil, Environmental, and Architectural Engineering at CU Scholar. It has been accepted for inclusion in Civil Engineering Graduate Theses & Dissertations by an authorized administrator of CU Scholar. For more information, please contact cuscholaradmin@colorado.edu.

SMALL STRAIN SHEAR MODULUS OF UNSATURATED, COMPACTED SOILS DURING HYDRAULIC HYSTERESIS

By

Ali Khosravi

B.A., Sharif University of Technology, 2003

M.A., Sharif University of Technology, 2005

A thesis submitted to the

Faculty of the Graduate School of the

University of Colorado in partial fulfillment

of the requirement for the degree of

Doctor of Philosophy

Department of Civil, Environmental and Architectural Engineering

2011

This thesis entitled:
Small Strain Shear Modulus of Unsaturated, Compacted Soils during Hydraulic Hysteresis

written by Ali Khosravi
has been approved for the Department of Civil, Environmental and Architectural Engineering

_____

Professor John McCartney, Committee Chair

_____

Professor Dobroslav Znidarcic

Date_____

The final copy of this thesis has been examined by the signatories, and we
find that both the content and the form meet acceptable presentation standards of scholarly work
in the above mentioned discipline.

Khosravi, Ali (Ph.D., Civil, Environmental and Architectural Engineering)

Small Strain Shear Modulus of Unsaturated, Compacted Soils During Hydraulic Hysteresis

Thesis directed by Professor John S. McCartney

A semi-empirical model was developed in this study to predict the impact of effective stress state and hydraulic hysteresis on the small strain shear modulus of unsaturated, compacted soils. Unlike previous empirical relationships for the small-strain shear modulus, this model incorporates constitutive relationships between effective stress, void ratio, stress history, hardening, and soil consistency. The model incorporates a stress-dependent hysteretic soil water retention curve relationship and a definition of mean effective stress equal to the product of the degree of saturation and matric suction.

The model is experimentally validated by considering small strain shear modulus data for a variety of soil types in the literature as well as from an independent testing program with a fixed-free resonant column device modified for suction control with the axis-translation technique. A flow pump was used to control the equilibrium matric suction and volumetric water content in a compacted silt specimen. The change in volume of the specimen was measured using a proximeter vertically mounted atop the soil specimen.

In both the model and experiments, for a constant net confining stress, the small strain shear modulus was observed to increase in a nonlinear fashion during drying, albeit at a reduced rate as the water occlusion conditions are reached. During subsequent wetting, the value

of G_{max} does not follow the same trend as during drying, similar to the hysteresis observed in the Soil Water Retention Curve (SWRC). Different from the SWRC, the value of G_{max} remains higher than that during drying. This hysteretic trend is attributed to hardening due to the effective stress changes associated with increased suction during drying. After calibration with parameters defined from the data available in the literature, the predictive model follows the experimental data.

DEDICATION

To the memory of my mother, J. S. Ghaffari

ACKNOWLEDGEMENT

First of all, I would like to dedicate this dissertation to the memory of my mother. She raised me and supported me through all the ups and downs. I am deeply indebted to her for her continued support and unwavering faith in me. She will be with me forever, in my heart and memories.

I would like to express my appreciation and sincere thanks to my advisor, Professor John S. McCartney, who guided and encouraged me throughout my studies. His advice and research attitude have provided me with a model for my entire future career. It has been an honor to be his first Ph.D student. I would like to thank Professor H.Y. Ko and Professor D. Znidarcic for their time and support during my PhD. I really appreciate the time and effort that they and the other geotechnical faculty have put into the coursework at CU. I would also like to thank Professor Judith Wang and Professor Abbie Liel for participating on my dissertation committee and providing new ideas about the subject.

Several individuals at the University of Colorado at Boulder helped make the resonant column test setup a reality. I am grateful for the perfect flow pump design and construction and the robust data acquisition design by Robert Wallen and Kent Polkinghorne. I would also like to acknowledge Dragan Mejic, the shop manager of the Chemical and Biological Engineering Department and Robert Geisert, the owner

of CNC Prototype Machine Inc. for their help in design and machining of different parts of the experimental setup. I learned about electronics, mechanics and machine installation from these people and I really appreciate it.

I would especially thank Majid Ghayoomi for his friendship, guidance, thoughtful discussion and many important contribution to this research. Thanks also to my friends at the University of Colorado Navid Plaseied, Masoud Arshadi, Thamer Alyaqoub, Christopher Lynch and JoonYung Lee for their sharing and help.

Finally, I would like to thank, although this is too weak a word, my mother, my wife and my brothers for their love, continual encouragement and support throughout this work.

CONTENTS

CHAPTERS

TABLES

Table

FIGURES

Figure

CHAPTER I

Introduction

1.1 Introduction

The shear modulus of soils is a key material property used in the evaluation of wave propagation through soil layers in dynamic response analyses for foundations, pavements, and embankments subjected to cyclic or earthquake loading. The shear modulus, G, is defined as the slope of the shear stress-strain hysteresis loop and is significantly influenced by the shear strain amplitude induced in a soil specimen. Of particular interest in geotechnical engineering is the value of shear modulus for strains less than 10^{-6} defined as the small strain shear modulus G_{max}. In analysis of soil behavior under cyclic or random loading conditions, when soil behavior is expected to stay within the range of the small strain of 10^{-6}, the use of an elastic model is justified and the small strain shear modulus becomes a key parameter to properly model the soil behavior (Hardin and Richart 1963). This parameter is used as the key reference value in pedictive relationships for G as a function of shear strain

amplitude, such as those developed by Hardin and Drnevich (1972), Vucetic and Dobry (1991), and Darandeli (2001).

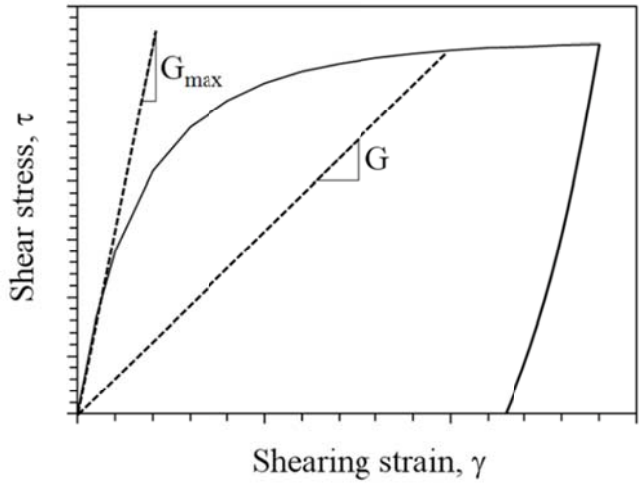

Figure 1.1: Example of a shear stress-strain hysteresis loop during a loading cycle

It is particularly relevant to understand the G_{max} for unsaturated soils. In many geotechnical systems, including bound and unbound pavements, laterally loaded foundations, machine foundations, foundations for wind turbines and retaining walls which are routinely subjected to dynamic loading, due to seasonal weathering changes, the soil underneath the structure may not be saturated anymore but experiencing unsaturated conditions. The seasonal wetting and drying of unsaturated soils in these systems imply that the stiffness of the soils may change during operation, complicating prediction of deformation. Although efforts have been made to develop analyses to consider the impact of seasonal weather interaction with soils in pavement design (i.e., the Enhanced-Integrated Climate Model of the Mechanistic Empirical Design Guide, MEPDG), they rely on

correlations between modulus and degree of saturation developed from tests with little consideration of unsaturated soil mechanics. Bringing these models to the next level will require an improvement to the prediction of G_{max} for unsaturated soils.

Studies on the shear modulus of soil at the small strain range of 10^{-6} revealed the significant influence of several factors on the magnitude of G_{max} of soils. Early involving measurement and prediction of G_{max} for dry and water saturated soils emphasized the importance of considering the void ratio e and mean effective stress (Hardin and Black 1968; Hardin and Black 1969; Hardin and Drnevich 1972; Iwasaki et al. 1978; Stokoe et al. 1995). Despite the significant body of work has been developed to evaluate the magnitude of G_{max} for saturated and dry soils, the variables that impact the magnitude of G_{max} for unsaturated soils are less well understood. Wu et al. (1984) and Qian et al. (1991; 1993) performed a careful series of resonant column studies on sands and silts compacted with different water contents under different total confining stresses to reveal strong nonlinear relationships between G_{max} and degree of saturation S_r.

Improvements in experimental unsaturated soil mechanics led to the definition of trends between G_{max} with net normal stress p_n (equal to the difference between the total mean stress p and pore air pressure u_a, i.e., $p_n = p - u_a$) and matric suction ψ (equal to the difference between pore air

pressure and pore water pressure u_w, i.e., $\psi = u_a - u_w$) using bender elements (Cabarkapa et al. 1999; Inci et al. 2003; Marinho et al. 2005; Sawangsuriya et al. 2009, Ng et al. 2009) and resonant column tests (Mancuso et al. 2002; Kim et al. 2003; Mendoza et al. 2005; Vassallo et al. 2007). However, except for the experimental studies by Sawangsuriya et al. (2009) and Ng et al. (2009), inter-relationships between G_{max}, S_r and ψ were not investigated. Concurrent measurement of S_r and ψ is not only necessary to interpret G_{max} measurements in terms of effective stress (Lu and Likos 2006; Lu et al. 2010; Khalili and Zargarbashi 2010), but it is also necessary to rationally consider the effects of drying and wetting (hydraulic hysteresis).

1.2 Objectives

The main objective of this study is to characterize the impacts of effective stress and degree of saturation S_r on the small strain shear modulus G_{max} of unsaturated, compacted soils during hydraulic hysteresis. Although recent studies have been performed in this area, this study compliments the measurement of matric suction with precise control of the degree of saturation. During hydraulic hysteresis, an element of soil may have different S_r values for the same value of ψ depending on whether the soil element is undergoing drying or wetting (Wheeler et al. 2003; Tamagnini 2004; Khalili and Zargarbashi 2010). The value of S_r during hydraulic hysteresis will reflect the amount of water in the soil,

and thus the cumulative number of air-water menisci affecting inter-particle connections, for a given matric suction (Wheeler et al. 2003). As a consequence, even though the suction may be the same magnitude upon drying and wetting, the different amounts of water in the soil will lead to different mechanical behavior (Wheeler et al. 2003; Tamagnini 2004; Khalili and Zargarbashi 2010).

1.3 Approach

The approach followed to reach the objective of this study is to develop a new constitutive modeling framework to consider the impact of hydraulic hysteresis on G_{max} for unsaturated soils, and to validate the framework using results from a resonant column (RC) test device with suction-saturation control. Unlike previous empirical relationships for the small-strain shear modulus, the constitutive modeling framework developed in this study incorporates inter-relationships between effective stress, void ratio, stress history, hardening, and soil consistency. The framework incorporates a hysteretic soil water retention curve measured under different net confining stresses and mean effective stresses.

The resonant column test device developed in this study incorporates the axis translation technique for suction control, a flow pump for degree of saturation control, and a vertically-oriented proximeter to infer changes in void ratio. A flow pump is essentially a syringe which can be moved to impose water flow rates on a specimen, and was originally used in

permeameter tests to measure the hydraulic conductivity of saturated clays (Olsen 1966).

After validation, the framework for G_{max} of unsaturated soils during hydraulic hysteresis is expected to be suitable for use in equivalent linear or nonlinear soil dynamics analyses that consider the effective stress state in unsaturated soils (i.e., matric suction and net confining stress). An improved understanding of the dynamic response of unsaturated soils is expected to lead to improved accuracy of design efforts for deformation prediction of geotechnical systems like pavements and machine foundations. More broadly, it will help provide tools to reveal linkages between moisture flow in unsaturated soils due to environmental fluctuations and their mechanical response.

1.4 Scope of the Study

The organization of this dissertation is arranged as follows. Chapter 2 provides a detailed description of previous research work on the effective stress of unsaturated soils, small strain shear modulus of saturated and unsaturated soils (measurement techniques and to proposed theoretical approaches) and hydraulic hysteresis and its effect on G_{max} of unsaturated soils. Material used for this study and its characterizations are described in Chapter 3. The semi-empirical framework proposed to analyze the impact of effective stress and hydraulic hysteresis on the small strain shear modulus of unsaturated, compacted soils is described in Chapter 4.

In this chapter, data from literature will be used to initially validate the proposed framework. The laboratory phase of this investigation containing the experimental equipment, the tests procedures and the results from various experiments is described in Chapter 5. A comparison of the results of the proposed framework to the test results are presented in Chapter 6. Then, Chapter 7 outlines a summary of the analyses and methods used in this study and gives general conclusions that may be drawn there from. Recommendations for future research into this subject are also provided. Chapter 8 contains a discussion on the definition of the effective stress of unsaturated compacted soil as an important parameter in predicting the small strain shear modulus, a mathematical relationship to define the air entry suction value of unsaturated soils, results obtained from flow pump during hysteresis changes of degree of saturation for specimens under different loading conditions and MATLAB programs which have been used to analyze the data..

CHAPTER II

Background

2.1 Small Strain Shear Modulus of Dry and Saturated Soils

Dynamic properties of soils have been studied theoretically and experimentally for several decades (Hardin and Black 1968, 1969; Hardin and Drnevich 1972; Hardin 1978; Iwasaki *et al.* 1978; Stokoe *et al.* 2004). Most of the work that has been performed on the dynamic shear modulus of soils has focused on either water-saturated or dry soil (Hardin and Black 1968, 1969; Hardin 1978; Iwasaki *et al.* 1978). Early experimental studies on the shear modulus of soils showed that G is highly dependent on different variables, such as shearing strain γ, mean effective stress p´, void ratio e, degree of saturation S_r, deviatoric stress τ, soil grain characteristics (shape, size, mineralogy), and gradation (Hardin and Richart 1963; Hardin and Drnevich 1972). However, further studies revealed that in elastic range of strain (shear strain amplitudes less than 10^{-6}), shear modulus of soil, defined as the maximum shear modulus G_{max},

is nearly independent of each of the variables except p´ and e (Hardin and Black 1969).

In attempts to describe the stiffness of the soil in the small range of strain, Rowe (1963) proposed an expression between relevant variables for the maximum elastic Yang's modulus E_{max} of soils:

$$E_{max} = \frac{1}{(1-n)C} E^{1-n} p'^{n} \quad (2.1)$$

where E is the Young's modulus of the particle material to satisfy the dimensions of the equation, C is dimensionless elastic compressibility coefficients and n is a constant. This expression was developed using the Hertz theory for elastic spheres in contact and considering isotropic behavior for soils in the elastic range of strain.

Later in 1963, due to difficulties in establishing the value of E for a given soil, Janbu (1963) found the atmospheric pressure P_a a better choice for satisfaction of the dimensions of the equation and defined the maximum Young's modulus E_{max} under an applied isotropic mean effective stress of p´ as follows:

$$E_{max} = K_E P_a^{1-n} p'^{n} \quad (2.2)$$

where P_a is the atmospheric pressure, n is a constant and K_E is a dimensionless elastic coefficient.

In 1978, Hardin evaluated the experimental measurements of the small strain shear modulus from wave propagation velocities and the small strain amplitude cyclic simple shear tests and from his observations

extended Janbu's expression to define an empirical relationship for G_{max} of saturated and dry soils with a general form of:

$$G_{max} = A\,(OCR)^{K} f(e) P_a^{1-n}\, p'^{n} \qquad (2.3)$$

In this equation, A and n are fitting parameters, p´ is the mean effective stress, OCR is the over-consolidation ratio, P_a is the atmospheric pressure, K is the hardening parameter related to the plasticity of soils PI and *f*(e) is referred to the void ratio function which was defined to consider the effect of void ratio on G_{max} of the soils. Different approaches were proposed to define the void ratio function. In early works by Hardin and Richart (1963), the effect of void ratio on G_{max} was expressed in the form of:

$$f(e) = \frac{(2.973-e)^2}{1+e} \qquad (2.4)$$

However, by the implementation of Eq. (2.3) in fitting experimental G_{max} data, later, Hardin (1978) proposed following relationship for *f*(e):

$$f(e) = \frac{1}{0.3+0.7e^2} \qquad (2.5)$$

Hardin and Richart (1963), Hardin and Black (1969), Hardin and Drnevich (1972), Seed et al. (1986), Ishihara (1996) also proposed similar expressions for the small strain shear modulus of saturated and dry soils.

2.2 Effective Stress in Soils

The principle of effective stress provides the most vital clue to understanding of dynamic behavior of soils and all experimental evidence supports the assertion that soil behavior is controlled by effective stress

and models which are intended for general application must be described in terms of history and changes of effective stresses. By considering the soil system as an equivalent continuum medium, Terzaghi (1936) defined the effective stress of saturated and dry soils as follows:

$$p' = p - u_w \tag{2.6}$$

where p is the total stress applied to the system and u_w is the pore water pressure between the particles. Use of Terzaghi's effective stress definition permitted the development of rational numerical methods to solve the governing partial differential equations for stress equilibrium under static and dynamic conditions in saturated soils.

However, it has become clear in recent years that improved solutions of many stress-related geotechnical engineering problems require not only sustained activities along the continuum based solid mechanics approach but also new theories along the discontinuous approach for describing effective stress under multiphase conditions. It has been recognized that theories describing the state of stress in unsaturated soil require consideration of the thermodynamic properties of the pore water in terms of soil suction, material variables such as grain size and grain size distribution, state variables such as degree of saturation, and inter-particle forces arising from matric suction (Lu and Likos 2006).

Different approaches have been recognized by researchers to describe the stress state of unsaturated soils. One approach that has been proposed

is the use of two independent stress-state variables, the net confining stress p_n (defined as the difference between total mean stress and pore air pressure $p_n = p - u_a$) and matric suction ψ (equal to the difference between the pore air pressure and pore water pressure $\psi = u_a - u_w$). This approach has been supported by observations that indicate volume change can occur due to either stress state variable (Fredlund and Morgenstern 1977). Several researchers have provided argued against using two stress state variables as it is not a natural extension of classical soil mechanics for saturated soils (Khalili et al. 2004; Lu 2008; Khalili and Zargarbashi 2010). Khalili et al. (2004) argued the concept proposed by Fredlund and Morgenstern (1977) requires a mixing of scales that is inconsistent with the continuum mechanics framework for multiphase systems. Lu (2008) argued that when matric suction and net confining stress are both selected as stress state variables to describe the state of stress in unsaturated soil, a transfer function is necessary to link the volumetric quantity of soil water with ψ and p_n.

Another approach was proposed by Bishop (1959) which describes the effective stress in unsaturated soils as a single stress state variable, as follows:

$$p' = p_n + \chi\psi \qquad (2.7)$$

where p_n is the net confining stress, χ is the effective stress parameter, ranging from 0 (for dry soils) to 1 (for saturated soils) and ψ is the matric

suction. Bishop's approach permits the straightforward use of Eq. (2.7) in engineering analyses developed using Terzaghi's definition of effective stress for saturated soils. Lu and Likos (2006) referred to the second term in Eq. (2.7) as the mean suction stress p_s, and indicated that it can be treated as a material relationship which depends on matric suction or degree of saturation S_r. They described the suction stress p_s as a macroscopic stress that collectively incorporates the effects of capillarity, as well as soil- and pore fluid-specific forces such as van der Waals forces, electrical double-layer repulsion forces, and net attraction forces arising from chemical cementation at the grain contacts (Lu and Likos 2006). They indicated that relationships between p_s and ψ can be defined for unsaturated soils for mechanical analyses in a similar manner to how soil-water retention curves (SWRCs) are defined for unsaturated soils in hydraulic analyses.

Different approaches are used to define the effective stress parameter χ in the definition of suction stress. Some studies have found that a value of χ equal to the degree of saturation S_r provides a successful representation of the mean effective stress when interpreting shear strength and deformation data (Gallipoli *et al.* 2003; Wheeler *et al.* 2003; Tamagnini 2004; Nuth and Laloui 2008). This definition of the effective stress parameter that is the basis of numerous recent constitutive stress frameworks includes a direct dependency of the overall behaviour of the

soil on the hydraulic state, reflected through variables suction and degree of saturation. However, by a comparison of S_r values and the effective stress parameter χ values obtained from the shear strength data, Khalili and Zargarbashi (2010) observed that the degree of saturation may not be a suitable choice for the effective stress parameter for the entire process of drying and wetting of the soil specimen, especially in the transition from drying to wetting for cohesive soils (Figure 2.1). It was observed that for cohesive soils, as the SWRC moves from drying to wetting, although degree of saturation increases slightly with decreasing suction, the effective stress parameter χ experiences a downward path to a minimum value beyond which it increases with decreasing suction (Khalili and Zargarbashi 2010).

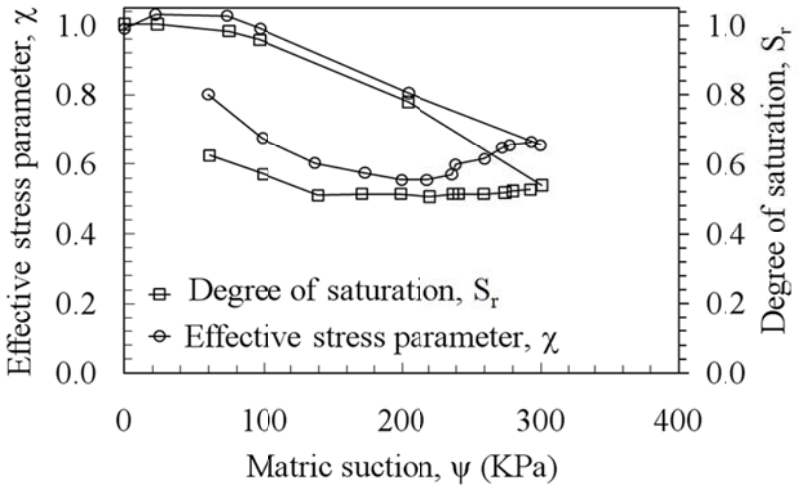

Figure 2.1: Variation of effective stress parameter χ and degree of saturation S_r versus matric suction ψ in the drying-wetting cycle for Sand-Kaolin mixture (Khalili and Zargarbashi 2010).

Lu and Likos (2006) proposed using an experimental approach involving a series of triaxial tests to define the relationship between p_s and ψ. A schematic highlighting their proposed experimental methodology is shown in Figure 2.2, in which p_s is equal to the tensile strength extrapolated from linear failure envelopes defined for different values of ψ.

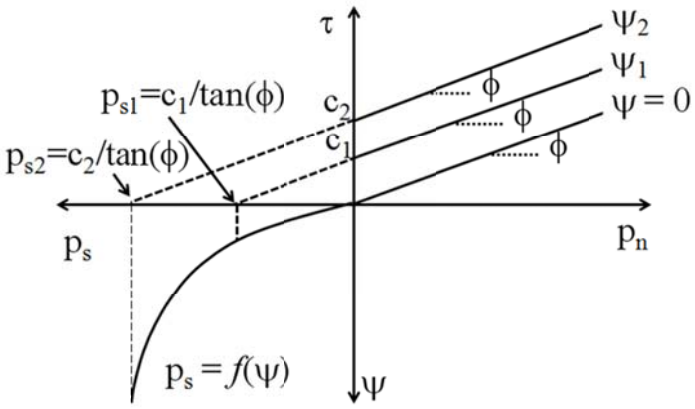

Figure 2.2: Illustrated methodology for evaluating the SSCC from shear strength data (Lu and Likos 2006; Khosravi and McCartney 2010).

By interpreting results obtained from this testing methodology, Lu et al. (2010) proposed following expression to define the suction stress of the unsaturated soil:

$$p_s = S_e \psi \qquad (2.8)$$

where S_e is the normalized degree of saturation by the value of S_r at residual saturation and ψ is matric suction. This assumption permits models for the SWRC relating S_e and ψ directly into Eq. (2.7), which implies that the effective stress can be predicted directly from the SWRC.

Using van Genuchten's (1980) SWRC model, following expression may be proposed to define the S_e of soils (Lu et al. 2010):

$$S_e = \frac{1}{(1 + (\alpha\psi)^N)^{\left(1-\frac{1}{N}\right)}} \quad (2.9)$$

where α and n are fitting parameters with "α" being the inverse of air entry suction for the soil and "N" being the pore size distribution parameter.

An issue encountered in implementing such an experimental methodology proposed by Lu and Likos (2006) is the effort and cost required to perform shear tests on multiple soil specimens. Previous round-robin tests on compacted soils for D18 revealed significant variability in compaction conditions, indicating that it may be difficult to obtain consistent samples for multiple triaxial tests. Also, if compression tests are to be carried out on intact field samples, the odds of recovering identical intact samples are low. In this regard, the use of drained multistage triaxial testing to determine the strength properties of unsaturated soils has been investigated by researchers for both eliminating variability in soils between tests and extracting the maximum amount of information from a single test (Ho and Fredlund 1982; Raharadjo et al. 1995; Khalili and Zargarbashi 2010). Several studies on saturated soils demonstrate the economic feasibility of performing multistage triaxial tests under saturated conditions (Saeedy and Mollah 1988; Soranzo 1988). By performing a series of multistage drained

shearing tests on residual soils, Ho and Fredlund (1982) made clear that the multistage testing procedure was only applicable to unsaturated soils with relatively high permeability, as the rate of shearing must be slower in soils with low permeability (such as unsaturated soils) to permit sufficient time for drainage of shear-induced pore water pressures. An interesting observation of Ho and Fredlund (1982) was that the strength of the soil specimen in the last stage of the multistage shearing test (i.e., having the highest applied suction) was found to be lower than the previous suction value.

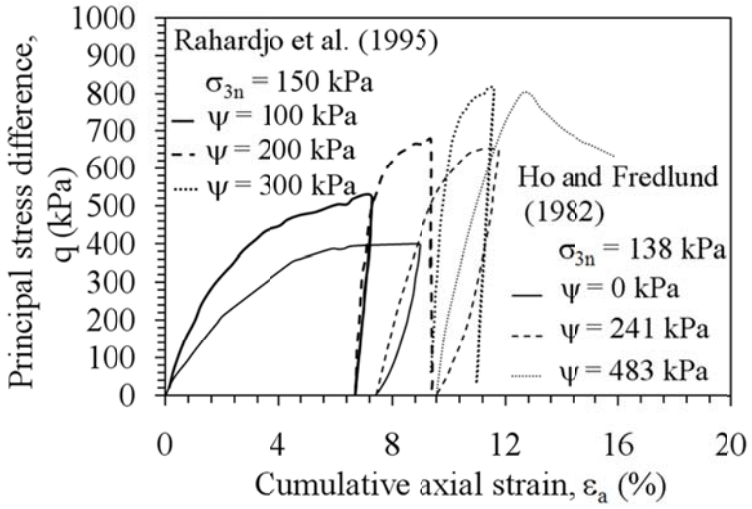

Figure 2.3: Results from multistage triaxial tests on unsaturated soils reported in the literature

This observation, which was also made by Rahardjo et al. (1995) in multistage tests on intact residual soil, was proposed to be related to the amount of strain accumulated while the specimen was failing. Examples of the axial stress-strain curves obtained by Ho and Fredlund (1982) and

Rahardjo et al. (1995) highlighting this feature are shown in Figure 2.3. Ho and Fredlund (1982) concluded that multistage testing is appropriate when soil specimens do not deform excessively during earlier stages of loading.

Recently, Khalili and Zargarbashi (2010) performed multistage triaxial tests on different soils to probe the critical state line (CSL) for different suction increments, with the goal of evaluating the variation of the effective stress parameter during hydraulic hysteresis (drying then wetting). A similar hysteretic trend observed in the SWRC was observed in relationships between χ and ψ for non-cohesive soils. Although Khalili and Zargarbashi (2010) observed that the degree of saturation may not provide representative values for the effective stress parameter, their results indicate that the SWRC and effective stress parameter are related. Their approach to define the CSL using multiple stages during drying was to apply increments of suction after shearing to the CSL, which increases the mean effective stress and departs away from the CSL. They defined points on the CSL during wetting by unloading the specimen through a reduction of matric suction, while maintaining constant net stress and axial strain. Based on observations from this study and observations by Khalili and Khabbaz (1998), the authors developed a semi-empirical expression to relate the effective stress parameter to the matric suction ψ and ψ_e which is defined as the suction value marking the transition

between saturated and unsaturated conditions (Khalili and Khabbaz 1998) for the main drying and wetting paths:

$$\chi = \begin{cases} 1 & \psi \leq \psi_e \\ \left(\frac{\psi}{\psi_e}\right)^{-0.55} & \psi \geq \psi_e \end{cases} \quad (2.10)$$

in which for the main wetting path $\psi_e = \psi_{ex}$ and for the main drying path $\psi_e = \psi_{ae}$ where ψ_{ex} is the air expulsion value and ψ_{ae} is the air entry value.

2.3 Small Strain Shear Modulus of Unsaturated Soils

By a theoretical study on the wave propagation of the soils in a fluid saturated porous medium, Biot (1956) reported that the presence of fluid between the voids produced only a minor effect on the shear wave velocity of the soil. Based on this observation, the difference between the curves for the dry and saturated conditions was accounted for by the effect of the weight of the water through the unit weight and effective stress of the soil (Richart et al. 1970). However, observations by Wu et al. (1984) and Qian et al. (1991; 1993) revealed the strong nonlinear relationships between G_{max} and degree of saturation S_r of the soils. Wu et al. (1984) performed one of the first studies to determine the difference in dynamic properties between unsaturated and saturated soils.

In their study, the effects of the degree of saturation, confining pressure, void ratio, and grain size distribution of the soil particles on the dynamic shear modulus of unsaturated soils were measured using a resonant column test device. Unsaturated soil specimens were prepared

by tamping the soil to reach the same void ratio but with different initial water contents. Their results indicated the significant effect of degree of saturation on the small strain shear modulus, especially at specimens subjected to a lower net confining stresses p_n or higher initial void ratio (Figure 2.4). In this study, G_{max} was observed to tend to increase to a peak value at a degree of saturation of 10 to 15%, after which it decreased as the soil became wetter. Same observations were reported by Qian et al. (1993).

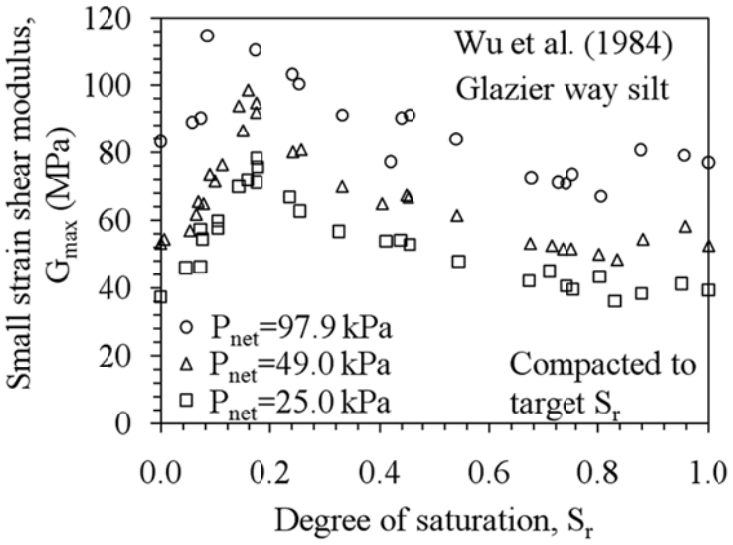

Figure 2.4: Variation of G_{max} with compacted degree of saturation for the Glazier way silt reported by Wu et al. (1984)

Although results by Wu et al. (1984) and Qian et al. (1991; 1993) revealed the significant influence of degree of saturation on G_{max} of soils, however, observations by Kim at al. (2003) revealed that G_{max} values at a given water content for specimen prepared by controlling compaction

moisture contents were smaller compared with those dried gradually by controlling the capillary pressure (Figure 2.5).

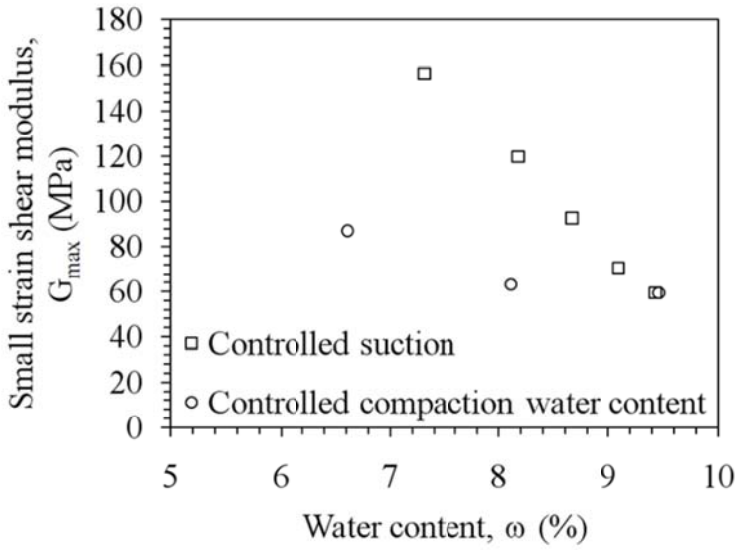

Figure 2.5: Comparison between specimens prepared with controlled compaction moisture content and those dried with controlled matric suction (Kim et al. 2003)

Kim et al. (2003) modified a Stokoe-type resonant column-torsional shear testing system to investigate the effect of various variables like matric suction, degree of saturation, void ratio, compaction moisture content and shear strain on the shear modulus of an unsaturated sand. In this study, contrary to previous studies which used various specimens of different compaction water contents, specimens were dried gradually by controlling the capillary pressure which is closer to the situation in the field where the water content of the soil is routinely fluctuated with seasonal weather changes.

In this test setup, the capillary pressure was controlled using the axis translation technique by increasing the air pressure applied to the system

while the water pressure was kept constant at the atmospheric pressure during the test. The volume of water passing through the specimen was monitored by a burette connected to the bottom of the high air entry porous stone. Based on this study, an increase in shear modulus was observed due to the increase in matric suction at the whole strain range applied to the specimen while an increase in degree of saturation resulted in the G_{max} decrease. Due to the method of testing, specimens tested in this study were not fully saturated at the beginning of the drying process but they were at the degree of saturation related to their compaction water content [Figure 2.6(a)].

Mancuso et al. (2002) performed an experimental study on the small strain shear modulus using a modified resonant column-torsional shear cell with the axis translation technique (Hilf 1956). Authors investigated the small strain behavior of an unsaturated, compacted silty sand under different net normal stresses, matric suctions and compaction water content. In this study, backpressure saturation was used to initially saturate the specimen by dissolving entrapped air bubbles (Schuurman 1966). Results in this study indicated the significant influence of net confining stress and matric suction on the G_{max} measurements of unsaturated soils.

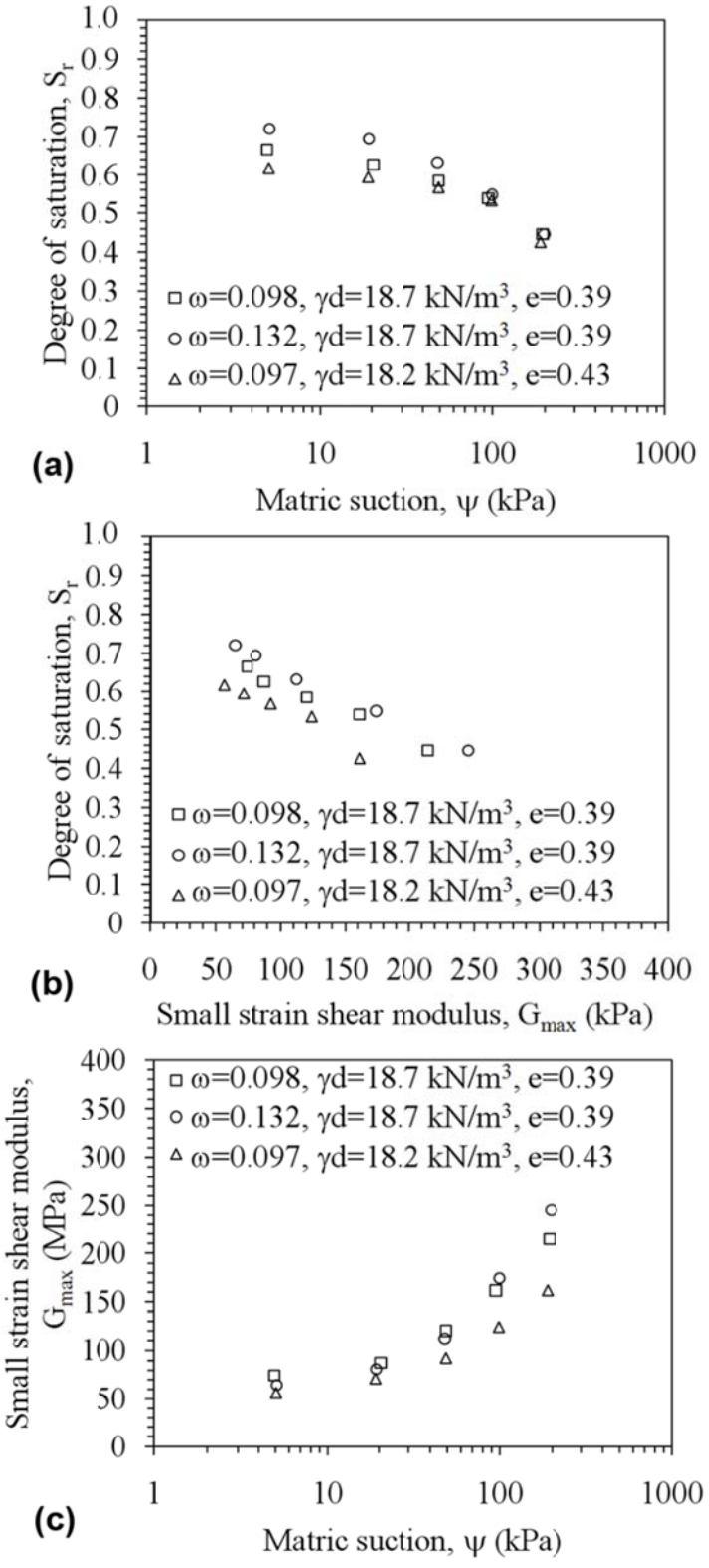

Figure 2.6: G_{max} data for different soils from Kim et al. (2003): (a) SWRCs; (b) G_{max} vs. S_r; and (c) G_{max} vs. ψ

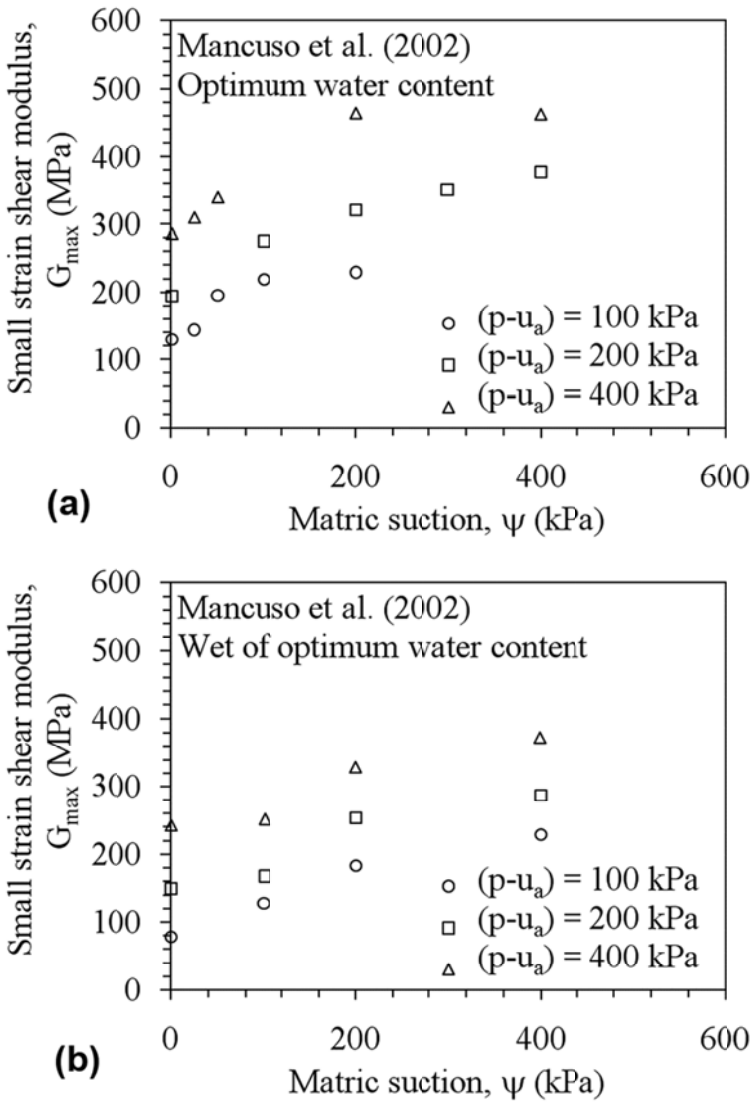

Figure 2.7: Variation of G_{max} with matric suction during drying for silty sand specimens with different compaction water content

The trend between G_{max} and ψ during drying was observed to have three distinct zones. The first zone was related to the drying process from saturation conditions to the air-entry suction, where the amount of air present in the specimen was negligible and a very small change in S_r occurred. In this zone, a slight increase in G_{max} with ψ was observed. For values of ψ greater than the air-entry suction, the soil desaturated at a

steeper gradient, which led to a greater increase in G_{max} with increasing matric suction. As the soil approached residual saturation conditions, G_{max} was observed to tend asymptotically toward a limiting value. Same observations are reported by Marinho et al. 1995; Inci et al. 2003; Mendoza et al. 2005; Vassallo et al. 2007; Sawangsuriya et al. 2009 and Vanapalli et al. 2009.

Trends in this study were also significantly affected by the initial compaction water content. Initial compaction water content, through its control of soil fabric, was observed to cause significant differences in the variation of G_{max} with matric suction. Specimens compacted wet of optimum water content had lower G_{max} and tended to exhibit a weaker soil fabric with respect to the specimen compacted dry of optimum. Increasing net confining stress applied to the soil was also observed to result in a considerable increase in G_{max}. However, specimens under higher net confining stress were observed to be less sensitive to the changes of matric suction. A limitation in the study by Mancuso et al. (2002) was that the variation of the degree of saturation of the soil specimen during the application of loading (ψ and p_n) was not monitored. From the observation by Ng et al. (2009), soil specimens subjected to higher net confining stresses were observed to have a better water retention ability and their rates of desorption and adsorption of the specimen were smaller.

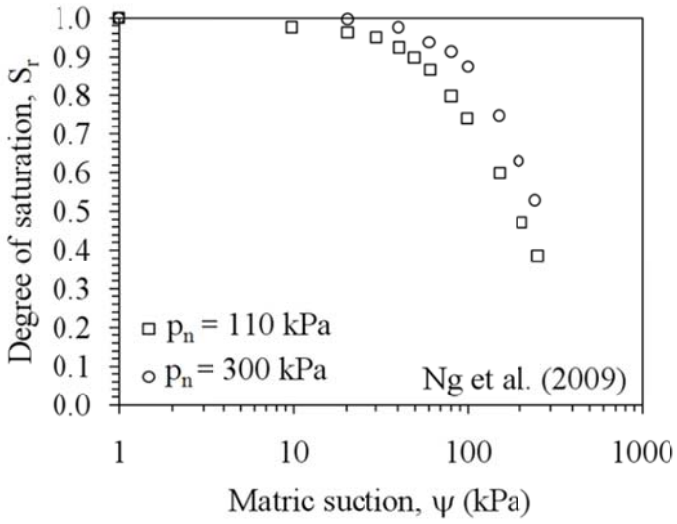

Figure 2.8: Effect of p_n on the degree of saturation of the soils during the process of drying (Ng et al. 2009)

In 2009, Khosravi et al. conducted a series of tests on Ottawa sand using a fixed-free Stokoe-type resonant column device modified with suction-control capabilities to evaluate changes in G_{max} of an unsaturated clean sand with the unsaturated stress state variables (matric suction and net stress) and degree of saturation, In this setup, the pore air pressure in the soil specimen was vented to atmosphere while the pore water pressure in the specimen was controlled using the hanging column technique with controlled water outflow (McCartney et al. 2008). In the hanging column technique, a static column of water is maintained below a water-saturated high air entry porous stone. The height of this column of water corresponds to the matric suction at the bottom boundary of the specimen. This device had the capability of applying matric suction values ranging from 0 to 10 kPa to the sand specimen.

The overall layout of this system is presented in Figure 2.9. The relationship between small-strain shear modulus and effective stress was evaluated for unsaturated sand specimens under different net confining stresses.

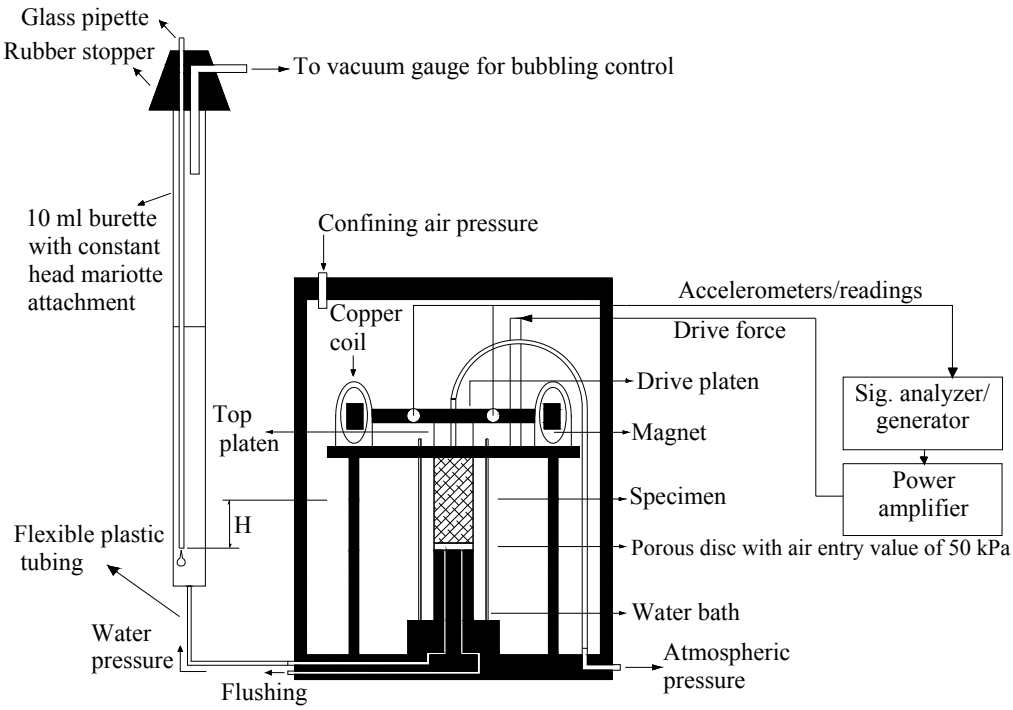

Figure 2.9: Cross-section of the suction-controlled resonant column apparatus

Especially, in this study, the effective stress was defined using the concept of the suction stress characteristic curve (SSCC) proposed by Lu and Likos (2006). The small-strain shear modulus was observed to follow a cane-shaped trend with matric suction, and reached a maximum value at a degree of saturation close to residual conditions (a matric suction approximately 5 kPa) after which it started decreasing to a value close to the value of small strain shear modulus at saturated conditions. This

observation is similar to the results by Wu et al. (1984) and Qian et al (1993) (Figure 2.10).

Comparing results for unsaturated non-cohesive (Figures 2.10 and 2.4) and cohesive soils (Figure 2.7), different trends in the small strain shear modulus are observed as suction increases beyond its residual value. Clayey soils are observed to tend toward a constant value with increasing suction while a decreasing trend for sandy specimens is observed. This difference in behavior may be due to differences in the interparticle forces concentrated at or near the interparticle contacts. Lu and Likos (2006) described the interparticle contacts as the combination of van der Waals attraction, electrical double-layer repulsion, and the net attraction arising from chemical cementation at the grain contacts referred as physicochemical forces as well as additional attractive forces arising from surface tension at air-water interfaces and attractive forces arising from negative pore water pressure in unsaturated sandy and clayey soils. As the suction applied to the system goes beyond its residual value, large increases in matric suction result in only very small changes in water content. In this stage, the capillary stress and double-layer stress significantly decrease or cease to exist, while van der Waals stress approaches a constant value. As a result, the interparticle forces may diminish to zero for sandy soils but could reach several hundred kPa for clayey soils.

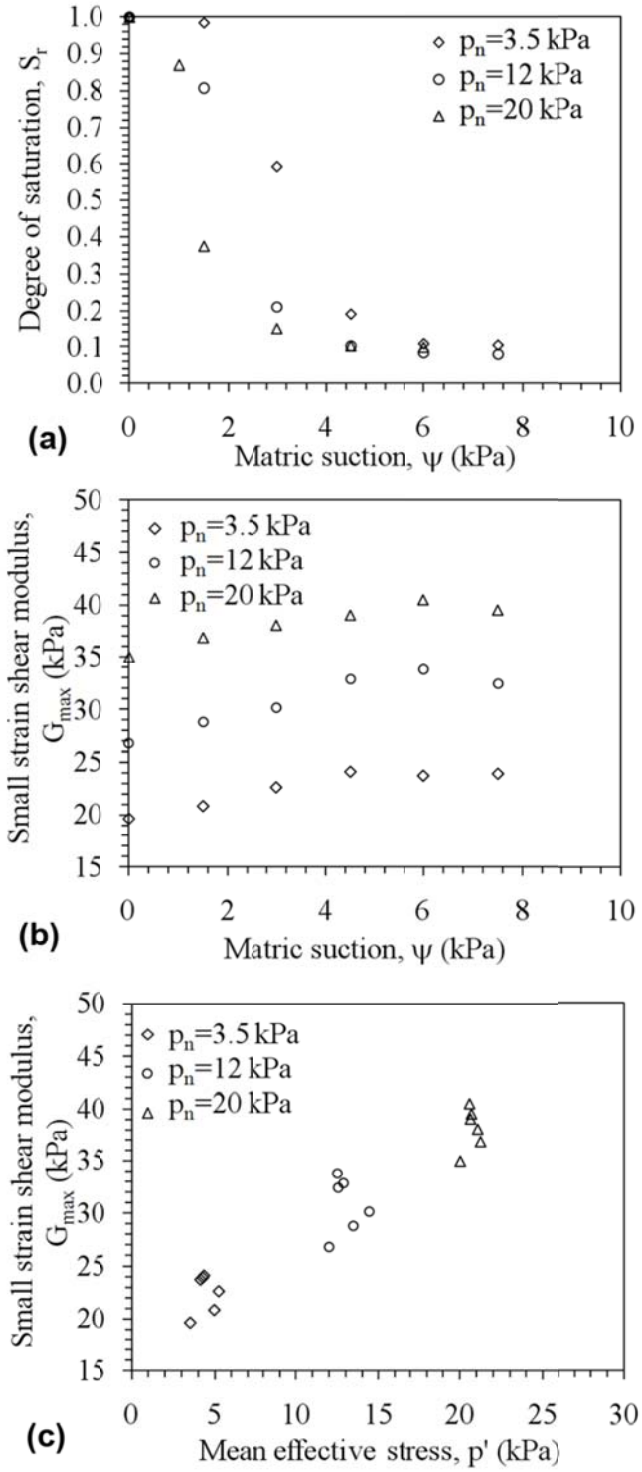

Figure 2.10: G_{max} data for different soils from Khosravi et al. (2009): (a) SWRCs; (b) G_{max} vs. ψ; and (c) G_{max} vs. p´

2.4 Relationships for the Small Strain Shear Modulus of Unsaturated Soils

In general, based on the definition of stress state considered for analysis and from the interpretation of G_{max} results measured using bender elements (Cabarkapa et al. 1999; Inci et al. 2003; Marinho et al. 2005; Sawangsuriya et al. 2009, Ng et al. 2009) and resonant column tests (Mancuso et al. 2002; Kim et al. 2003; Mendoza et al. 2005; Vassallo et al. 2007), two different types of relationships can be recognized for the small strain shear modulus of unsaturated soils. One type of relationship is based on the use of independent stress state variables (Fredlund and Morgenstern 1977) as the stress state of unsaturated soils. For example, using this concept and the evaluation of experimental measurements of G_{max} for unsaturated, compacted soils, Sawangsuriya et al. (2009) proposed an empirical relationship for G_{max} along the drying path of the SWRC that relied on the physical soil properties and the SWRC of the soil as follows:

$$G_{max} = Af(e)p_n{}^n + B\psi \qquad (2.11)$$

where n and A are parameters defined by fitting Eq. (2.11) to a set of G_{max} data under a constant value of p_n and f(e) is a void ratio function. Mancuso *et al.* (2002); Mendoza *et al.* (2005); Oh and Vanapalli (2009); and Ng *et al.* (2009) also proposed similar empirical relationships for G_{max}. Although these relationships provide a good prediction of G_{max} with stress state

during drainage-path tests for a given initial void ratio, they have not been evaluated for hydraulic hysteresis.

Accordingly, Inci et al. 2003; Sawangsuriya et al. 2009; Khosravi and McCartney 2009; Khosravi et al. 2010 have incorporated the single-value mean effective stress definition proposed by Bishop (1959) for unsaturated soils into the expression of G_{max} proposed by Hardin and Black (1968) , as follows:

$$G_{max} = Af(e)p'^{\,n} \tag{2.12}$$

where A and n are fitting parameters and p´ is the effective stress of unsaturated soils defined as Eq.(2.7). In the definition of Eq. (2.12), different approaches for the effective stress parameter were considered. Sawangsuriya et al. (2009) used following expression for the effective stress parameter:

$$\chi = \Theta^K = \left(\frac{\theta}{\theta_{sat}}\right)^K \tag{2.13}$$

while Inci et al. (2003), Kawajiri et al. (2009) and Khosravi et al. (2010) used an effective stress parameter of 1 in their analysis.

As observed in Eqs. (2.11) and (2.12), implementation of both equations in fitting experimental G_{max} data almost always incorporates a relationship for *f*(e) defined by Hardin and Black (1969) (Eq. 2.4) and Hardin (1978) (Eq. 2.5). In both equations, definition of *f*(e) was developed assuming that e and p´ are uncoupled and G_{max} is proportional to the square root of p´. Other studies (Stokoe et al. 1999; Tatsuoka et al. 1996;

Darendeli 2001) found that the coefficient of proportionality between G_{max} and p´ [i.e., the fitting parameter n in Eq. (2.5) and (2.6)] may not be the same for all soils.

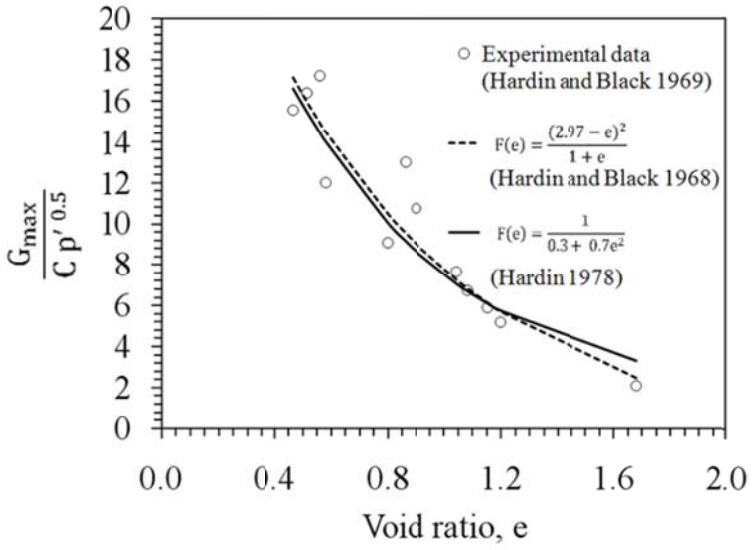

Figure 2.11: Empirical relationships proposed to represent the trend in void ratio with G_{max} for undisturbed clay specimens

The value of n for most of normally consolidated soils was reported in a range of about 0.5 to 0.6 while for the over-consolidated soils, G_{max} was observed to be less sensitive to p´, resulting in values of n smaller than 0.5 (Darendeli 2001). Accordingly, a model G_{max} which incorporates coupling between e and p´ may better represent hardening phenomena noted during hydraulic hysteresis.

2.5 Effect of Hydraulic Hysteresis on the Small Strain Shear Modulus of Unsaturated Soils

The common experimental techniques to measure the small strain shear modulus of unsaturated soils are the fixed-free resonant column and

pulse wave (i.e., bender element) tests combined with a hydraulic permeameter modified with the axis translation technique (Hilf 1956). Axis translation permits the control of the suction in the specimen by applying (or measuring) a difference in air and water pressure across a soil specimen resting atop a high air-entry ceramic disk or porous membrane. The high air-entry ceramic disk permits independent control of the pore water pressure on the boundary of the specimen as only water is transmitted through the ceramic disk for suction values less than the air-entry suction of the ceramic disk. The pore water pressure in the axis translation technique needs not be zero as the suction is equal to the difference in the air and water pressure. Accordingly, backpressure saturation can be used to initially saturate the specimen by dissolving entrapped air bubbles (Schuurman 1966). The axis translation technique with backpressure permits improved accuracy of outflow measurements from unsaturated materials. However, water flow from or into the specimen during the application of increments of ψ values in most of available technique is typically measured using visual observation of the water level in a graduated burette connected to the water drying line from the specimen. Although this water flow measurement approach may yield appropriate results at equilibrium, it is particularly difficult to ascertain whether or not equilibrium has been reached and the temporal resolution of water flow can be difficult to assess for small flow volumes.

This shortcoming of the conventional axis translation technique makes it difficult to ensure that a uniform value of suction has been reached in the specimen, especially during wetting. Partially due to difficulties in tracking outflow during suction control with the conventional axis translation technique, most studies on G_{max} of unsaturated soils presented results of only the primary drying path of the SWRC and did not report trends with degree of saturation (Cabarkapa et al. 1999; Mancuso et al. 2002; Inci et al. 2003; Mendoza et al. 2005; Vassallo et al. 2007). The value of S_r is critical to measure in unsaturated soils experiencing hydraulic hysteresis, as an element of soil may have different S_r values for the same value of ψ depending on whether the soil element is undergoing drying or wetting (Wheeler et al. 2003; Tamagnini 2004; Khalili and Zargarbashi 2010).

The value of S_r during hydraulic hysteresis will reflect the amount of water in the soil, and thus the cumulative number of air-water menisci affecting inter-particle connections, for a given matric suction (Wheeler et al. 2003). As a consequence, even though the suction may be the same magnitude upon drying and wetting, the different amounts of water in the soil will lead to different mechanical behavior (Wheeler et al. 2003; Tamagnini 2004; Khalili and Zargarbashi 2010).

Khoury and Zaman (2004) conducted a comprehensive study on the variation of resilient modulus M_R as a soil stiffness parameter with water

content and matric suction upon drying and wetting. Their results indicated that M_R-moisture content relationships exhibited a hysteretic behavior due to wetting and drying. Same observation was reported by Khoury (2010) on silt specimens. Ng et al. (2009) investigated the effects of wetting–drying and stress ratio on anisotropic shear stiffness of an unsaturated completely decomposed tuff (CDT) at small strains using a modified triaxial testing system equipped with three pairs of bender elements. During drying, the measured small strain shear moduli increased in a nonlinear fashion. A sharp increase in G_{max} first occurred in the soil. The G_{max} was then observed to increase at a reduced rate as the matric suction increased. During wetting, at the same suction level, the measured small strain shear moduli were observed to be consistently higher compared to those measured during drying. Ng et al. (2009) interpreted this observation as the direct influence of degree of saturation on G_{max}, in addition to any influence of matric suction and net confining stress (Figure 2.12).

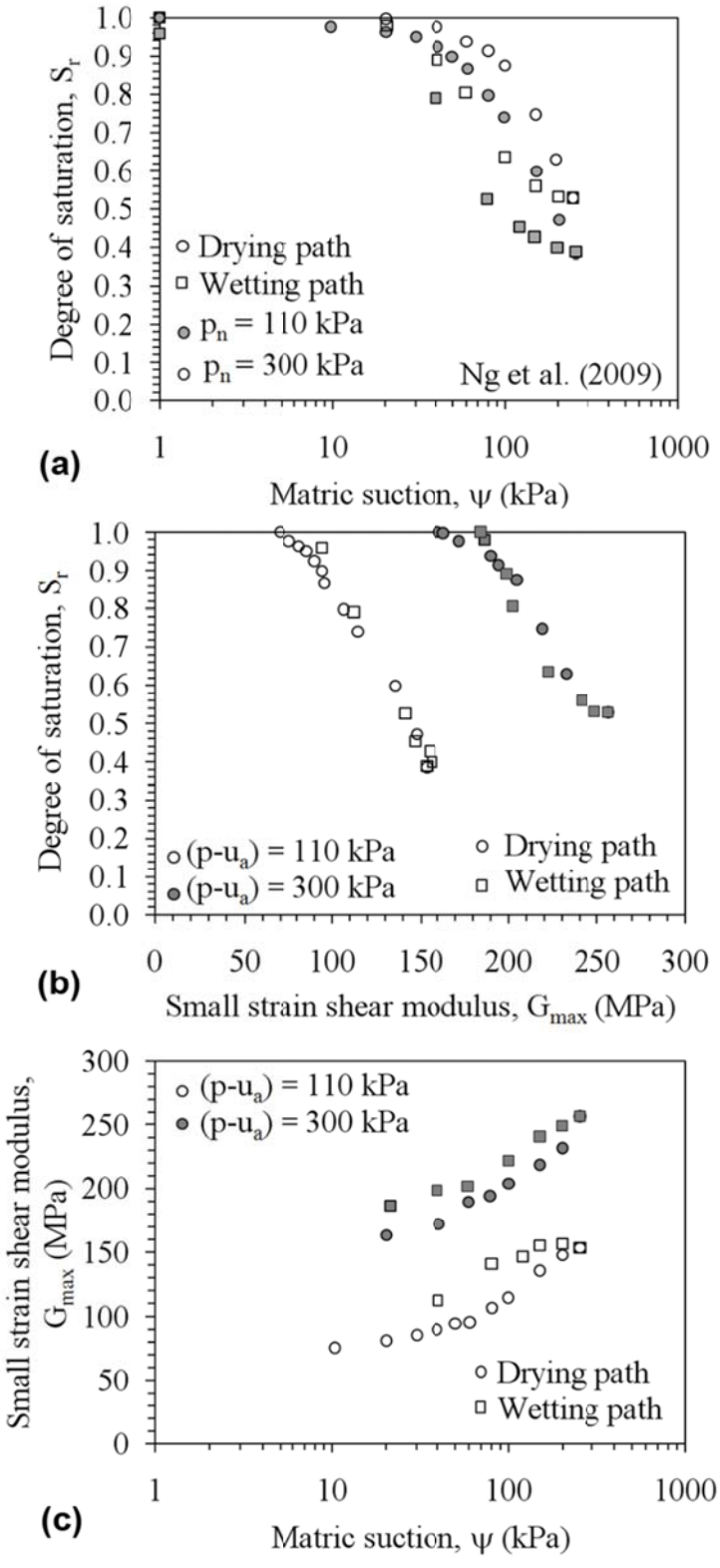

Figure 2.12: G_{max} data for ML soil from Ng et al. (2009): (a) SWRCs; (b) G_{max} vs. S_r; and (c) G_{max} vs. ψ

CHAPTER III

Material Properties

3.1 Introduction

A silt obtained from the Bonny dam near the Colorado-Kansas border (Figure 3.1) was used to demonstrate the capabilities of the new suction-saturation controlled resonant column setup and to validate the framework for the prediction of G_{max} of unsaturated soils during hydraulic hysteresis. The information gained through the use of low plasticity clay will facilitate interpretation of the impact of unsaturated stress state because they vary in moisture content over a wide range of suction with negligible volume change during SWRC testing. These materials are expected to be straightforward to test in the resonant column and triaxial setups without significant scale effects. The liquid and plastic limits of the soil measured according to ASTM D 4318 are 26 and 24 and the soil has a specific gravity G_s of 2.6. The grain size distribution of the soil is shown in Figure 3.2. Based on this information, the soil classifies as a ML according to the Unified Soil Classification System (USCS).

Figure 3.1: The location of the Bonny dam

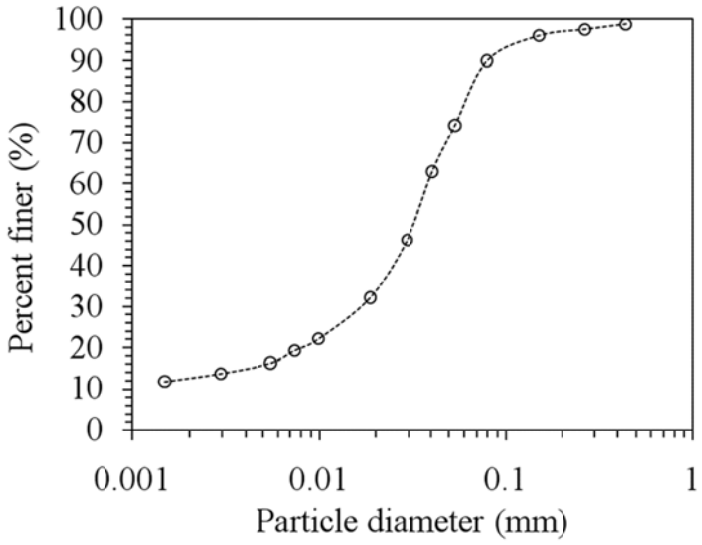

Figure 3.2: The grain size distribution

3.2 Compaction Characteristics

Modified and standard Proctor compaction tests were performed on the Bonny silt following ASTM D 698 to determine the optimum water content and maximum dry unit density of the soil. The compaction curves, shown in Figure 3.3, show maximum dry unit weights of 16.5 kN/m^3 and

18.8 kN/m^3 for specimens compacted using the standard and modified Proctor efforts, respectively. The optimum water content for the standard Proctor effort is approximately 14%, while that for the modified Proctor effort is approximately 11%.

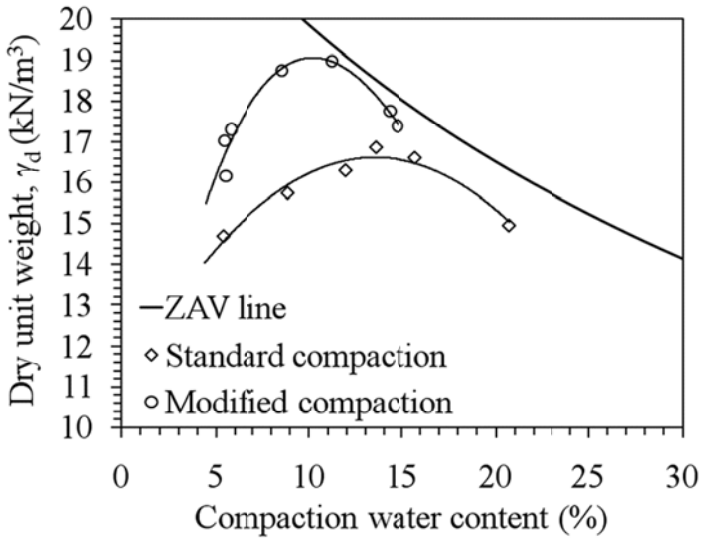

Figure 3.3: Modified and standard Proctor test results

3.3 Shear Strength Parameters

The shear strength parameters of Bonny silt was determined using a series of consolidated undrained triaxial tests on the soil specimens under different mean effective stresses of 100, 200 and 350 kPa with pore pressure measurement, following ASTM D4767 for consolidated-undrained triaxial compression test. Specimens were prepared at an initial void ratio of 0.53 and a compaction water content of 14%. The stress-strain curves are shown in Figure 3.4(a) and the pore water pressure response is shown in Figure 3.4(b). The pore water pressure

response clearly shows that the soils have a transition in behavior near the previous preconsolidation pressure induced by compaction.

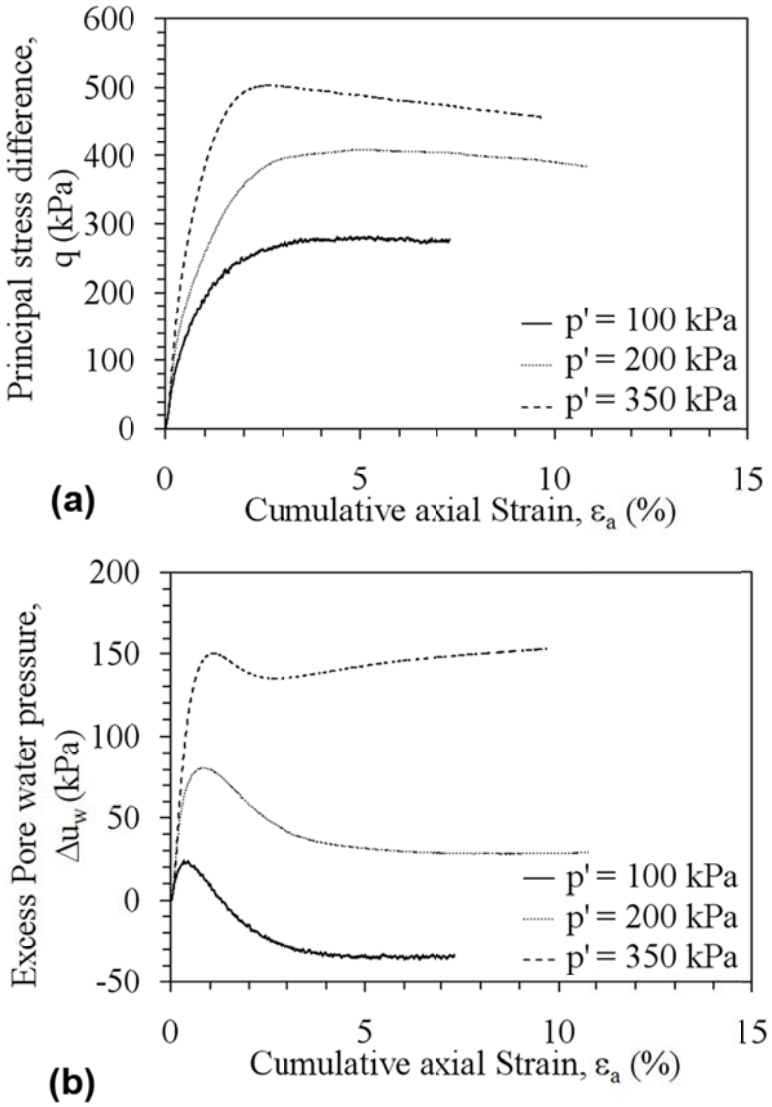

Figure 3.4: Shear strength results for saturated specimens subjected to different net confining stresses (a) Principal stress difference vs. axial strain (b) Pore water pressure vs. axial strain

The stress paths shown in Figure 3.5 indicate a unique critical state line for specimens under different mean effective stresses. As it is observed in the figure, along shearing the specimen for all cases, the

stress path follows an upward path tending toward a critical state line with a slope of M = 1.305 corresponding to an effective friction angle of 29 degrees.

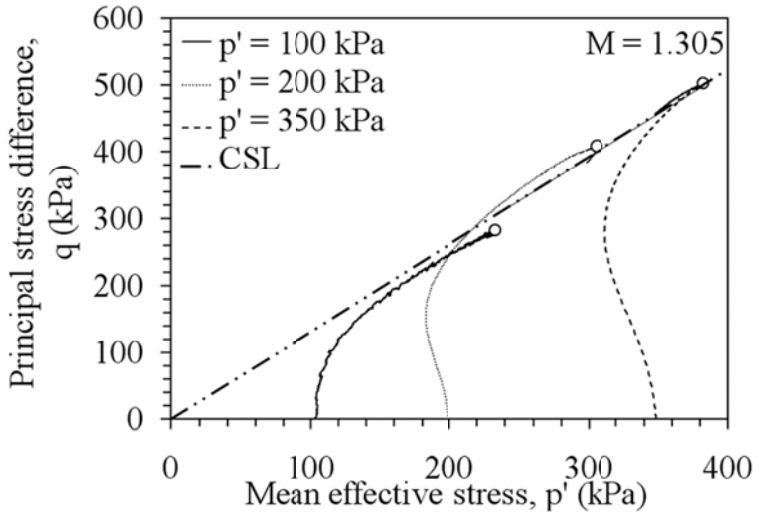

Figure 3.5: Stress paths of the soil specimens subjected to different mean effective stress during shearing

3.4 Hydraulic Conductivity of Saturated Bonny Silt

Hydraulic conductivities for Bonny silt specimens with different void ratios at saturated state measured using the flow pump technique (Aiban and Znidarcic 1989) are shown in Figure 3.6. The flow pump technique was introduced to the soil science discipline by Olsen (1966) and Aiban and Znidarcic (1989) to improve the measurement of the saturated hydraulic conductivity. Znidarcic *et al.* (1991) adopted the flow pump technique to measure the SWRC and K-function of unsaturated soils by combining it with the axis-translation technique.

The first step in the flow pump technique for the measurement of the hydraulic conductivity is saturation of the soil specimen in the triaxial cell

using the back pressure technique under a constant confining stress. After saturation, a known constant quantity of flow is forced through the specimen by the pump and the corresponding pressure difference, from which the hydraulic gradient is evaluated, is measured by a pressure differential transducer (Figure 3.7). The saturated hydraulic conductivity is then measured as:

$$k_{sat} = \frac{Q}{Ai} \tag{3.1}$$

where Q is the flow rate applied to the specimen, A is the area of the specimen and I is the hydraulic gradient.

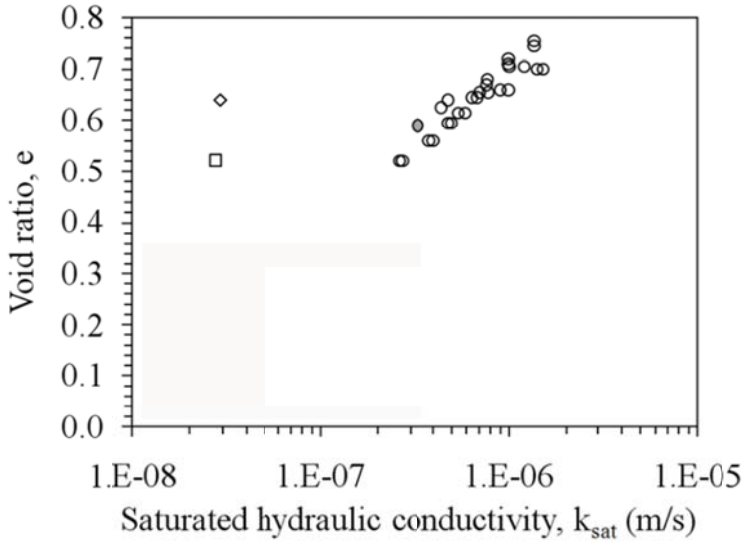

Figure 3.6: Void ratio vs. saturated hydraulic conductivity relationship for Bonny silt specimens reported in literature

The advantage of this test arises from the fact that it is much easier to control small flow rates precisely than to measure them accurately. With the flow pump technique, the specimens are subjected to steady state conditions.

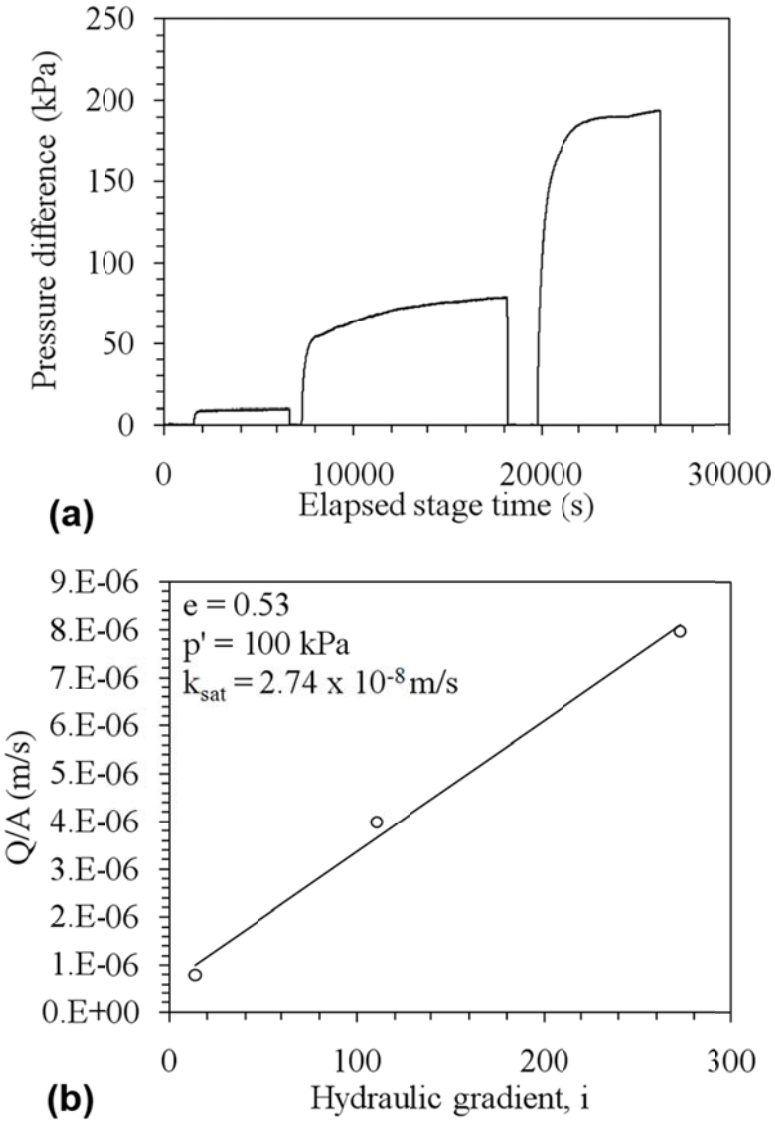

Figure 3.7: Flow pump results for Bonny silt specimen with an initial void ratio of e=0.53 under a mean effective stress of 100 kPa

3.5. SWRC of Monolithic Bonny Silt

In Figure 3.8, the SWRC measurements using the flow pump technique (Znidarcic et al. 1991) for Bonny silt specimens prepared at different initial void ratios are presented. In this technique, after saturation of the specimen using the back pressure technique under a constant net

confining stress, the soil specimen was de-saturated by maintaining a constant air pressure at the top of the specimen and drawing water from the bottom of the soil specimen using the flow pump. The pump is operated in the withdrawal mode which caused pore water reduction at the bottom of the specimen.

A differential pressure transducer connected to the air pressure (top of the specimen) and water pressure (bottom of the specimen) lines is used to measure the matric suction during the test. The flow pump withdraws water from the specimen at a constant rate until the differential pressure transducer indicates that a target suction (i.e., a difference between the pore air on the top of the soil specimen and the pore water on the bottom of the saturated porous disc) has been reached at the boundary of the specimen. However, this suction level is only representative of the boundary. In order to gain a uniform suction through the specimen, a feedback control loop in the flow pump stepper-motor is used to continue drawing water from the specimen in increments until the matric suction ($u_a - u_w$) is stabilized for a desired period of time.

After reaching the suction equilibrium at the specimen for a specific matric suction, this step will be repeated for several values of matric suction to obtain the SWRC. The degree of saturation for a corresponding matric suction is measured by calculating the volumetric moisture content from the outflow data after each stable suction value has been reached.

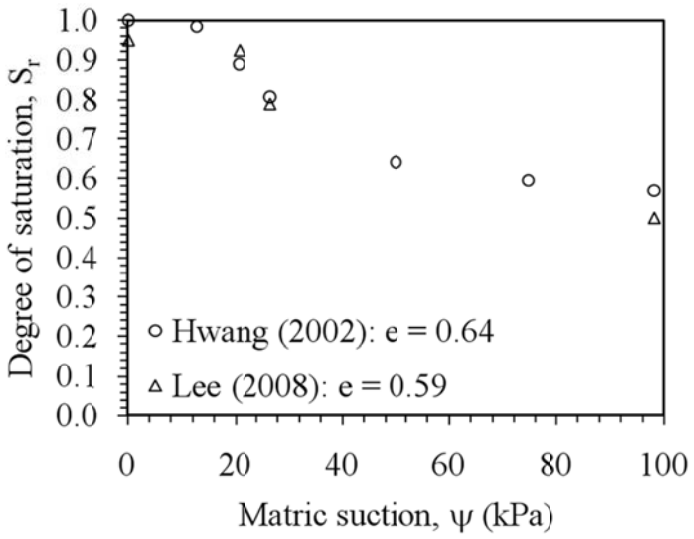

Figure 3.8: SWRC for Bonny silt reported in literature

CHAPTER IV

Prediction of the Small Strain Shear Modulus of Unsaturated Soils during Hydraulic Hysteresis

4.1 Introduction

In this chapter, a semi-empirical framework for G_{max} of unsaturated soils incorporating recent advances in the definition of the effective stress state in unsaturated soils, relationships for hydraulic hysteresis in the soil water retention curve (SWRC), and established constitutive relationships for unsaturated soils is proposed. From the interpretation of the small strain shear modulus results, different definition of trends between G_{max} with the stress state of the soils (net confining stress p_n and matric suction ψ) and material properties (void ratio e and over consolidation ratio OCR) were proposed (Cabarkapa et al. 1999; Mancuso et al. 2002; Inci et al. 2003; Kim et al. 2003; Marinho et al. 2005; Mendoza et al. 2005; Vassallo et al. 2007; Sawangsuriya et al. 2009, Ng et al. 2009; Ng et al. 2009). However, in these trends, an empirical manner between the stress state and void ratio is considered. Besides, except for the experimental

studies by Sawangsuriya et al. (2009) and Ng et al. (2009), inter-relationships between G_{max}, S_r and ψ were not investigated. Although these trends may work well for saturated soils (Hardin and Black 1968; Hardin and Black 1969; Hardin and Drnevich 1972; Hardin 1978), it is not likely to work for unsaturated soils, where the behavior may change upon wetting and drying due to hydraulic hysteresis.

4.2 Model Description

Similar to the approach of Hardin (1978), a multiplicative relationship between the relevant variables is used as the starting point to define G_{max} for unsaturated soils, as follows:

$$G_{max} = A\,(OCR)^K\,{P_a}^{1-n}\,{p'}^{n} \qquad (4.1)$$

where A and n are fitting parameters, P_a is the atmospheric pressure used for normalization, OCR is the over-consolidation ratio, p′ is the mean effective stress, and K is referred to as the consistency constant which is sensitive to the plasticity index of the soil. The OCR is defined as:

$$OCR = \frac{{p_0}'}{p'} \qquad (4.2)$$

where p_0′ is the apparent mean preconsolidation stress of the soil specimen and p′ is the current mean effective stress.

The mean effective stress employed in the proposed framework was defined using an approach similar to Wheeler et al. (2003), Tamagnini (2004), and Nuth and Laloui (2008):

$$p' = p_n + S_r\psi \qquad (4.3)$$

where p_n is the net confining stress equal to $(p-u_a)$ and ψ is the matric suction equal to (u_a-u_w). This equation is similar to Bishop's (1959) single value effective stress variable with an effective stress parameter χ equal to S_r. As presented in Appendix A, this definition of effective stress was found acceptable over the initial drying paths of the SWRC for compacted soils. Khalili and Zargarbashi (2010) also showed that using S_r as the effective stress parameter over the initial drying and wetting paths of hysteresis cycle for non-cohesive soils is deemed acceptable.

The concept of the double-hardening mechanism experienced by unsaturated soils during hydro-mechanical hysteresis (Wheeler et al. 2003; Tamagnini 2004) is used in this framework. Based on this concept, hydraulic hysteresis and mechanical behavior of soils are linked in a single framework to describe changes in stiffness of a soil during two coupled physical processes. The first process is the mechanical process of displacement of the soil skeleton under changes of applied effective stresses, with elastic displacements attributed to the elastic deformation of soil particles, and plastic compression related to the slippage between the particles.

Plastic compression, arising from slippage between the particles, causes a new arrangement of the particles with lower void ratio. In this new arrangement, the soil skeleton will experience a hardening process as it shows a more stabilized state against yielding under subsequent loading

and unloading. Employing the extended Cam-Clay model, following expression can be used to describe the evolution of yield function (e.g. hardening) produced by the plastic changes in volume of the soil specimen during isotropic loading (Wheeler et al. 2003, Tamagnini 2004):

$$\frac{dp_0{}'}{p_0{}'} = \frac{(1+e_0)d\varepsilon_v^p}{(\lambda-\kappa)} \tag{4.4}$$

where λ and κ are the slopes of the normal compression curves and the elastic swelling line on the e-lnp´ diagram for saturated soils, respectively [Figure 4.2(a)] and e_o is the initial void ratio of the soil specimen.

The second physical phenomenon is the hydraulic process of water flow during wetting and drying. In this regard, hydraulic hysteresis in the soil water retention curve (SWRC) is modeled as an "elasto-plastic" process with plastic changes in S_r as the soil state is moving along a primary drying curve or primary wetting curve and elastic changes in S_r as long as the soil state remains between the primary drying and primary wetting curves (Wheeler et al. 2003). This process may be clearly explained by tracking changes of air-water interface with matric suction changes (Figure 4.1). As suction increases from zero suction during drying, the air-water interface between the particles moves from position A to B as shown in Figure 4.1. This movement of the interface during drying is modeled as a reversible process and changes in the degree of saturation during this stage are considered as the elastic changes of S_r. However, increasing suction beyond the air entry suction, air will break through into the voids

from position B and will push water to neighboring water-filled voids. The process of air breakthrough into the voids is considered as the irreversible (plastic) process of the SWRC during drying because the voids will not immediately re-flood with water as the suction reduces to a lower value.

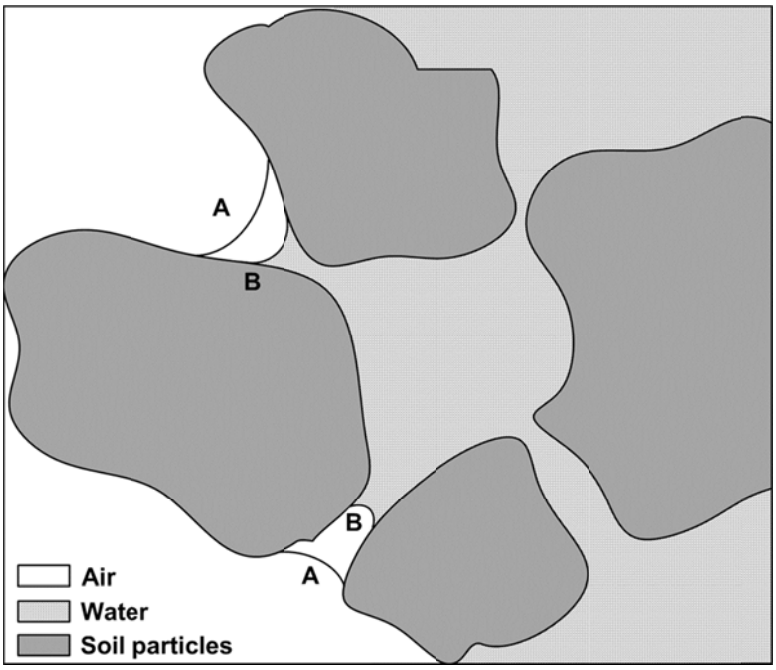

Figure 4.1: Movement of air-water interfaces during the hydraulic hysteresis

In this study, the hysteretic changes in degree of saturation S_r are described using a piece-wise log linear model as shown in Figure 4.2(b). In this model, the primary drying and wetting curves (i.e., when the soil is undergoing rapid changes in S_r beyond the air entry suction and during water re-entry after drying to water occlusion conditions) have gradients of λ_s and elastic paths including parts of the SWRC before reaching the air entry suction or after wetting up to the water-entry suction have a gradient of κ_s.

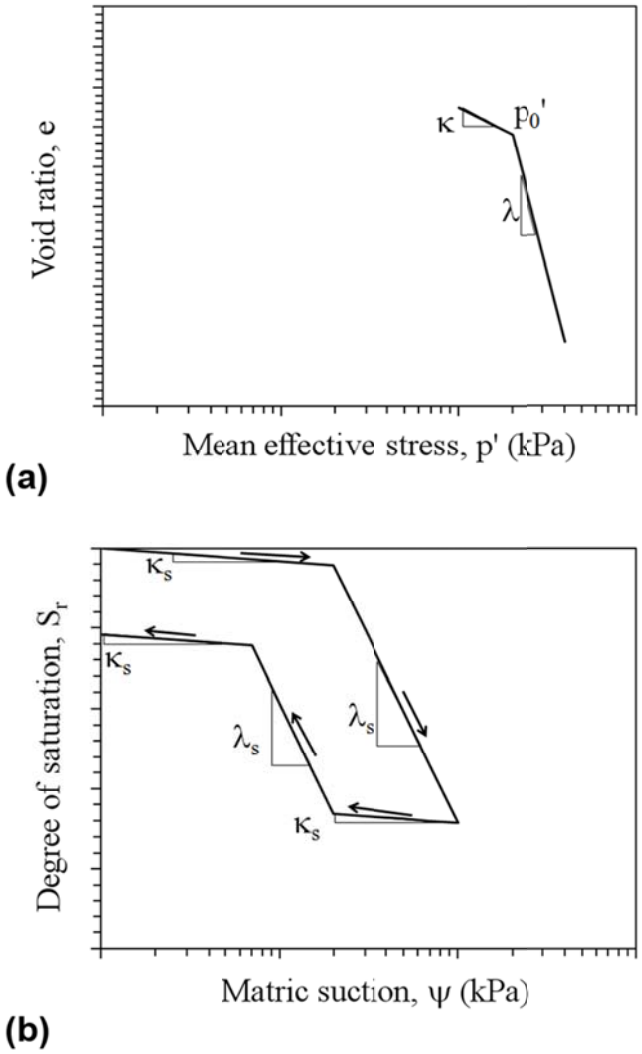

Figure 4.2: Models for (a) The void ratio and (b) The SWRC

Based on the SWRC model, changes in the degree of saturation in the "elastic" portions of the SWRC, dS_r^e are defined as:

$$dS_r^e = -\kappa_s \frac{d\psi}{\psi} \tag{4.5}$$

where κ_s is an elastic constant representing the slope of the elastic paths of the SWRC. Plastic changes of S_r, dS_r^p, are given by:

$$dS_r^p = -(\lambda_s - \kappa_s) \frac{d\psi}{\psi} \tag{4.6}$$

where λ_s is the slope of the plastic portions of the SWRC. This type of elasto-plastic modeling of the SWRC was suggested previously by Dangla et al. (1997) and Wheeler et al. (2003). The main difference between the SWRC defined by Wheeler et al. (2003) and that used in this study is that the piece-wise log-linear curves are arranged to consider the effect of entrapped air on the shape of the wetting SWRC (i.e., the wetting SWRC does not return to $S_r = 1$). Strict evaluation of the SWRC model indicates that it is incorrect as S_r changes before reaching the air entry suction. However, this gradual decrease in S_r represents the gradual entry of air into pores with different sizes on the air-water interface at the border of the soil specimen. The piece-wise log-linear model has been observed to fit the experimental SWRCs of different soils. However, if this feature is not desired in an analysis, a very small value of κ_s can be used to define the SWRC.

During plastic changes of S_r during drying or wetting of the soil, Wheeler et al. (2003) proposed that there is a difference in the distribution and quantity of water menisci throughout the soil, and consequently in the magnitude of interparticle contact stresses and thus the mechanical properties of the soil. Based on the definition of the SWRC shown in Figure 4.2(a), Wheeler et al. (2003) proposed the following expression to describe the evolution of the yield surface (i.e., hardening) produced by "plastic" changes in S_r:

$$\frac{dp_0{}'}{p_0{}'} = -b\frac{dS_r^p}{(\lambda_s - \kappa_s)} \tag{4.7}$$

where b is a constitutive constant referred to as the double-hardening constant controlling the rate of changes in hardening of the soil caused by changes in S_r.

Combining Eq. (4.7) with Eq. (4.4) gives the general equation that represents the movement of the yield surface under the hydro-mechanical loading, as follows:

$$\frac{dp_0{}'}{p_0{}'} = -b\frac{dS_r^p}{(\lambda_s - \kappa_s)} + \frac{(1+e_0)d\varepsilon_v^p}{\lambda - \kappa} \tag{4.8}$$

Integration of Eq. (4.8) leads to following expression for p_0':

$$\int_{p_0{}'_m}^{p_0{}'_{m+1}} dp_0{}' = \int_{\Delta S_r^p, \Delta e^p} p_0' \left(-b\frac{dS_r^p}{(\lambda_s - \kappa_s)} - \frac{de^p}{\lambda - \kappa}\right) \rightarrow$$

$$p_0{}'_{m+1} = p_0{}'_m exp(-b\frac{\Delta S_r^p}{\lambda_s - \kappa_s} - \frac{\Delta e^p}{\lambda - \kappa}) \tag{4.9}$$

where the subscripts m and m+1 denote the old and new values of p_o' after a change in S_r or e. Substituting Eq. (4.9) into Eq. (4.2) permits definition of changes in the OCR during changes in S_r or e, as follows:

$$(OCR)_{m+1} = \frac{p_0{}'_m}{p'_{m+1}} exp\left(-b\frac{\Delta S_r^p}{\lambda_s - \kappa_s} - (1+e_0)\frac{\Delta \varepsilon_v^p}{\lambda - \kappa}\right) \tag{4.10}$$

where p'_{m+1} is the $(m+1)^{th}$ term of mean effective stress, which changes with S_r. Assuming negligible changes in e during changes in S_r, Eq. (4.10) can be split in two terms, as follows:

$$OCR_{m+1} = \frac{p_0{}'_{sat}}{p_n} exp\left((1+e_0)\frac{\Delta \varepsilon_v^p}{\lambda - \kappa}\right) + \frac{p_n p_0{}'_m}{p_0{}'_{sat} p'_{m+1}} exp\left(-b\frac{\Delta S_r^p}{\lambda_s - \kappa_s}\right) \tag{4.11}$$

where the first term represents changes in OCR due to changes in e during mechanical loading, while the second term represents changes in OCR due to changes in S_r. During changes in S_r, the terms $p_o'_{sat}$, which represents the mean consolidation pressure due to mechanical loading of saturated soil, and p_n, the net normal stress, are assumed constant. Substituting Eq. (4.11) into Eq. (4.1), the new value of G_{max} after a change in S_r or e can be obtained as follows:

$$(G_{max})_{m+1} = A\left(\frac{{p_0}'_{sat}}{p_n} exp\left((1+e_0)\frac{\Delta\varepsilon_v^p}{\lambda-\kappa}\right)\right)^K$$

$$\left(\frac{{p_0}'_m p_n}{{p_0}'_{sat} {p'}_{m+1}} exp\left(-b\frac{\Delta S_r^p}{\lambda_s-\kappa_s}\right)\right)^{K'} {P_a}^{1-n} {p'}^n_{m+1} \qquad (4.12)$$

where K′ and K are the parameters to control the rate of changes in G_{max} with hardening due to changes in S_r and e, respectively.

The parameters required to solve the evolution of Gmax during hysteretic hydro-mechanical loading include those from elasto-plastic compression curve (κ, λ), the SWRC (κ_s, λ_s), the coupling parameter (b), hardening parameters (K and K′), and empirically fitting parameters specific to a given soil (A, n). The value of K for a given soil is typically defined using guidance from Hardin (1978) and the fitting parameters, A and n, are determined from fitting a curve to G_{max} data at zero matric suction (saturation condition) under different net confining stresses. In the definition of G_{max} in Eq. (4.12), it is assumed that there is a negligible

change in void ratio during S_r changes. Therefore, the proposed model is only suitable to represent the behavior of non-expansive or non-collapsible soils.

4.3 Parametric Evaluation of the Model

A parametric evaluation was performed in order to demonstrate the capabilities of the model during hydraulic hysteresis. The evaluation considers the following initial values of the state variables: p_n = 100 kPa, ψ = 0 kPa, e = 0.6 and S_r = 1, p' = 100 kPa and p_o' = 200 kPa. Based on the initial p_o' and the initial stress state conditions, this hypothetical soil is considered over-consolidated. During the initial drying process from points A to B along the SWRC in Figure 4.2(a) (i.e., before the air entry suction), a small change in S_r is predicted by the model.

During this stage, p_o' predicted using Eq. (4.9) remains constant [Figure 4.3(b)] and p' defined using Eq. (4.3) increases slightly [Figure 4.3(c)]. These changes lead to a small increase in G_{max} as the suction changes from A to B [Figures 4.4(b) and 4.4(c)]. In this stage, both mechanical and hydraulic behaviors could be considered elastic as described by Wheeler et al. (2003). After reaching the air entry suction at point B (plastic regime), S_r decreases at a faster rate with increasing suction from B to C.

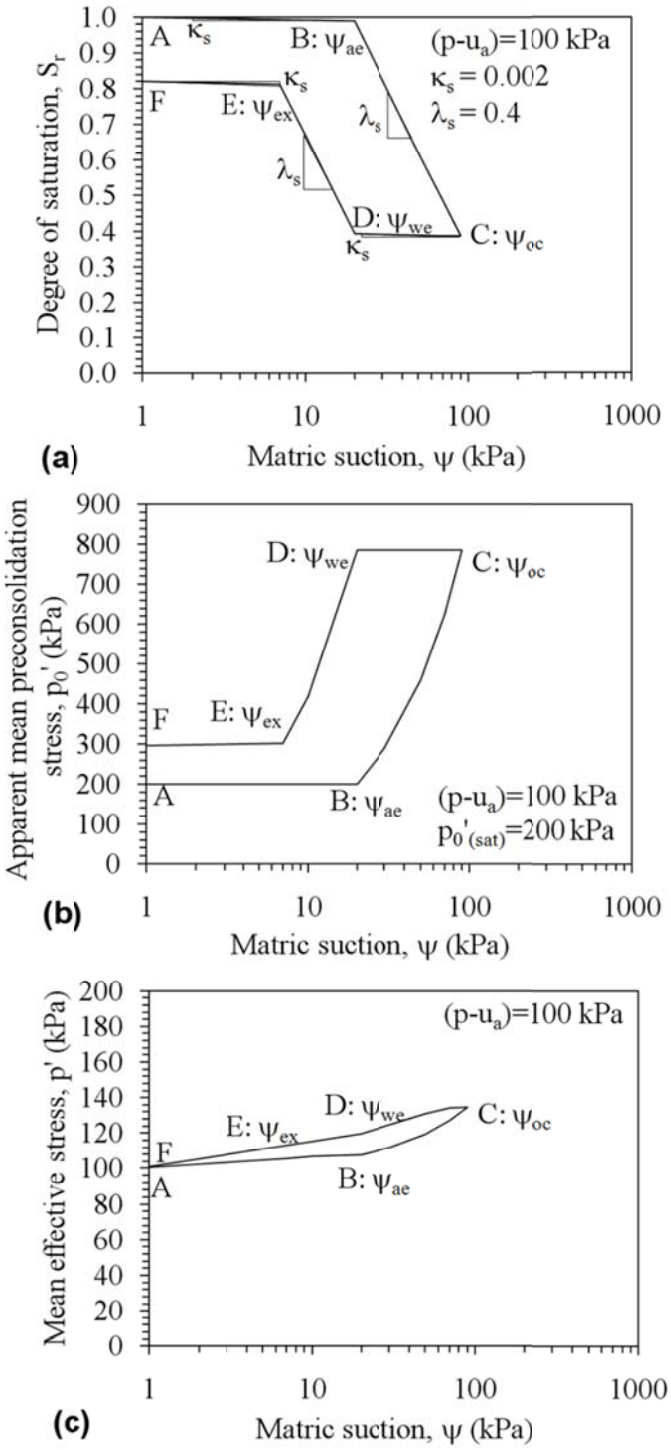

Figure 4.3: Transition points in the key relationships in the elasto-plastic model for Gmax during hydraulic hysteresis: (a) SWRC; (b) Suction-hardening relationship (p_0´ vs. ψ); (c) Effective-stress suction relationship (p´ vs. ψ)

During movement along this portion of the curve, both p_o' [Figure 4.3(b)] and p' [Figure 4.3(c)] experience a considerable increase with ψ. Accordingly, G_{max} increases at a greater rate with ψ before tending toward a threshold value as water begins to become occluded [Figures 4.4(b) and 4.4(c)]. The wetting process from a suction of 100 to 1 kPa is shown as path C-D-E-F in Figure 4.3(a). During the decrease in suction from C to D, only a small change in S_r is observed and p_o' remains with no change. In this stage, the most significant change would be the considerable reduction in p', which results in a slight reduction in G_{max} from C to D. At point D, water will start breaking through the middle-size voids of compacted soils, resulting in a plastic increase in S_r. After this point, p_o' decreases linearly with a slope of b due to changes in S_r while p' is still decreasing as the suction decreases from D to E. This causes a sharp decrease in G_{max}. Point E is considered as the air expulsion suction defined as the point of separation between the saturated and unsaturated conditions during wetting of SWRC. After this point, only small changes in S_r are observed and G_{max} will follow the same slope as observed in path A-B. The influence of the hardening parameter K' and the coupling parameter b on G_{max} during drying and wetting are shown in Figures 4.5(a) and 4.5(b) respectively. In all of the curves, G_{max} has a greater magnitude upon wetting than it does during drying, following a similar trend to that noted in p_o' curve shown in Figure 4.3(b).

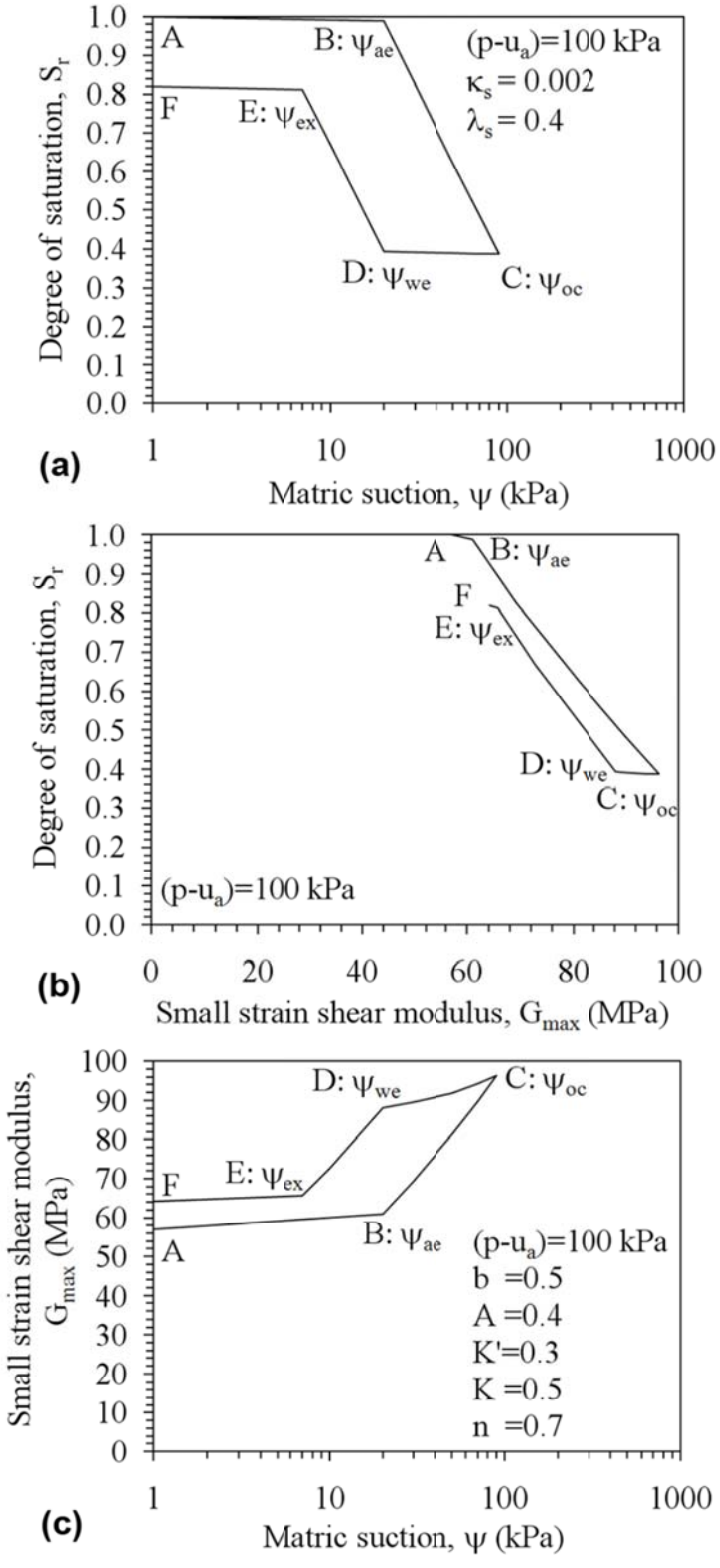

Figure 4.4: Model predictions showing key transition points: (a) SWRC; (b) G_{max} vs. S_r; (c) Gmax vs. ψ

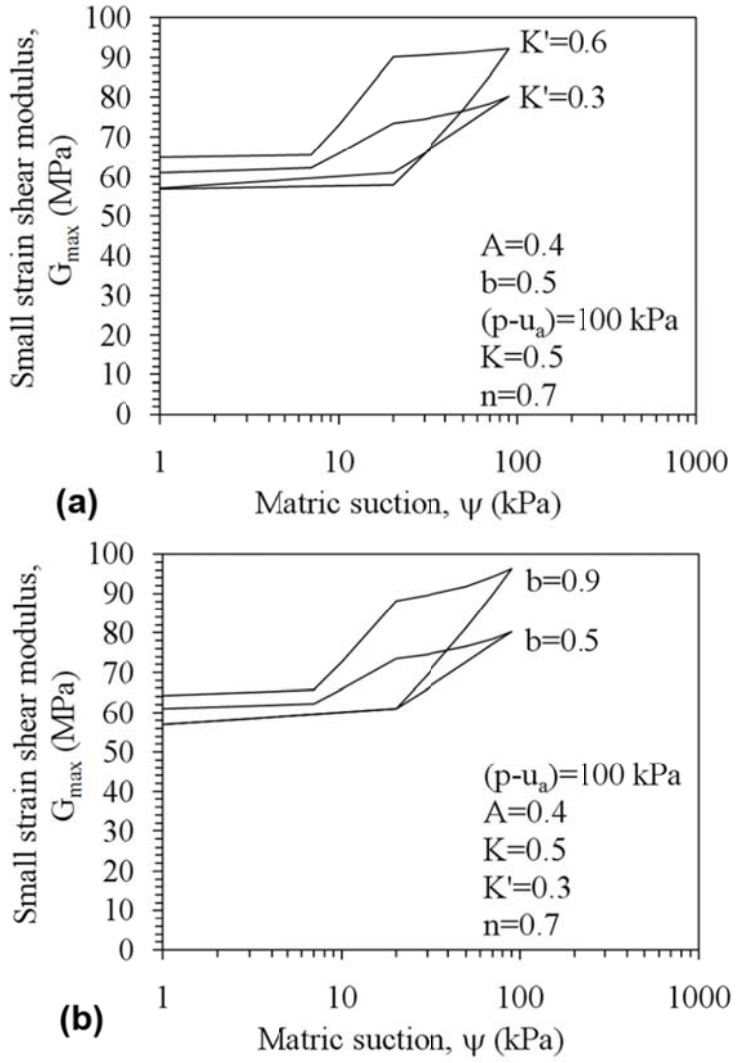

Figure 4.5: Parametric evaluation of the elasto-plastic model showing the impact of hardening parameters on G_{max} during drying and wetting: (a) Effects of hardening parameter K´ on G_{max}; and (b) Effects of double hardening parameter b on G_{max}

Greater values of the hardening parameter K´ lead to an upward shift in the magnitude of G_{max}, as well as a slightly flatter shape of the wetting portion of the loop. A slight upward trend in G_{max} is noted in the drying path before reaching the air entry suction for lower values of K´. Greater values of the double-hardening parameter b lead to a steeper increase in

G_{max} on the drying path after reaching the air entry suction (path B-C). The results of the parametric evaluation indicate that p´ and S_r have the most significant impact on G_{max} for a constant value of p_n. This effect is especially significant during the wetting process of SWRC. As the change of S_r during wetting is less than that during drying, G_{max} during wetting is larger than that during drying.

4.4 Verification of the Model with G_{max} data from the Literature

Results from unsaturated small strain shear modulus tests reported in the literature may be used to validate the proposed model. Figures 4.6 to 4.8 present experimental small strain shear modulus data in the space of matric suction and degree of saturation for SW (Kim et al. 2003), SC, ML and CH (Sawangsuriya et al. 2009) and ML (Ng et al. 2009) at matric suction ranging from 0 (saturated) up to 1000 kPa. In this study, the initial p_o´ was assumed for the materials and the SWRC parameters (λ_s, κ_s) were defined using the SWRC data reported in literature as shown in Figures 4.6(a), 4.7(a) and 4.8(a). The parameters A, n, K, K´ and b were found by fitting the best-fitted curves to the measured G_{max} data (Table 4.1).

As it is observed in all cases, the trend between G_{max} and ψ during drying was observed to have three distinct zones. The first zone, a slight increase in G_{max} with ψ was noted as the suction changed from zero to the air entry suction. A greater increase in G_{max} was observed for values of ψ

greater than the air-entry suction, after which G_{max} approached an asymptotic value as the water occlusion condition was reached.

Table 4.1: Material properties of the soils used for analysis

Researcher	Sawangsuriya et al. (2009)			Kim et al. (2003)	Ng and Yung (2009)	
Material	ML	CH	SC	SW	ML	
K	0.3	0.6	0.6	0.33	0.1	0.1
K'	0.4	0.2	0.8	0.2	0.45	0.45
b	0.5	0.8	0.4	2	0.55	0.55
λ_s	0.14	0.12	0.18	0.12	0.35	0.35
κ_s	0.01	0.001	0.001	0.002	0.001	0.001
p_0'	300	400	100	300	400	400
ψ_e	10	200	60	10	45	45
p_{net}	34.5	34.5	34.5	41	110	300
n	0.6	0.7	0.8	0.6	0.8	0.8
A	0.5	0.1	0.5	0.62	0.65	0.65

Upon wetting, a hysteretic behavior was noted in G_{max}. For the same values of suction, the G_{max} values of wetting path of the SWRC were consistently higher than those obtained during drying. During wetting, a small reduction in the G_{max} with decreasing ψ was observed. A greater reduction in G_{max} was noted for lower suctions during wetting, where a greater amount of water was absorbed by the specimen. The model was then compared against the trends in G_{max} with S_r [Figures 4.6(b), 4.7(b) and 4.8(b)]. The data in these figures indicate that the model shows a good fit with the data for the particular fitting values shown in Figures 4.6 to 4.8.

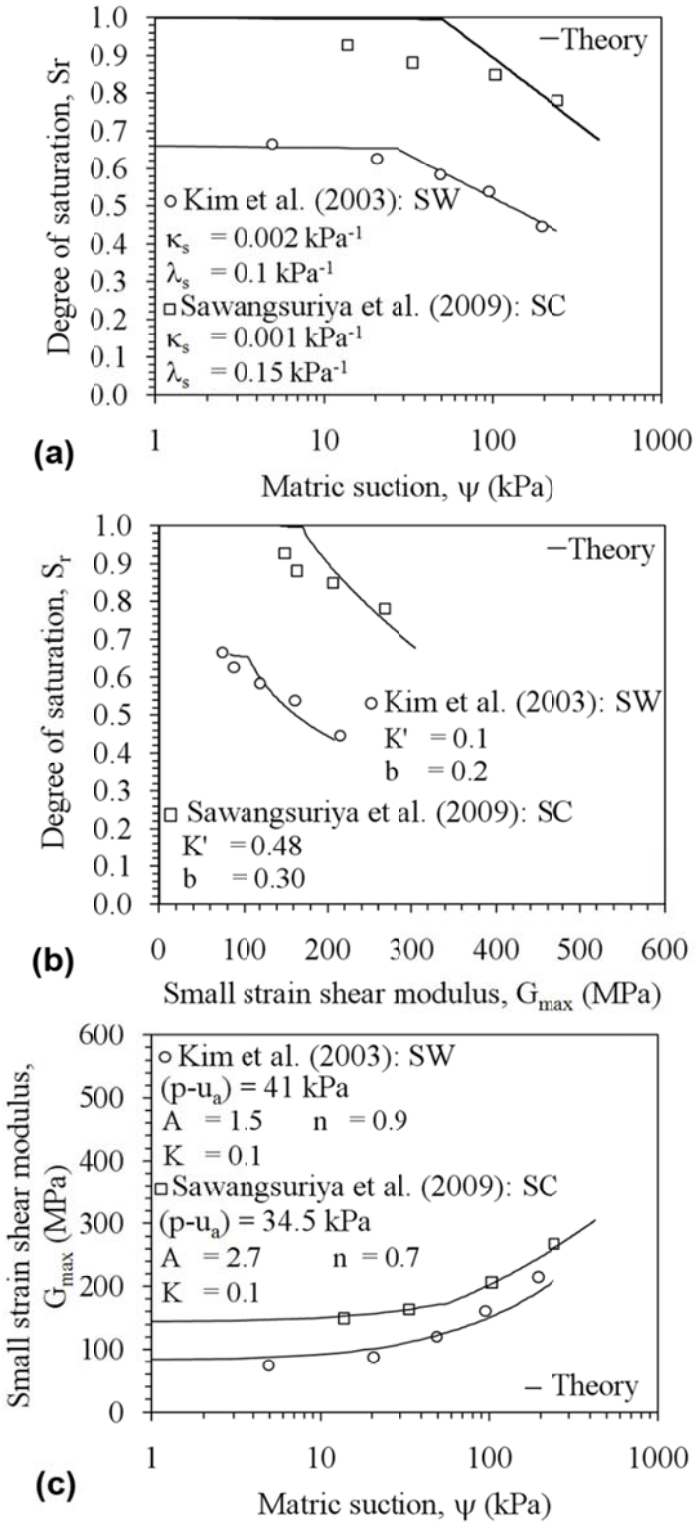

Figure 4.6: Fitted model relationships to sand data (Kim et al. 2003; Sawangsuriya et al. 2009): (a) The SWRC of the soils; (b) Variation in G_{max} with S_r; and (c) Variation in G_{max} with ψ

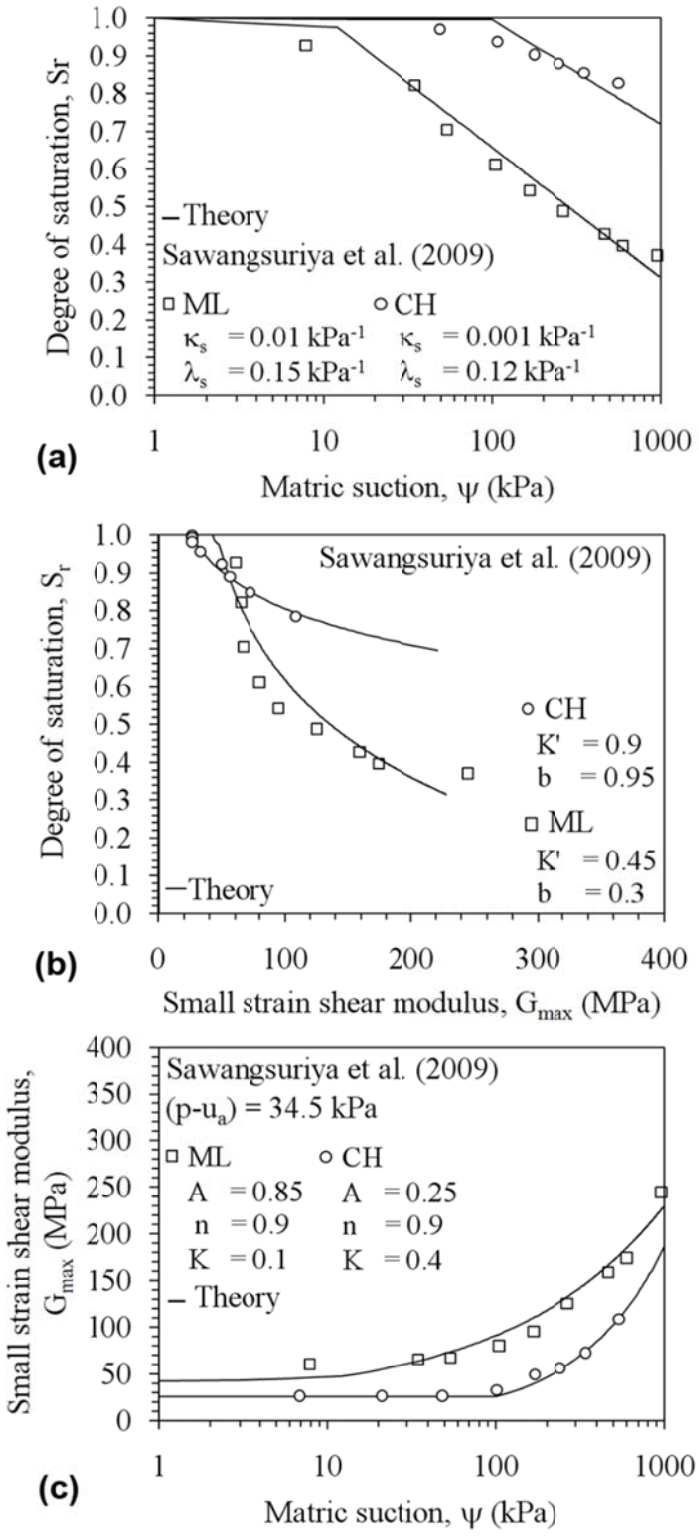

Figure 4.7: Fitted model relationships to clay and silt data (Sawangsuriya et al. 2009): (a) The SWRC of the soils; (b) Variation in G_{max} with S_r; and (c) Variation in G_{max} with ψ

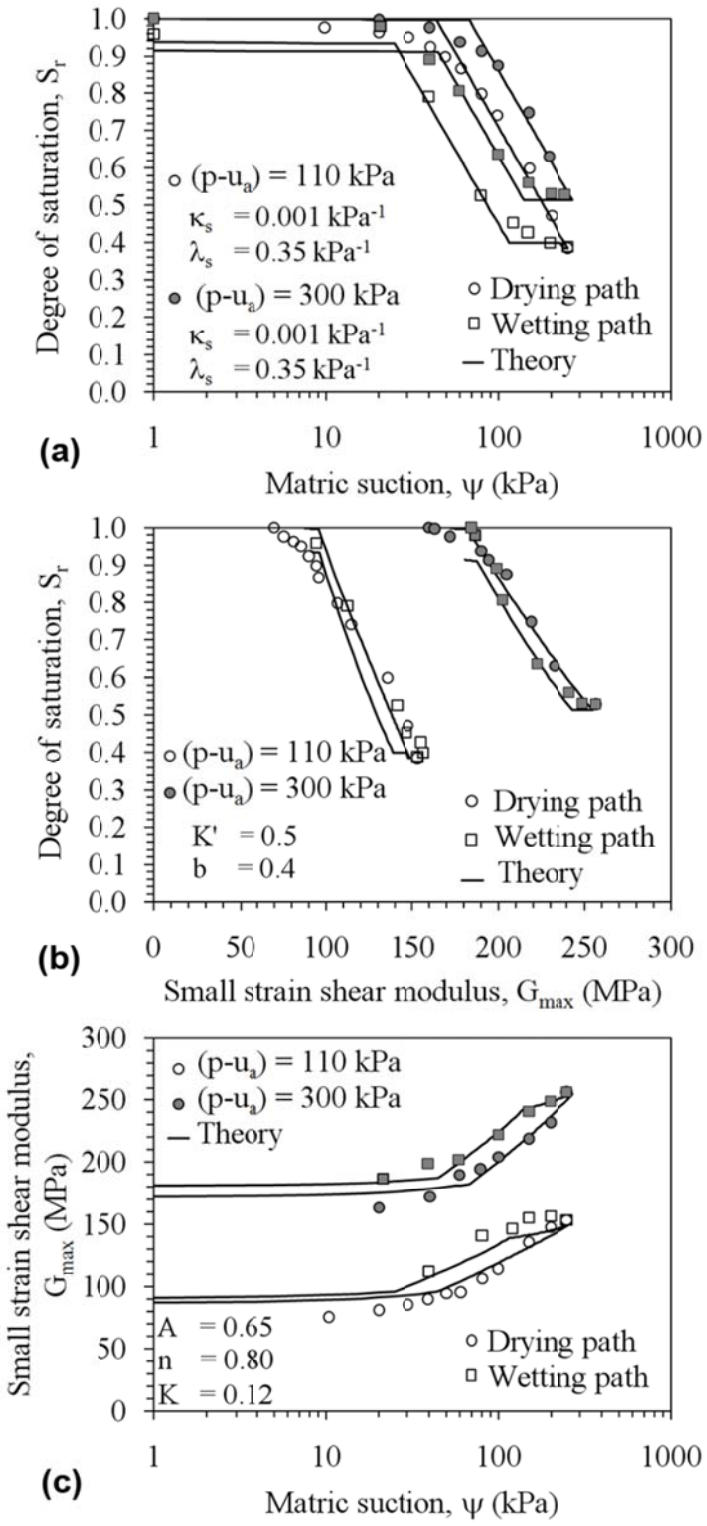

Figure 4.8: Fitted model relationships to silt data (Ng et al. 2009): (a) The SWRC of the soils; (b) Variation in G_{max} with S_r; and (c) Variation in G_{max} with ψ

CHAPTER V

Experimental Measurement of the Small Strain Shear Modulus of Unsaturated Soils

5.1 Introduction

This chapter describes the details and typical results from a test method to measure the path-dependent changes in G_{max} during hydraulic hysteresis. Specifically, the axis translation technique for suction control, a flow pump for degree of saturation control, and a vertically-oriented proximeter to infer changes in void ratio are incorporated into a fixed-free resonant column setup. A flow pump is essentially a syringe which can be moved to impose water flow rates on a specimen, and was originally used in permeameter tests to measure the hydraulic conductivity of saturated clays (Olsen 1966). The waterflow rate is later used to determine the volume of water inserted into or extracted from the specimen and consequently the water content of the soil during the matric suction changes. Flow pumps have been used to impose transient water flow processes on unsaturated soils in order to infer the soil-water retention

curve (SWRC; also referred as the soil-water characteristic curve, SWCC) and hydraulic conductivity of unsaturated soils using inverse analyses (Znidarcic et al. 1991, Abu-Hejleh et al. 1993; Bicalho et al. 2000; Znidarcic et al. 2002). However, because G_{max} is particularly sensitive to degree of saturation and matric suction, transient flow is not appropriate as part of a measurement program for G_{max} for unsaturated soils. Accordingly, the flow pump is operated with suction feedback measurements to reach equilibrium conditions for G_{max} measurement.

5.2 Sample Preparation

To prepare the soil specimen, Bonny silt was first mixed at a gravimetric water content of 14% (the optimum water content corresponding to standard Proctor compaction conditions) and placed in a sealed plastic bag for 24 hours for the water content to homogenize. Static compaction (i.e., compression under a static load) was then used to form soil specimen with different void ratios. Compaction was performed in three 23.7 mm-thick lifts in a 35.6 mm diameter split mold. The static compaction approach was observed to lead to uniform specimen density and repeatable conditions. The interfaces between the layers were scarified to minimize formation of weak zones in the compacted soil specimen.

5.3 Experimental Setup

The Overall shape of the system is presented in Figure 5.1. Following, different components of the setup are explained in detail.

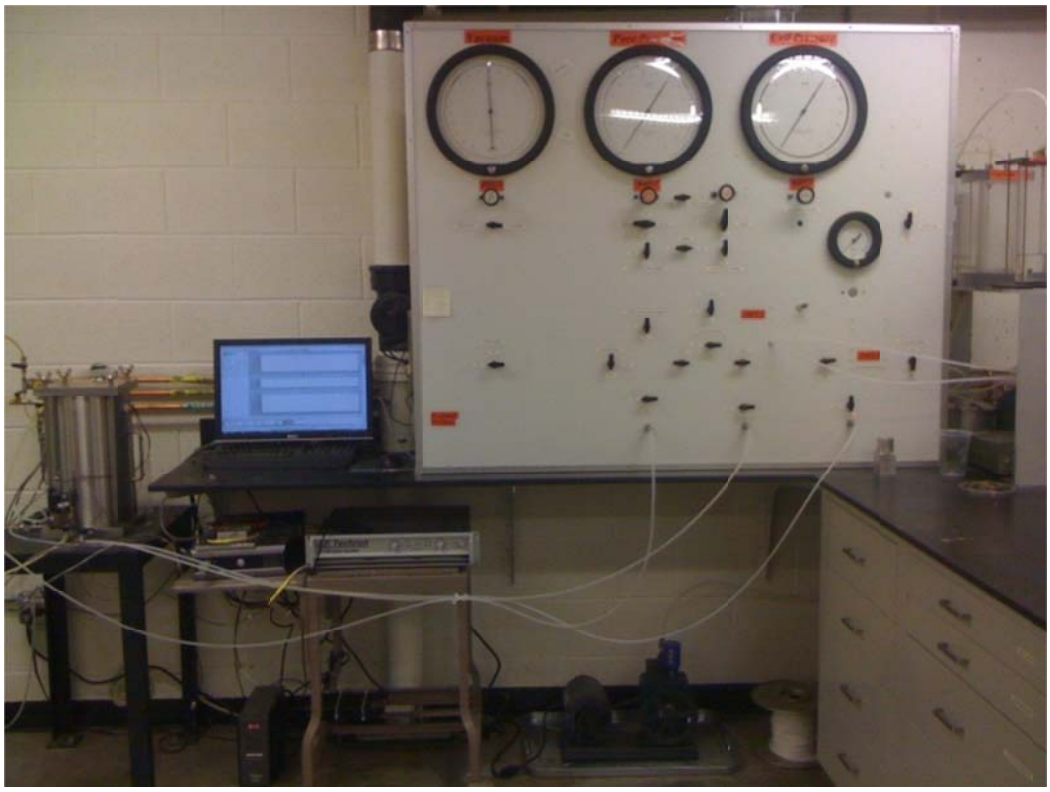

Figure 5.1: The overall shape of the system used in this study

5.3.1 Resonant Column Device

The fixed-free Stokoe-type resonant column device modified with suction-saturation control is shown in Figure 5.2. The basic operational principle in the resonant column test is vibration of a cylindrical specimen in the first-mode torsional resonance. This type of system has been used to determine the shear modulus at small strain since the 1960's (Hall and Richart 1963; Hardin and Black 1968, 1969; Stokoe et al. 1999).

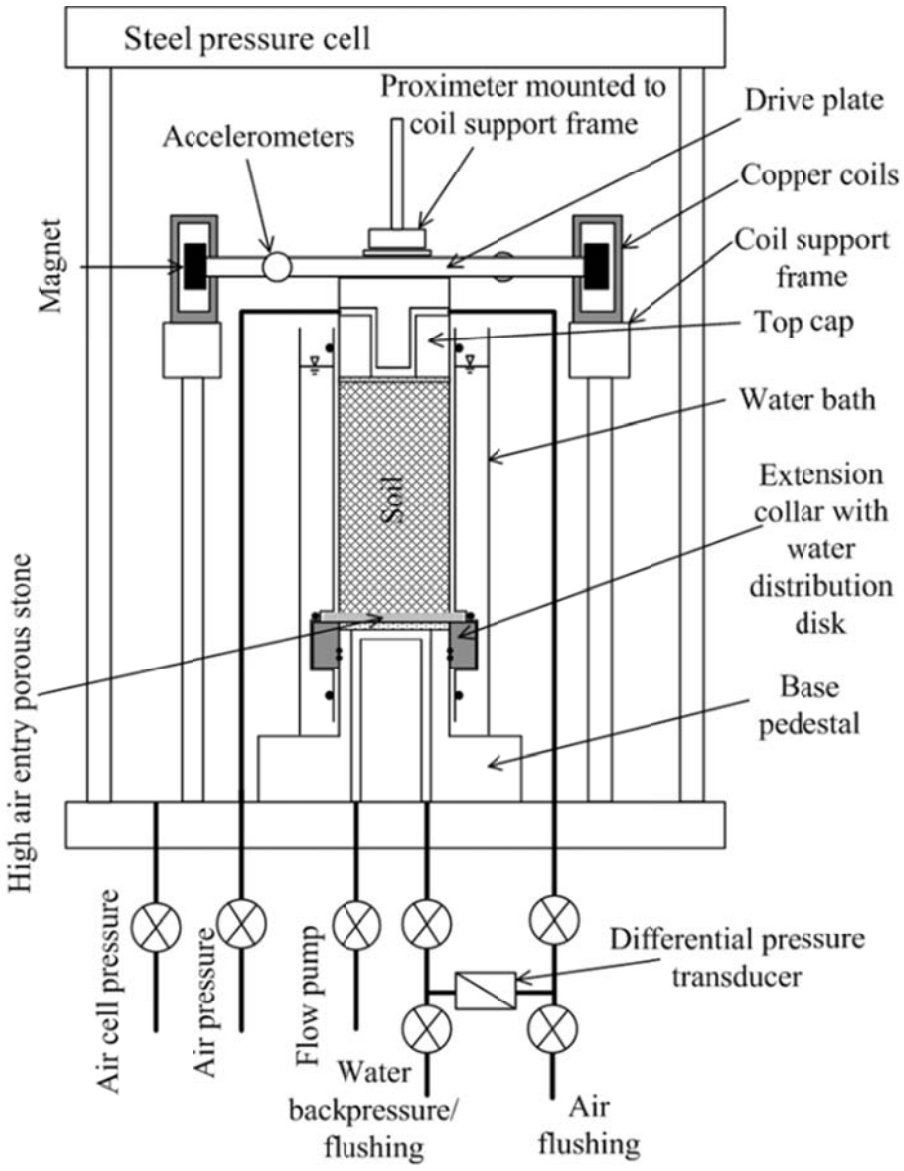

Figure 5.2: Schematic of the resonant column device adapted for suction control using the axis translation technique

In the resonant column device, the cylindrical soil specimen having a diameter of 35.6 mm and height of 71.1 mm is placed atop a high air-entry ceramic disk with an air entry suction value of 100 kPa mounted atop the bottom pedestal of the resonant column test setup. Tests were performed by the authors using ceramic disks with higher air entry suction values of

300 and 500 kPa, but because the point of water occlusion in the silt was observed to be less than 100 kPa the ceramic disk with a lower air entry suction was used. The disk with lower air entry suction has the advantage of a higher hydraulic conductivity, so equilibration of water pressures across the ceramic disk is faster. Different from other axis translation setups where the ceramic disk is affixed with epoxy to the bottom pedestal, the ceramic disk has a greater diameter than the specimen (40 mm), and is placed directly atop a modified extension collar on the bottom platen (Figure 5.3).

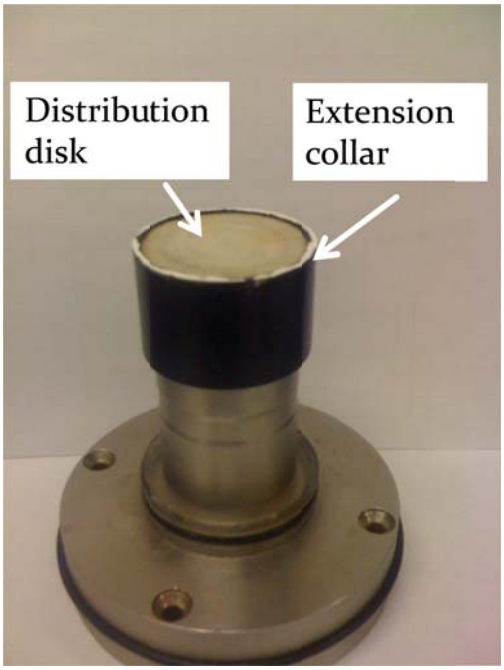

Figure 5.3: Details of the modified extension collar

A latex membrane is placed around the specimen, ceramic disk, and extension collar. Under application of a confining pressure, the latex membrane is used to provide the hydraulic seal that prevents air from

short-circuiting past the high air entry ceramic, and a fixed bottom boundary condition during resonant column testing.

For additional security under low confining pressures, an "O"-ring was placed around the latex membrane on the ceramic disk. Although the slight stretch in the latex membrane may produce a stress concentration at the bottom of the specimen, this approach was observed to show consistent resonant frequency results even under relatively low confining pressures.

A high permeability water distribution disk is placed within the extension collar beneath the ceramic disk to ensure a uniform distribution of water across the ceramic disk and to prevent stress concentrations which may cause the ceramic to crack. A water bath surrounding the specimen within the resonant column chamber is used minimize diffusion of air from the cell through the membrane and into the specimen during long-term tests. Flexible 3.175 mm Tygon® tubing with Swagelok® connectors were used to connect the backpressure air/water supply lines to the top cap of the specimen in order to minimize interference with measurement of the resonant frequency of the soil specimen. Similar resonant frequency measurements were obtained in tests with and without the tubing connected to the top cap.

5.3.2 Dynamic Loading System

Torsional vibration of the cylindrical soil specimen was used in the fixed-free resonant column test to identify the first-mode of resonance. Specifically, a torsional force is applied through a non-contact electromagnetic drive plate resting on top of the specimen. The drive plate consists of a cross-shaped disk with four rectangular permanent magnets mounted at the end of each arm of the cross. A pair of copper coils having opposing polarities is mounted to a separate pedestal, with a coil surrounding each end of the rectangular magnets. Application of an electrical current through the coils generates a magnetic field which imposes a force on the magnet, inducing a torque on the specimen through the drive plate.

A swept sine signal with constant amplitude is supplied to the copper coils using a Quattro® dynamic signal analyzer from DataPhysics. The Quattro dynamic signal generator provides over 120 dB dynamic range with up to 40 kHz real-time rate and facilitates high-resolution measurements to 25,600 lines. The range of frequency provided by this system is significantly larger than the range that is needed for the resonant column test (A frequency range up to 1 kHz). This signal analyzer is capable of both dynamic signal analysis and signal generation.

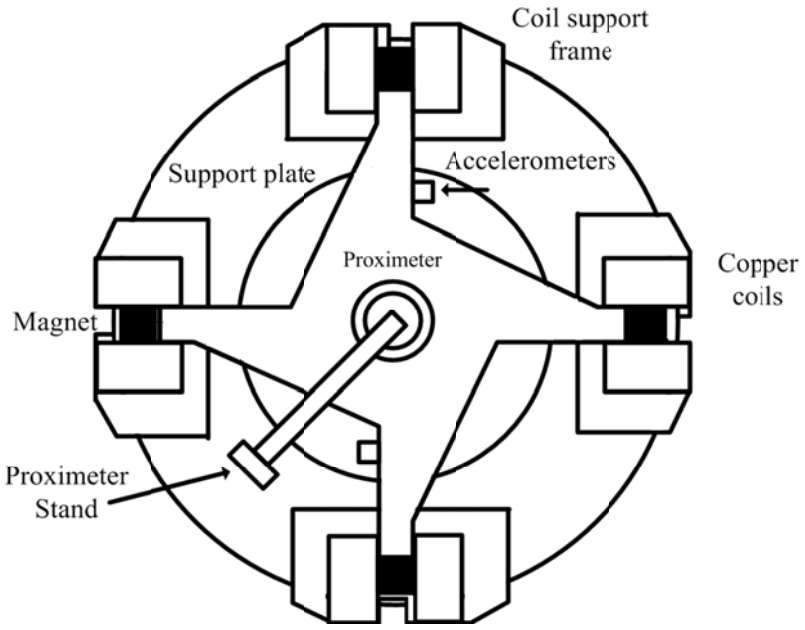

Figure 5.4: Schematic of the non-contact electromagnetic drive plate resting on top of the specimen

Figure 5.5: The Quattro dynamic signal analyzer

The output channel from the signal analyzer was connected to a Techron power amplifier (Model LVC608) to amplify the voltage supplied

to the copper coils. The frequency of the imposed current was swept to identify the angular frequency at which the specimen reaches resonance. The angular frequency response is measured using a pair of PCB Piezotronics miniature ceramic shear ICP accelerometers (Model 352C67) connected to the drive plate which is mounted on top of the specimen.

This shear mode accelerometer is characterized by having a seismic mass mounted on the side of a piezoelectric material. Application of acceleration to the mass causes a shear stress on the face of the crystal and, consequently, a proportional electric signal. This signal generated is very small but is then amplified by the internal signal conditioning of the ICP, or "Integrated Circuit - Piezoelectric," after which it becomes an actual usable signal. This particular model of accelerometer has fixed voltage sensitivity, a force measurement range up to 50g peak, and a frequency range from 0.5 to 10,000 Hz, which made them a suitable choice for this particular application. In addition, they are small and lightweight so any mass loading effect on the test article is negligible.

Using the measured resonant frequency, the shear wave velocity of the soil specimen V_s is calculated for fixed-free boundary conditions as follows (Richart et al. 1970):

$$\frac{I}{I_0} = \left(\frac{\omega_r L}{V_s}\right) \tan\left(\frac{\omega_r L}{V_s}\right) \qquad (5.2)$$

where I is the polar mass moment of inertia of the specimen, I_0 is the polar mass moment of inertia of top cap and drive plate, L is the length of the

sample, and ω_r is the resonant frequency of the specimen obtained from the frequency curve. G_{max} can be calculated from V_s as follows:

$$G_{max} = \rho V_s^2 \quad (5.3)$$

where ρ is the mass density of the soil specimen.

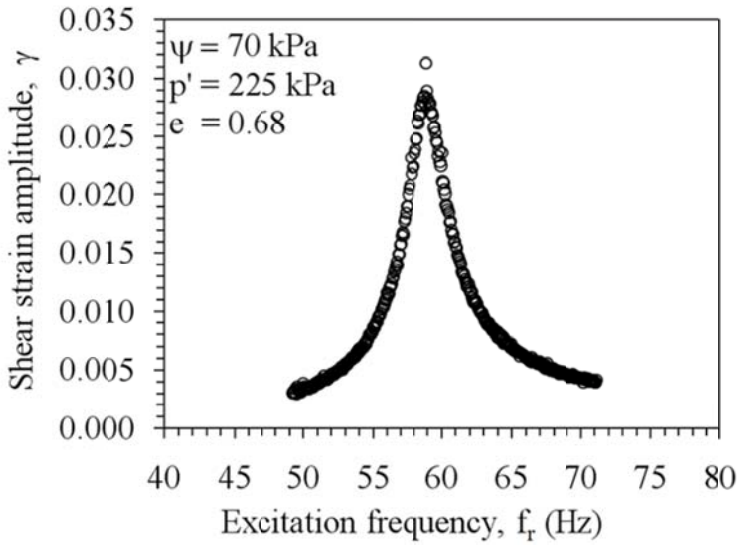

Figure 5.6: Typical Frequency curve obtained from the RC test

5.3.3 Volume Change Measuring System

A non-contact proximity sensor manufactured by the Bentley-Nevada Corp is used to measure the changes in height of the specimen, as a means of estimating the volumetric strain during isotropic loading.

The proximeter has a 2 mm range and is mounted vertically on top of the drive plate as shown in Figure 5.7. The proximeter uses the induction to determine the distance between a conductive target mounted to the top of the drive cap and a coil embedded in the tip of the measuring probe. The coil is oscillated at a high frequency by the proximitor detector-driver unit. A change in the gap width between the coil and the target will

produce perturbation in magnetic field of the coil resulting in a change in the DC output voltage of the driver unit.

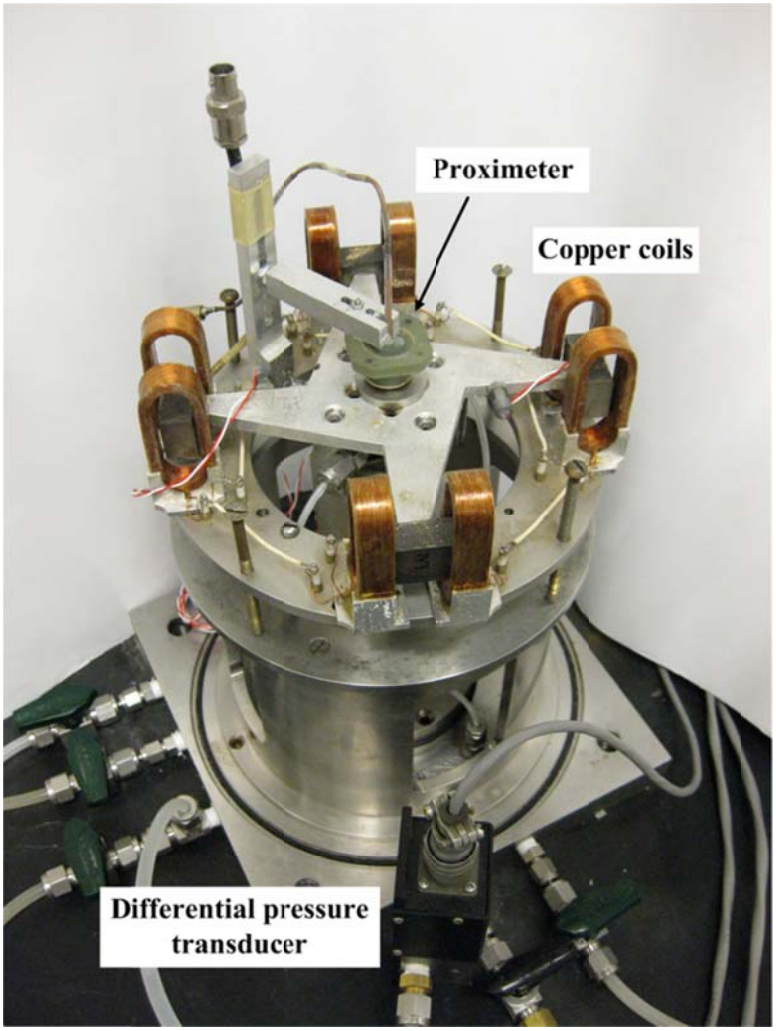

Figure 5.7: Picture of the resonant column device highlighting the mounting of the proximeter

5.3.4 Hydraulic Control System

The degree of saturation of the soil specimen is controlled using a flow pump system constructed as part of this study (5.8). The flow pump operates by moving a precisely machined circular piston having a cross-sectional area of 792 mm^2 into or out of a rigid steel water reservoir. An

"O"-ring bushing is used to provide a pressure seal between the circular piston and the water reservoir. A stepper motor is used to move the piston by turning a fixed threaded rod into the piston whose alignment is maintained using a pair of low friction guide bearings. The stepper motor records the rotational position of the threaded rod, permitting accurate measurement of the flow volume into or out of the specimen. The flow pump is capable of moving at velocities ranging from 5 to 0.00001 mm/s, which correspond to the flow rates ranging from 3.96×10^{-6} to 7.92×10^{-12} m^3/s. The flow pump is connected to the bottom platen of the resonant column device as shown in Figure 5.8(b). Operation of the pump will cause water to flow out or into the soil specimen through the ceramic disk.

During testing, the port connecting the bottom of the specimen to the back-pressure reservoir is closed, which means that pump operation will lead to a change in the water pressure at the bottom of the specimen. The difference between the water pressure at the base of the specimen and the air pressure applied to the top of the specimen is measured using a Validyne® wet-wet differential pressure transducer. Accordingly, the differential pressure transducer is used to monitor the matric suction at the bottom boundary of the specimen. The differential pressure transducer is incorporated into a suction-feedback control loop used by McCartney and Znidarcic (2010) to reach different equilibrium values of suction and degree of saturation in the soil specimen.

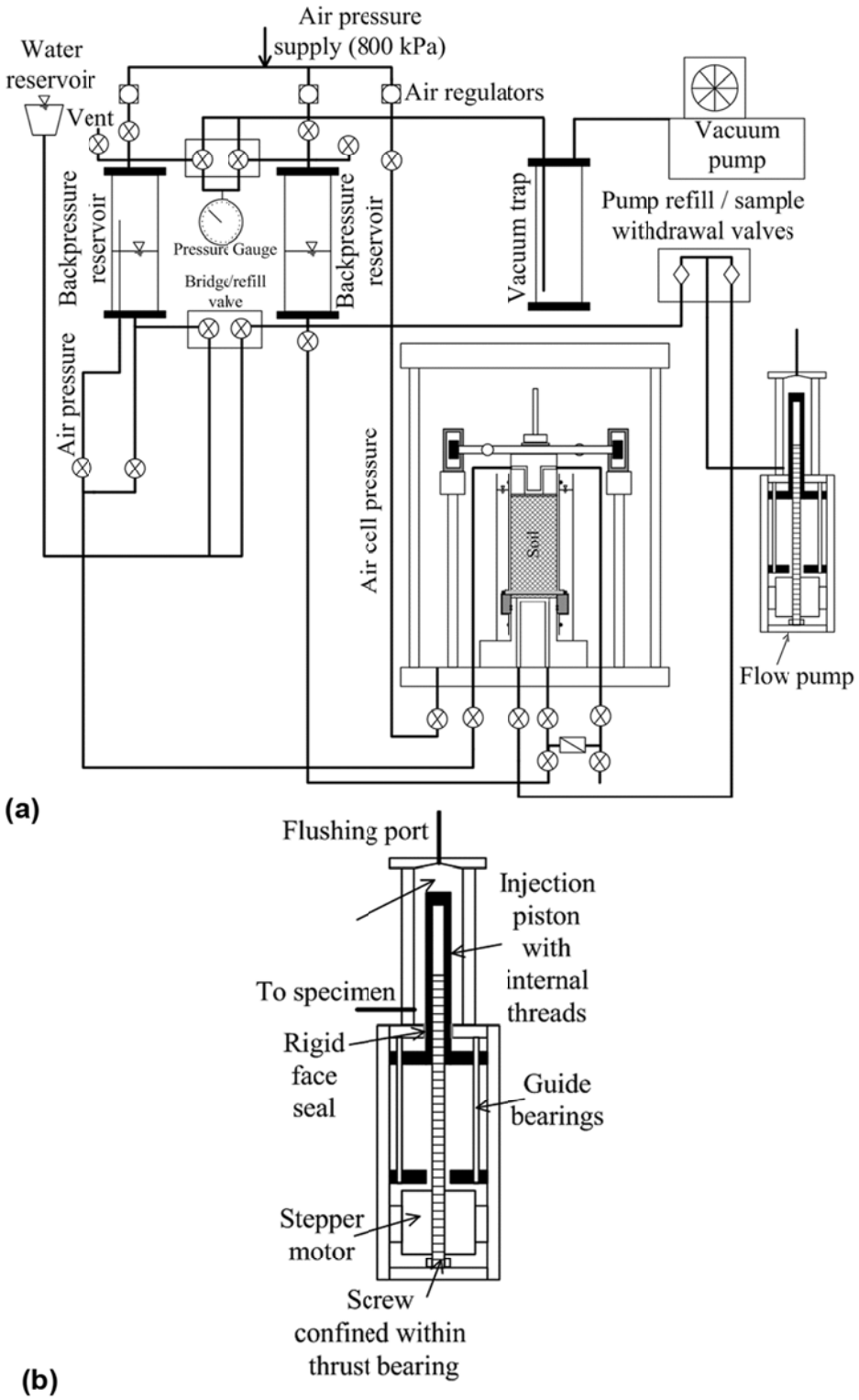

Figure 5.8: (a) Schematic of the hydraulic control system (b) The flow pump for degree of saturation control

As suction imposed by flow pump operation is only representative of the suction at the boundary of the specimen, the feedback loop is needed to control the flow of water to or from the specimen until the matric suction at the boundary equilibrates with the suction in the rest of the specimen.

5.4 Experimental Procedures

To demonstrate the suction-saturation control procedures used to measure the effects of hydraulic hysteresis on G_{max} of unsaturated soils, drying-wetting tests under different confining net stresses were performed on compacted silt specimens with initial void ratios of 0.53 and 0.69. After the soil specimen was prepared within the resonant column setup and the drive plate was been properly aligned and leveled, a high vacuum pump was used to apply a vacuum with a magnitude of -80 kPa to the inside of the specimen. The specimen and all plumbing lines on top and bottom of the specimen are then permitted to de-air for approximately one hour. During this time, the cell was assembled around the specimen. An air pressure of 20 kPa was applied to the cell as a seating confining pressure. De-aired water from the backpressure reservoirs was then introduced into the bottom platen to saturate the ceramic disk, soil specimen, top platen, and all supply lines from the bottom up. During this upward flow of water, de-aired water was flushed through both chambers of the pressure transducer, all valves, tubing, and the flow pump in order to ensure that

the system is fully water-saturated. The cell pressure was then increased to 90 kPa and the backpressure was increased to 20 kPa, corresponding to an initial mean effective stress of 70 kPa. After ensuring that the volume of the specimen is constant, the cell pressure and backpressure were increased in stages to 520 kPa and 450 kPa, respectively, maintaining the effective stress equal to 70 kPa. Skempton's B-value parameter was checked during this process to evaluate the initial saturation of the specimen. A B-value of 0.98 was observed for the test presented in this study. After this point, the confining pressure was increased to reach the desired net confining stress. After a 24 hour consolidation period, a resonant column test was performed on the specimen to determine the value of G_{max} corresponding to saturated conditions.

After conducting the resonant column test under water-saturated conditions, the line connecting the bottom of the specimen to the backpressure water reservoir was closed for the remainder of the test, while the hydraulic connections leading to the flow pump and one side of the differential pressure transducer remain open. The air was then flushed from the top platen of the specimen while maintaining an air pressure of 450 kPa. Air was also flushed from the line connecting the top platen to the other side of the differential pressure transducer. While water is flushed from the top platen and associated tubing, the soil specimen will not desaturate because the pore air and water pressures are

both equal to 450 kPa (i.e., a suction of 0 kPa) and the connection to the backpressure reservoir is closed.

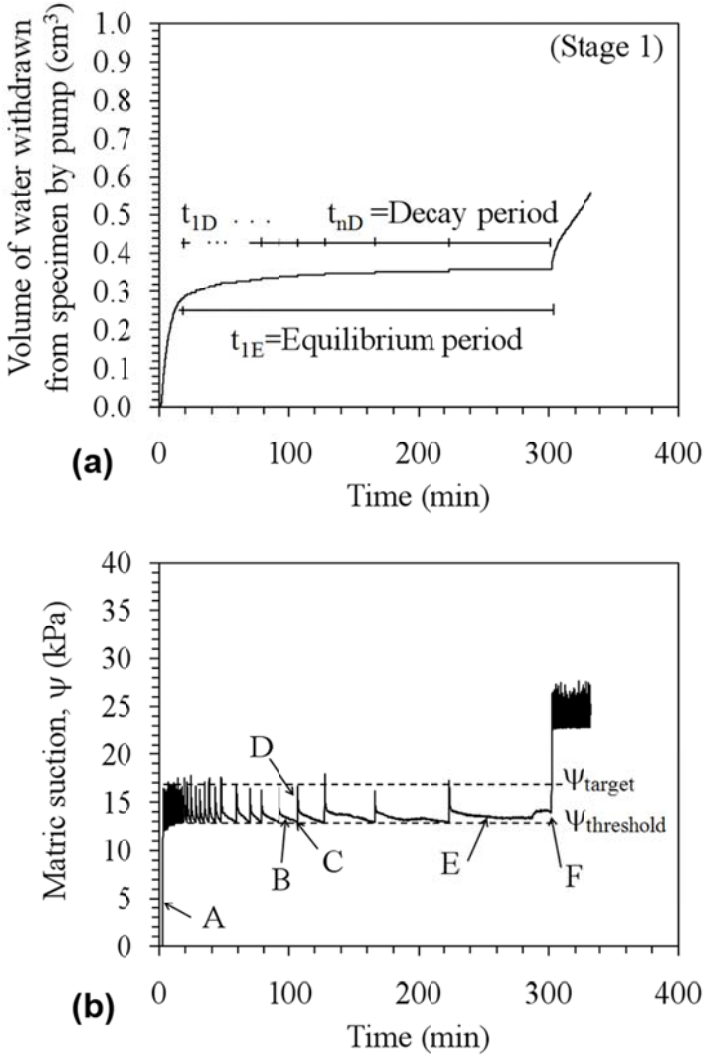

Figure 5.9: Flow pump operation data highlighting the suction control procedures for specimen with e=0.53 and p_n=100 kPa: (a) Water volume withdrawn from the soil specimen during the first increment of matric suction applied to the soil specimen; (b) Measured changes in matric suction at the outflow face of the soil specimen during the first increment of matric suction

However, if water is withdrawn from the bottom of the specimen by the flow pump, air will be free to take its place within the soil pores, resulting

in desaturation of the specimen. The approach used to impose the first target suction value of 17 kPa for the specimen prepared with an initial void ratio of 0.53 is shown in terms of the volume of water withdrawn from the specimen in Figure 5.9(a) and the measured matric suction at the bottom boundary of the specimen in Figure 5.9(b) for the specimen under a confining nets stress of 100 kPa. During drying of the specimen, the flow pump is used to withdraw water from the bottom of the specimen (through the ceramic disk) at a constant rate until a target suction value at the boundary of the specimen measured using the differential pressure transducer [Point A in Figure 5.9(b)]. After reaching the target suction value, the flow pump is stopped, and the suction imposed at the bottom boundary of the specimen is permitted to equilibrate with the suction within the rest of the specimen [Point B in Figure 5.9(b)]. If the suction at the boundary decays to a threshold suction value [Point C in Figure 5.9(b)], the pump is restarted until the suction at the boundary reaches the target value again [Point D in Figure 5.9(b)].

The threshold suction used in this study was 3 kPa below the target suction. This value can be adjusted by the test user depending on the soil type and the time required for equilibration. The time required for the suction to reduce from the target value to the threshold value is defined as the decay period. As equilibrium signifies no-flow conditions, the decay period will increase during each successive operation of the pump. The

decay period can be used as an indicator of whether the soil is at equilibrium. A target decay period of 5000 second was used to signify equilibrium conditions for low suctions in this study. This value represents a compromise between practical testing times and the equilibration of flow in the specimen; longer equilibration times were used in preliminary tests and similar results were obtained. The iterative operation of the pump is repeated until the suction remains above the threshold suction value for a decay period equal to the target value. The entire time required for equilibration is defined as the equilibration period. Point E in Figure 5.9(b) shows the case when the soil specimen has maintained a suction above the threshold suction for the target decay period, and is defined as being at hydraulic equilibrium. A resonant column test was then performed immediately on the soil specimen to measure G_{max} of the soil specimen at the equilibrium suction value. The volume of water withdrawn from the specimen to reach equilibrium (no flow) conditions can be obtained from the flow pump data shown in Figure 5.9(b). This process can be repeated to define multiple points on the SWRC and the relationship between G_{max}, ψ, and S_r for different net confining stresses. Point F in Figure 5.9(b) shows when the pump was operated to reach the second target suction. After defining the drying path of the SWRC, definition of the wetting process involves reversing the

direction of movement of the pump piston to supply water to the specimen in controlled increments.

The flow pump speed has a significant effect on the accuracy of the feedback control loop and consequently on the resolution of suction values which can be imposed on the specimen. If the pump operates too fast, it will be difficult for the feedback control loop to stop the pump after reaching the threshold suction, resulting in "overshooting" of the target suction before the feedback-loop tells the pump to stop. To avoid overshooting, the pump speed can be adjusted throughout the test as the hydraulic conductivity of the specimen decreases. A pump speed of 0.0009 mm/s was used for all of the suctions applied in this study. This speed is more suited for the higher suctions applied in this study than to the low suctions, which only means that the test may have had a longer duration than it needed.

5.5 Results

5.5.1 SWRC of the Soil Specimens Subjected to Different Net Confining Stresses

To illustrate the interpretation of results obtained from the flow pump, the volume of water withdrawn from the specimen by the flow pump during the test and the measured suction at the bottom boundary of the specimen for the case of specimen with an initial void ratio of 0.53 subjected to a net confining stress of 100 kPa, are shown in Figures

5.10(a) and 5.10(b), respectively. Results for other cases are presented in Appendix A. The vertical dashed lines in these figures separate the test results into stages in which different target suction values were applied. In this case, the first stage of the test [shown in detail in Figures 5.10(a) and 5.10(b)] involved application of a target suction value of 15 kPa. Comparison of this first stage to later stages shows that a small amount of water was needed to reach equilibrium through the soil specimen, indicating that this first target suction was less than or near the air entry suction of the soil. Equilibration of the specimen under the second target suction of 25 kPa required a longer time, which means that a greater amount of water had to be withdrawn from the specimen before the suction remained above the threshold suction for a decay period longer than 5000 seconds. The duration of this second stage is also associated with the water withdrawn from the soil; the greater amount indicates that the second target suction value was greater than the air entry suction of the soil.

The stage involving a target suction value of 70 kPa had a relatively smaller equilibration time than the previous stages. Other tests performed by the authors indicate that application of suctions above 70 kPa for this compacted silt resulted in equilibration of flow after a single iteration. This indicates that the water phase in the soil was approaching occluded conditions, and the water at the top of the specimen was not

hydraulically connected to the water at the bottom of the specimen. This observation of the point of water occlusion is consistent with other tests performed on this soil by Bicalho (1999) and Hwang (2002). Accordingly, after reaching equilibrium under a suction of 70 kPa, the direction of the pump was reversed to evaluate the SWRC and G_{max} along an imbibition scanning path. During the wetting process, desired suction values were obtained comparatively quickly to the drainage stages. During wetting, it was observed that only a small amount of water entered the specimen before equilibrium of suction occurred, although more water entered the specimen during application of target suction less than 20 kPa. The same amount of water that was withdrawn from the specimen was not reabsorbed for a target suction of 3 kPa, likely due to occlusion of air in the specimen during wetting. The SWRC of the soil specimen was then defined by plotting the measured values of ψ [Figure 5.10(b)] against the values of S_r calculated from the water flow measurements [Figure 5.11(a)], and identifying the points of equilibrium. The van Genuchten (1980) SWRC model was also fitted to the points of equilibrium to define the primary drying path and the wetting scanning curve of the SWRC. The primary drying path measured using this approach is consistent with data defined by other authors as shown in Figure 5.12). In the case of soil specimen with e=0.53 under the net confining stress of 100 kPa, the air entry suction was approximately 21 kPa and water occlusion occurred at approximately a S_r of 0.63. During wetting from this point, the soil returned to a degree of saturation of 0.83.

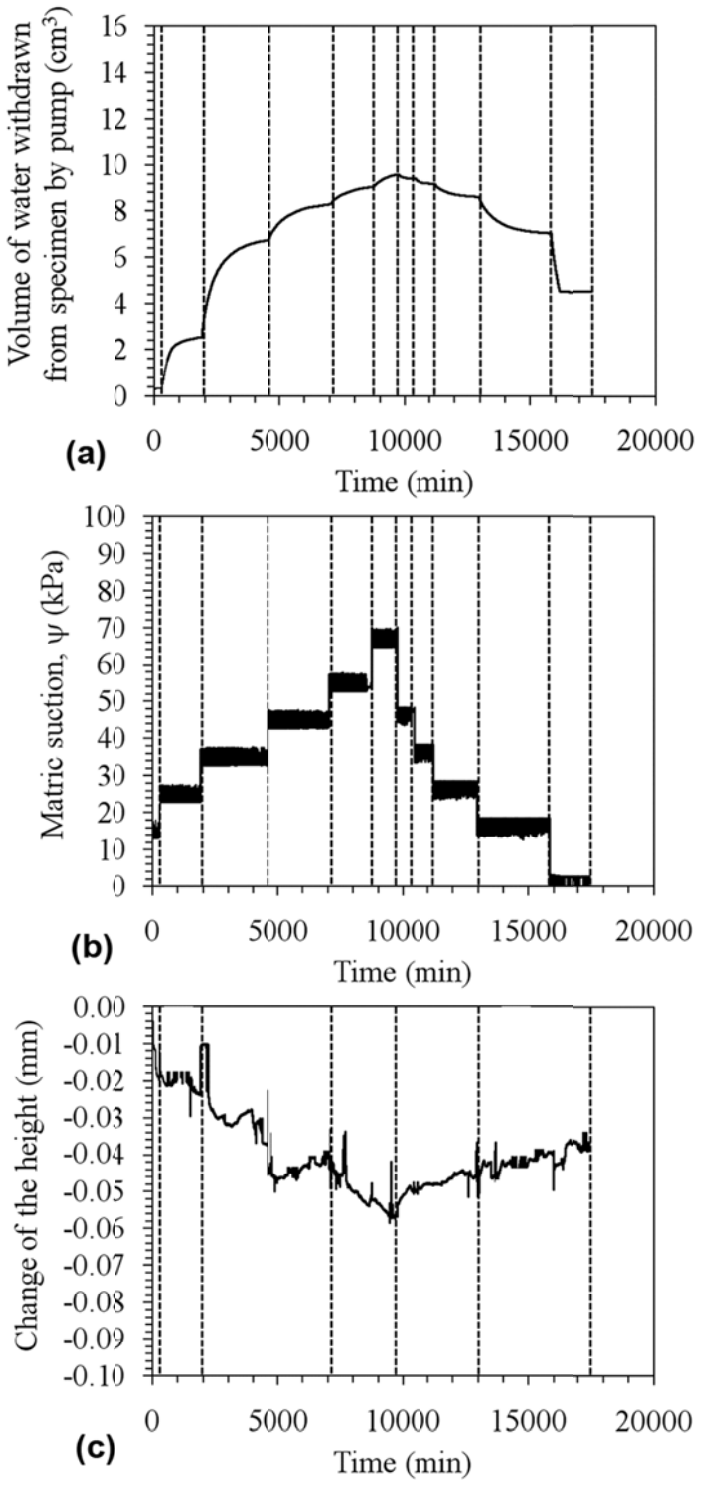

Figure 5.10: Flow pump operation data highlighting the suction control procedures: (a) Variation in the volume of water; (b) Measured changes in ψ; and (c) Measured change in height during drying and wetting

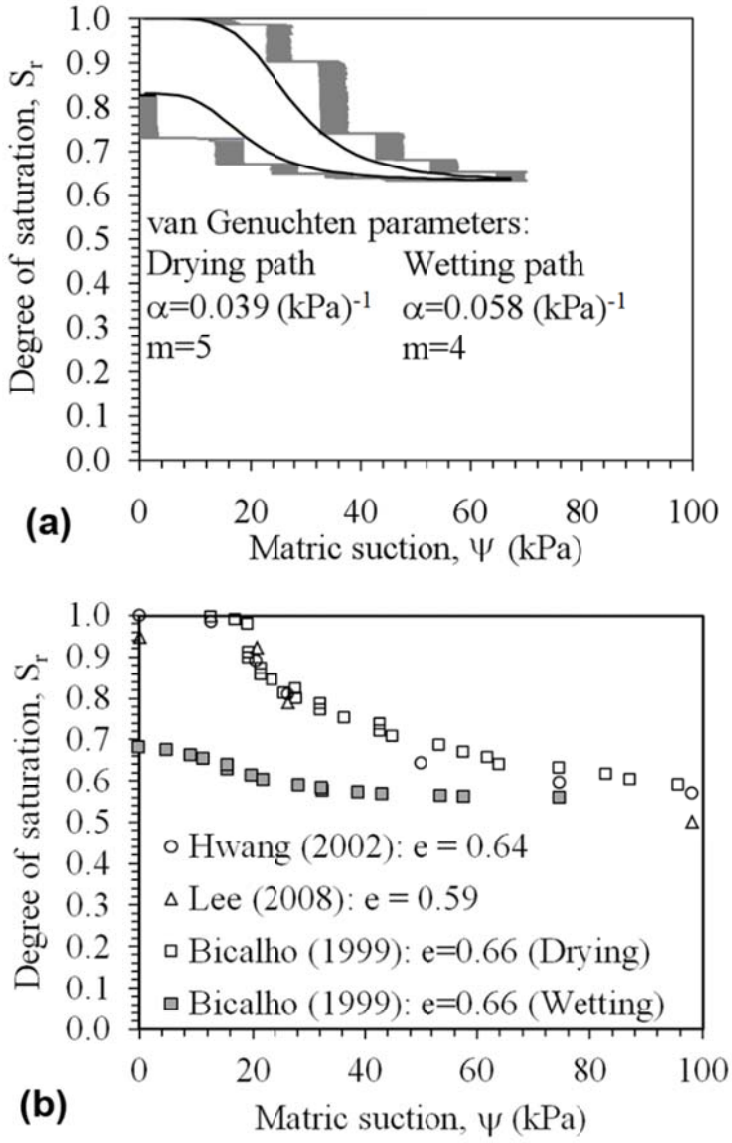

Figure 5.11: SWRC of compacted Bonny silt for specimen with e=0.53 subjected to p_n=100 kPa: (a) van Genuchten SWRC model fitted to the equilibrium points of degree of saturation and matric suction; (b) Comparison of SWRCs from this approach with those reported in previous studies

It should be noted that the value of S_r measured at the point of water occlusion is not representative of the value of S_r at residual saturation conditions. To reach residual saturation, the soil must be dried using a relative humidity technique with vapor flow. The axis translation is not

appropriate for use in measuring suction values beyond the point at which water flow is negligible. Nonetheless, the information in obtained over a degree of saturation from 0.63 to 1.00 attained with this testing method is suitable to evaluate the behavior of soils in the range of conditions affected by liquid water flow in the field.

Figure 5.12 shows the hysteretic SWRCs obtained from the drying and wetting tests for specimens subjected to different net confining stresses. As it is observed in both Figures 5.12 (a) and 5.12 (b), there is a significant difference between the SWRC of the soil specimens under different net confining stresses, suggesting that net confining stress has a great influence on the soil water retention curve. In the case of specimens prepared at an initial void ratio of 0.53, the air-entry values of the specimens are estimated to be 18 to 21 kPa as the net confining stress increases from 100 to 200 kPa. Besides, soil specimen with higher net confining stress is shown to have a better retention ability (lower desorption rate) compared to that under lower net confining stress, resulting in a shift to right in the measured SWRC. This observation may be due to a new arrangement between the particles in a smaller average pore-size distribution in the soil specimen due to a higher applied net confining stress (Ng and Pang 2000a). The size of the hysteresis loop also appears to be affected by the net confining stress with smaller loop at a higher net confining stress. This is likely due to the presence of a smaller

average pore-size distribution in the soil specimen under higher net confining stress and its effect on the mechanisms attributed in the hysteresis on the SWRC.

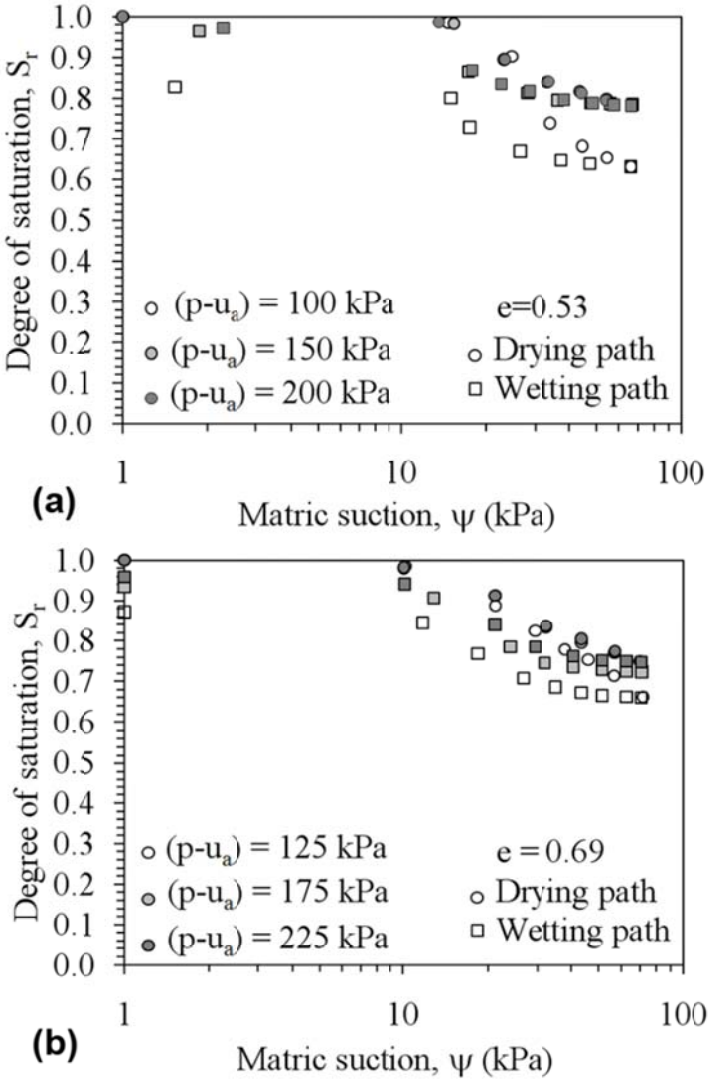

Figure 5.12: The SWRC measurement for specimens prepared at (a) e=0.53; and (b) e=0.69

In fact, several mechanisms have been observed to attribute in the hysteretic process of the SWRC. Major theorized mechanisms include: (1) geometrical effects associated with non-homogenous pore size distribution,

(2) entrapped air, which refers to the formation of occluded air bubbles in "dead-end" pores during wetting, (3) swelling and shrinkage, which may alter the pore fabric of fine-grained soil differently during wetting and drying processes, and (4) contact angle hysteresis, which is related to the intrinsic difference between drying and wetting contact angles at the soil particle–pore water interface. Contact angle is an intrinsic property of any two contacting phases in a solid-liquid-gas system. For unsaturated soil systems, contact angle may be defined as the angle between a line tangent to the air-water interface and a line defined by the water-solid interface (Lu and Likos 2006). When the average pore-size distribution is smaller, the effects of these mechanisms on the SWRC will be smaller (Ng and Pang 2000a) and consequently, the hysteresis loops of the SWRC for the specimens subjected to the higher net confining stresses are smaller. As shown in Figure 5.12, the end point of the wetting curve is back to a degree of saturation of 0.96 under an applied net confining stress of 200 kPa, while the degree of saturation at zero suction during wetting with a net confining stress of 100 kPa is a lower degree of saturation of 0.88.

Specimen with a higher initial void ratio of 0.69 [Figure 5.12(b)] tends to have a lower air-entry suction value. In this case, for the range of net confining stresses of 125 to 225 kPa applied to the specimen, the air entry suction changes from 12 (for cases with lower net confining stress) to 16 kPa (for higher net confining stress). In the specimen prepared at a higher

initial void ratio, the effect of net confining stress is more pronounced compared to that prepared at a lower void ratio. In this case, since the size of the pores between the particles is larger, a higher energy is required during the hydraulic hysteresis to displace air trapped in the large pores of the soil specimens and the hysteresis loop will be larger compared to that prepared at a lower initial void ratio (Ng and Pang 2000a).

5.5.2 Variation in Axial Displacement during the Hydraulic Hysteresis and application of p_n

The axial displacements for specimens under different loading conditions prepared at initial void ratios of 0.53 and 0.69 are shown in Figure 5.13(b) and 5.14(b), respectively. These measurements were obtained from the proximeter readings [Figure 5.10(c)] mounted on top of the specimen. As observed in the figures, distinct decrease in height was noted during drying, and a rebound in height was noted during wetting. During the first stage of drying, the height of the specimen decreases only slightly with an increase in matric suction, because the first target suction is less than the air entry suction. After this stage, the height of the specimen decreases in a faster rate with increasing suction. During the wetting process, at either net confining stress, the specimen expands slightly with a decrease in matric suction becoming constant at low suction values. A smaller change in the height of the specimen was measured during the wetting process.

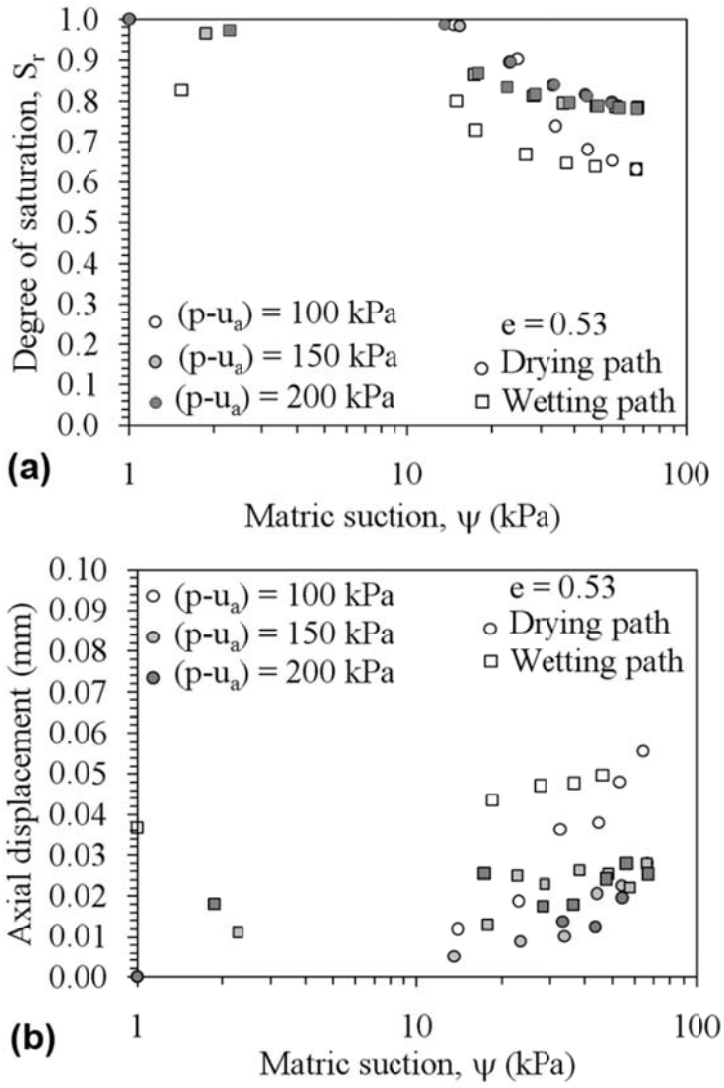

Figure 5.13: (a) SWRC and; (b) axial displacement vs. matric suction for specimen prepared at an initial void ratio of 0.53

In this study, the magnitudes of the axial displacement the specimen subjected to a higher net confining stress was observed to be mostly lower than those at a smaller net confining stress. In the case of the soil specimen prepared at an initial void ratio of 0.53, a maximum axial displacement of 0.06 mm is obtained under a net confining stress of 100

kPa, while the maximum displacement under a higher net confining stress of 200 kPa was 0.024 mm.

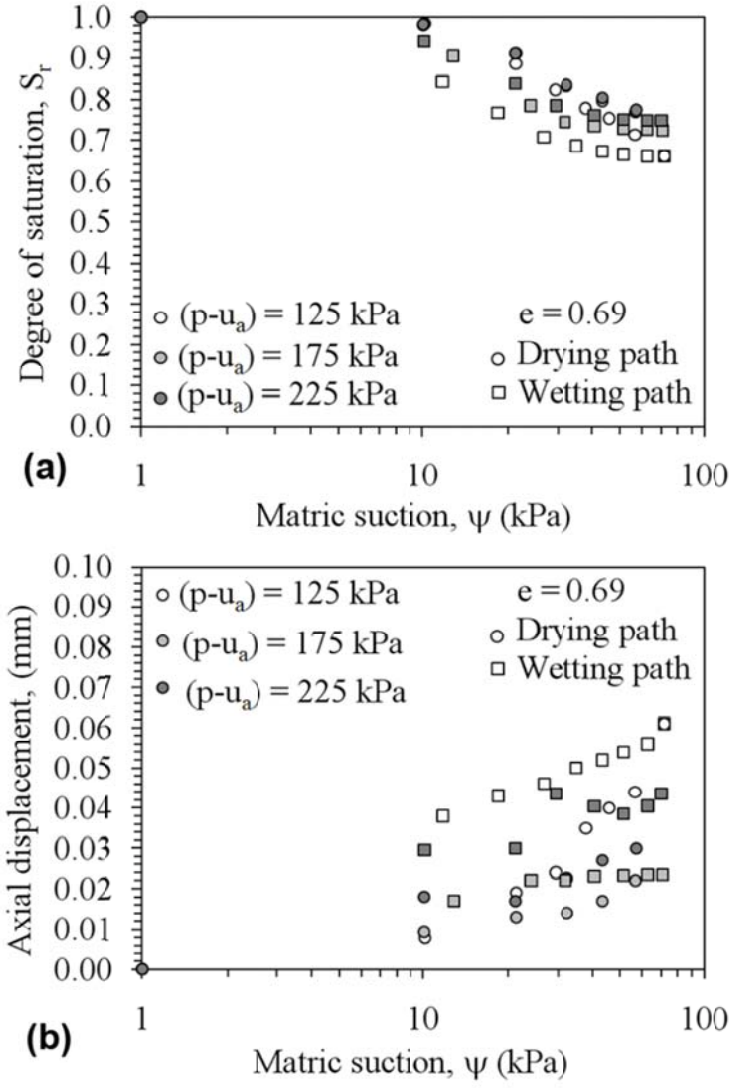

Figure 5.14: (a) SWRC and; (b) axial displacement vs. matric suction for specimen prepared at an initial void ratio of 0.69

The size of the hysteresis observed in axial displacement was also affected by the net confining stresses with smaller loop for specimens subjected to higher net confining stresses [Figure 5.11(b)]. For specimen prepared at an initial void ratio of 0.69 [Figure 5.12(b)], a higher axial

displacement during the process of drying and wetting was observed and the effect of net confining stress was more pronounced.

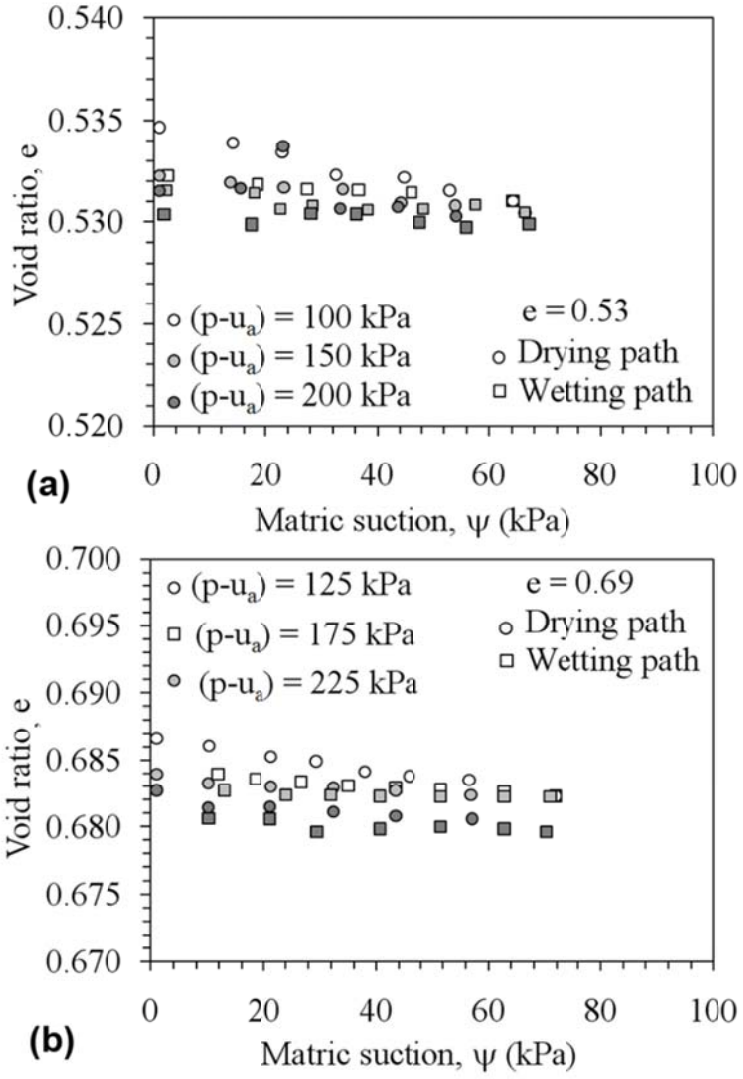

Figure 5.15: Changes in void ratio during the hydraulic hysteresis for specimens prepared at an initial void ratio of: (a) e = 0.53 and; (b) e = 0.69

The change in the specimen height measured using the proximeter was used to estimate the changes in void ratio during the hydraulic hysteresis. Specifically, in order to calculate the changes of the void ratio from the proximeter measurement, the soil was assumed to deform isotropically.

The void ratio changes during hydraulic hysteresis for different cases calculated from the axial displacement measurements are shown in Figures 5.15(a) and 5.15(b). Only minor changes in void ratio are noted during the hydraulic hysteresis. Although the changes in void ratio were then used to adjust the value of S_r in the calculation of the SWRC, these changes had a negligible effect on the measured SWRC and G_{max} relationships for the compacted silt. Accordingly, the value of ε_v^p in Eq. (4.12) was assumed to be zero. The change in volume may be a more important variable to measure for other types of soils evaluated using this testing method.

5.5.3 Small Strain Shear Modulus of Unsaturated Compacted Silt

The values of G_{max} measured after reaching equilibrium during each stage of the drying and wetting tests for specimens with the initial void ratios of 0.53 and 0.69 are shown in Figures 5.14(b) and 5.15(b), respectively. During drying, regardless of the initial void ratio, G_{max} followed an S-shaped curve complying with the S-shaped of the SWRC. In all cases, during the drying process from saturated condition, G_{max} is initially observed to have a slight increase in magnitude with suction or S_r when below or near the air entry suction. However, a greater increase in G_{max} is measured for suctions greater than the air entry suction, although the trends started to flatten out for higher values of suction.

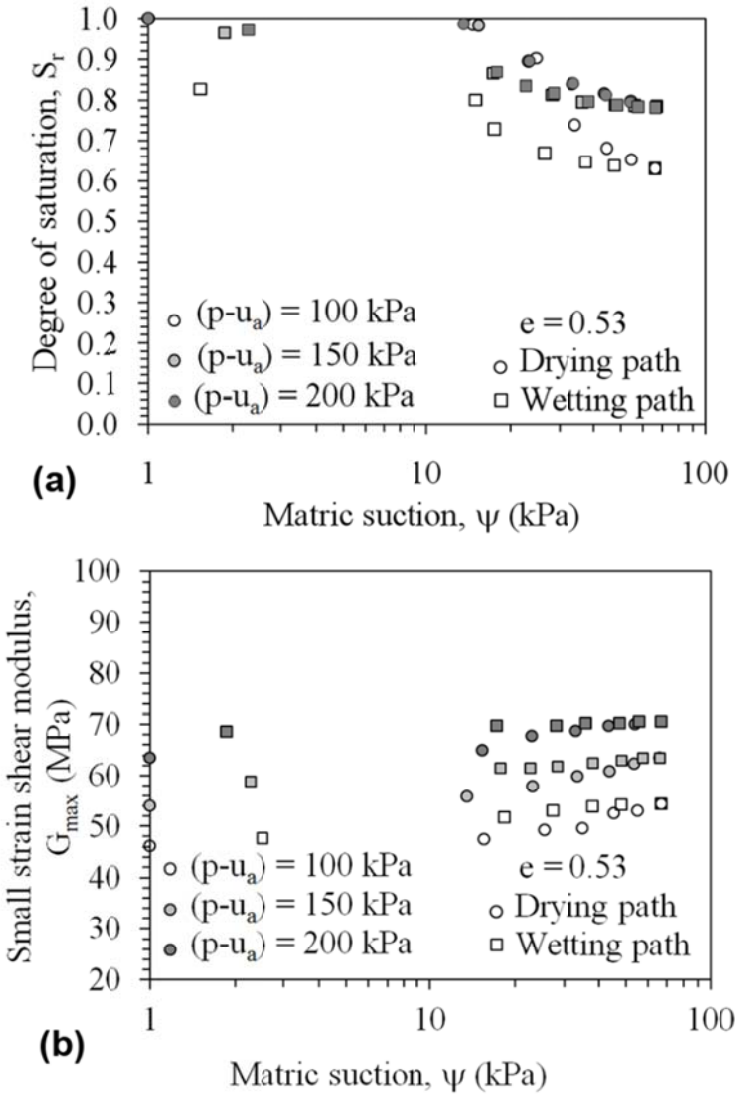

Figure 5.16: Results during drying and wetting of compacted Bonny silt specimen with an initial void ratio of e=0.53: (a) SWRC; (b) G_{max} measured as a function of degree of saturation; and (c) G_{max} measured as a function of matric suction

A limiting value is not expected for this test because of the relatively high degree of saturation. During wetting, a hysteretic behavior is noted in G_{max} similar to that noted by Ng et al. (2009). For the same values of equilibrium suction, the G_{max} values measured during wetting are consistently higher than those obtained during drying. During wetting, a

small reduction in G_{max} with decreasing ψ is observed. A greater reduction in G_{max} is noted for low suctions during wetting, where a greater amount of water is absorbed by the specimen.

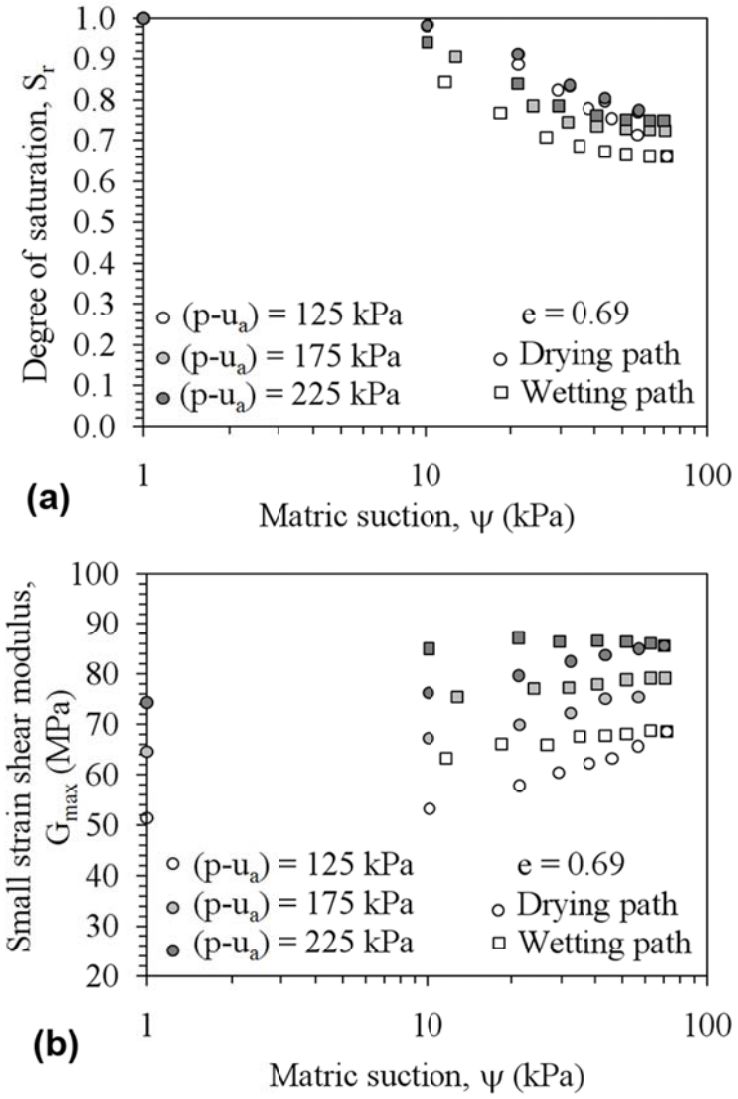

Figure 5.17: Results during drying and wetting of compacted Bonny silt specimen with an initial void ratio of e=0.69: (a) SWRC; (b) G_{max} measured as a function of degree of saturation; and (c) G_{max} measured as a function of matric suction

As explained in Chapter 4, the hysteretic behavior in G_{max} is due to drying-induced hardening that is not fully recovered during wetting, as

well as due to the different distributions in water throughout the specimen during the wetting process.

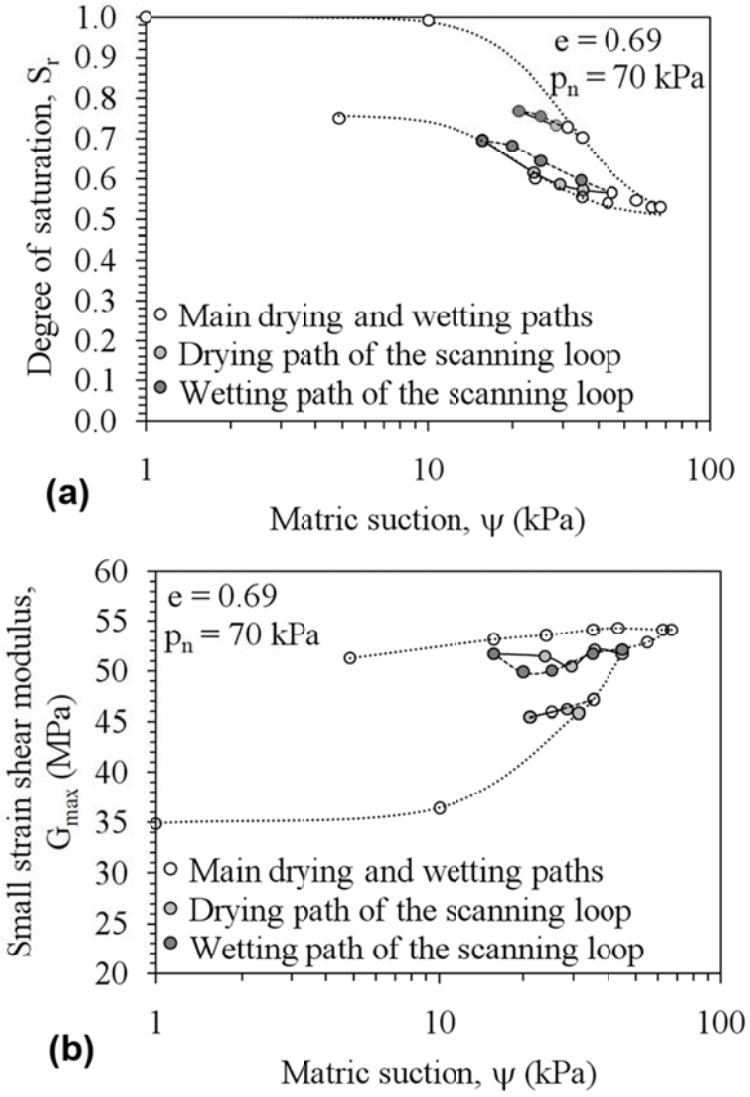

Figure 5.18: Results during drying and wetting of compacted Bonny silt specimen with an initial void ratio of e=0.69 and under p_n=70 kPa: (a) SWRC; (b) G_{max} measured as a function of matric suction

The distribution of water may vary because of entrapped air bubbles, and may lead to different spatial impacts of air-water menisci on the inter-particle connections throughout the soil specimen (Khalili and

Zargarbashi 2010). Increasing the net confining stress, as observed in Figures 5.16 and 5.17, decreases the effect of matric suction on the small strain shear modulus.

Changes in the small strain shear modulus through the scanning curves of the SWRC were also examined by performing a series of resonant column tests on a specimen with an initial void ratio of 0.69 through the scanning loop. As it is observed in Figure 5.18, due to the small change in the degree of saturation of the soil specimen with matric suction, a small change in the small strain shear modulus through this part of the SWRC is observed.

CHAPTER VI

Model Validation

6.1 Model Validation

To validate the model and parameter selection methodology, the values of G_{max} predicted from the model were compared with those measured using the modified resonant column with suction-saturation control. The SWRCs of the silt specimen prepared at initial void ratios of 0.53 and 0.69 defined under different net confining stresses are shown in Figures 6.3 (a) and 6.4(a). The piece-wise linear SWRC model was fit to this set of data to define the values of λ_s and κ_s, which are reported in the figures. Since the SWRCs for different net confining stresses differ, soil specimens subjected to a higher net confining stress were found to have greater water retention ability with smaller rates of desorption and adsorption, which means a smaller slope of the plastic portions of the SWRC, λ_s.

The measured G_{max} data at zero suction (saturation conditions) for specimens was used to define values of A and n [Figures 6.1(a) and 6.1(b)]. Similar to the literature results, the value of K was predicted using guidance in Hardin (1978) (Table 6.1). The parameters K´ and b were

defined using the trend lines in Figures 6.2(a) and 6.2(b), respectively. Using these parameters, the model provided a good fit to the G_{max} data plotted as a function of S_r in Figures 6.3(b) and 6.4(b) and ψ in Figures 6.3(c) and 6.4(c) for specimens with initial void ratio of 0.53 and 0.69, respectively. The trends observed in the experimental data and the model predictions are consistent with those observed in the data from the literature by Ng et al. (2009). Specifically, the value of G_{max} was observed to decrease at a different rate during wetting than during drying due to the suction-induced hardening.

Table6.1: A guidance for the determination of hardening parameter K from plasticity index, PI (Hardin 1978)

K	PI
0	0
0.18	20
0.3	40
0.41	60
0.48	80
0.5	100
0.125	13.7

The results in Figures 6.3 and 6.4 are re-plotted in Figure 6.5 in terms of the single-value effective stress. Although the G_{max} results followed an approximately linear trend with p', hysteresis is still observed. A difference in magnitude of G_{max} of up to 10 MPa is noted from the wetting and dying paths. This highlights the importance of using a model such as the one in Eq. (4.12) to capture the effect of hydraulic hysteresis instead of

relying solely on a model for G_{max} such as that in Eq. (4.1) which is only a function of p´.

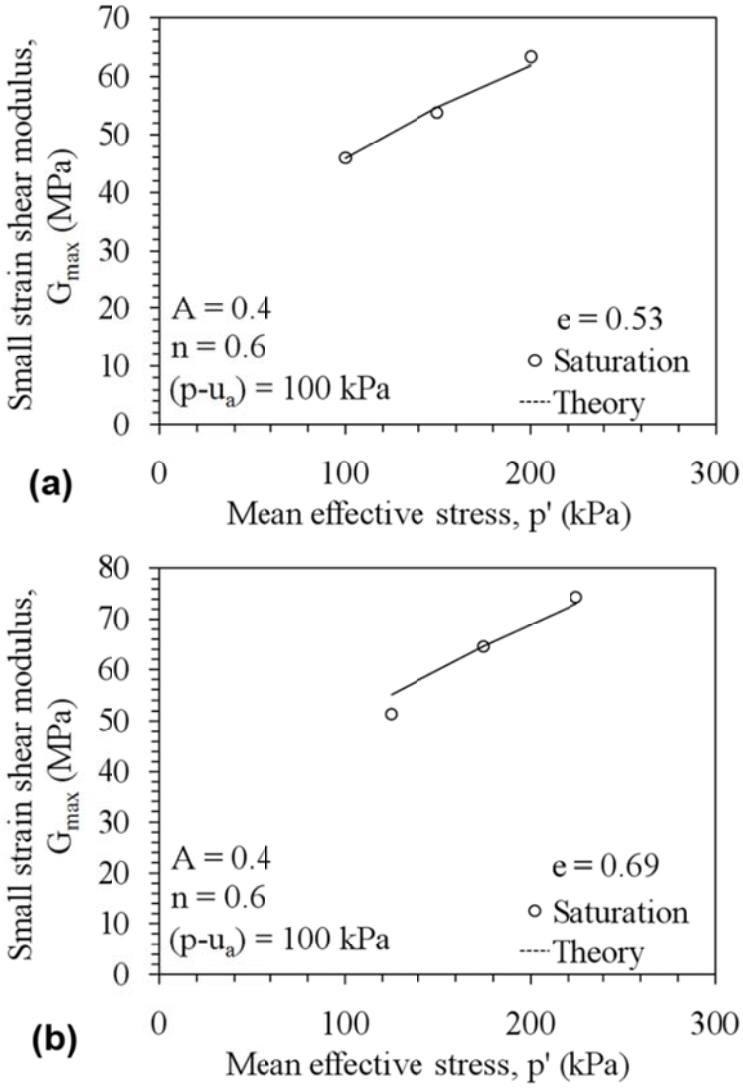

Figure 6.1: Parameters A and n definition for specimens prepared at an initial void ratio of: (a) e = 0.53 and (b) e = 0.69

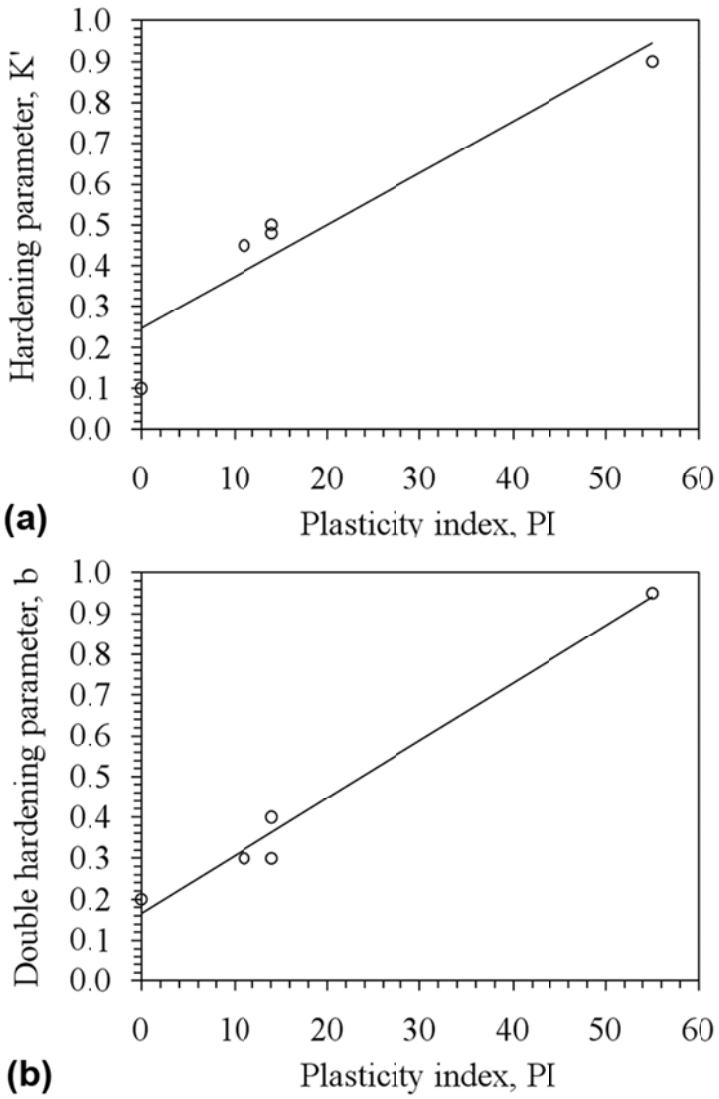

Figure 6.2: Preliminary guidance on model parameter definition for different soils (using data from literature): (a) Hardening parameter K´; (b) Double-hardening parameter b

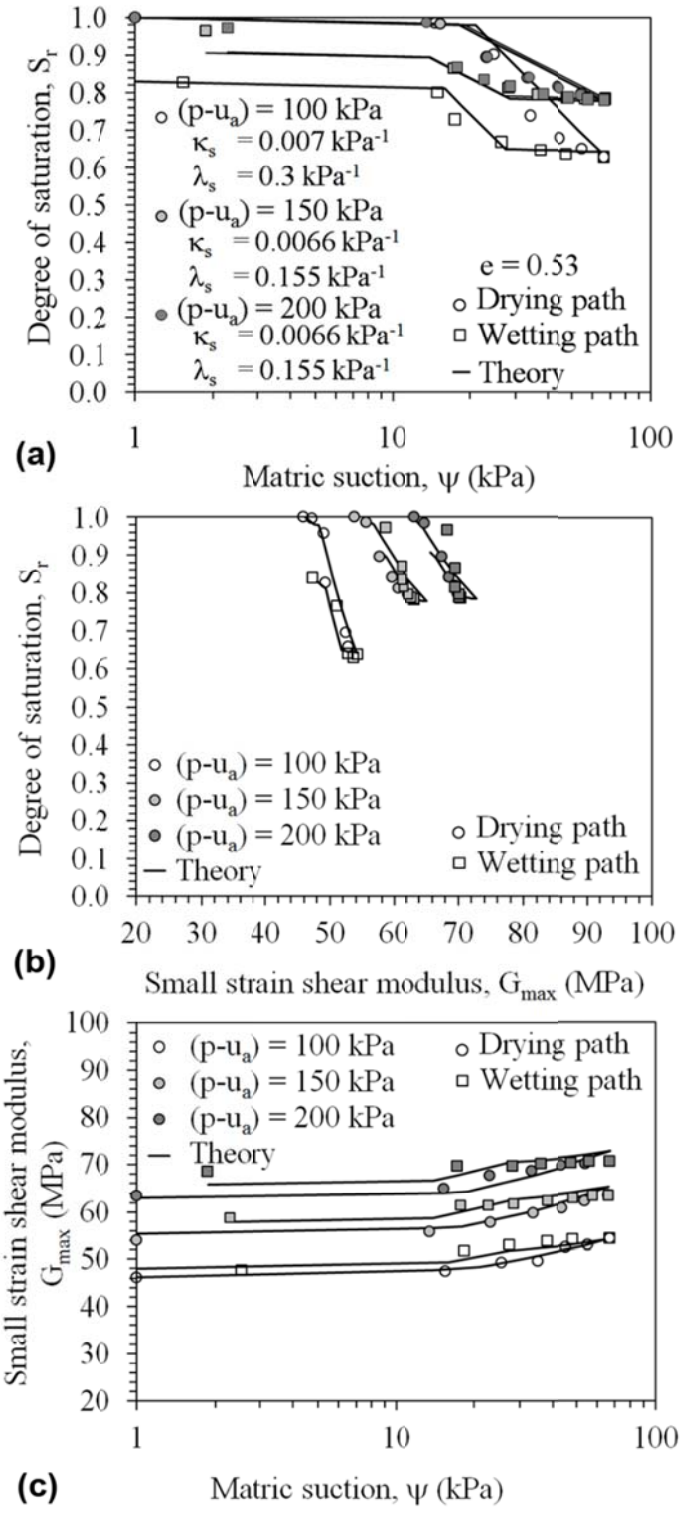

Figure 6.3: Model validation for Bonny silt drying and wetting data (A = 0.39, n = 0.55, K = 0.1, K' = 0.37 and b = 0.23): (a) SWRCs; (b) Gmax vs. Sr; and (c) Gmax vs. ψ

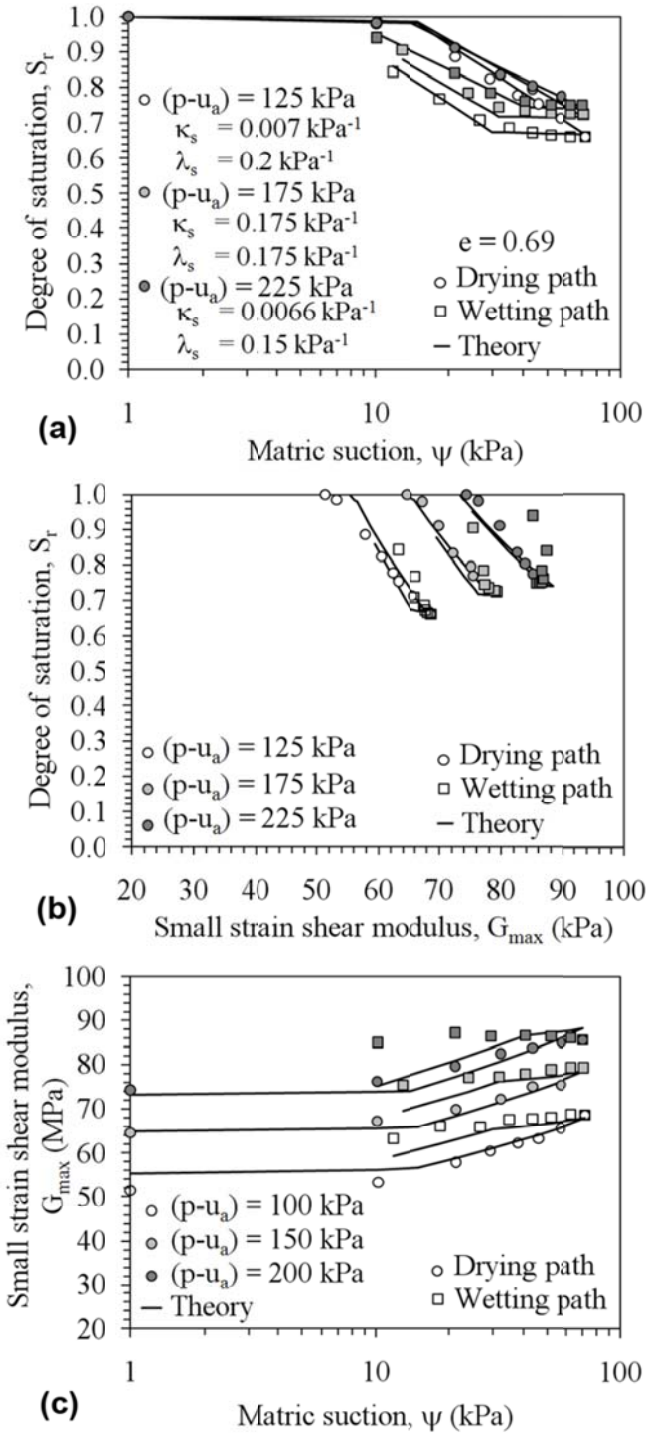

Figure 6.4: Model validation for Bonny silt drying and wetting data (A = 0.42, n = 0.58, K = 0.1, K' = 0.37 and b = 0.23): (a) SWRCs; (b) G_{max} vs. Sr; and (c) G_{max} vs. ψ

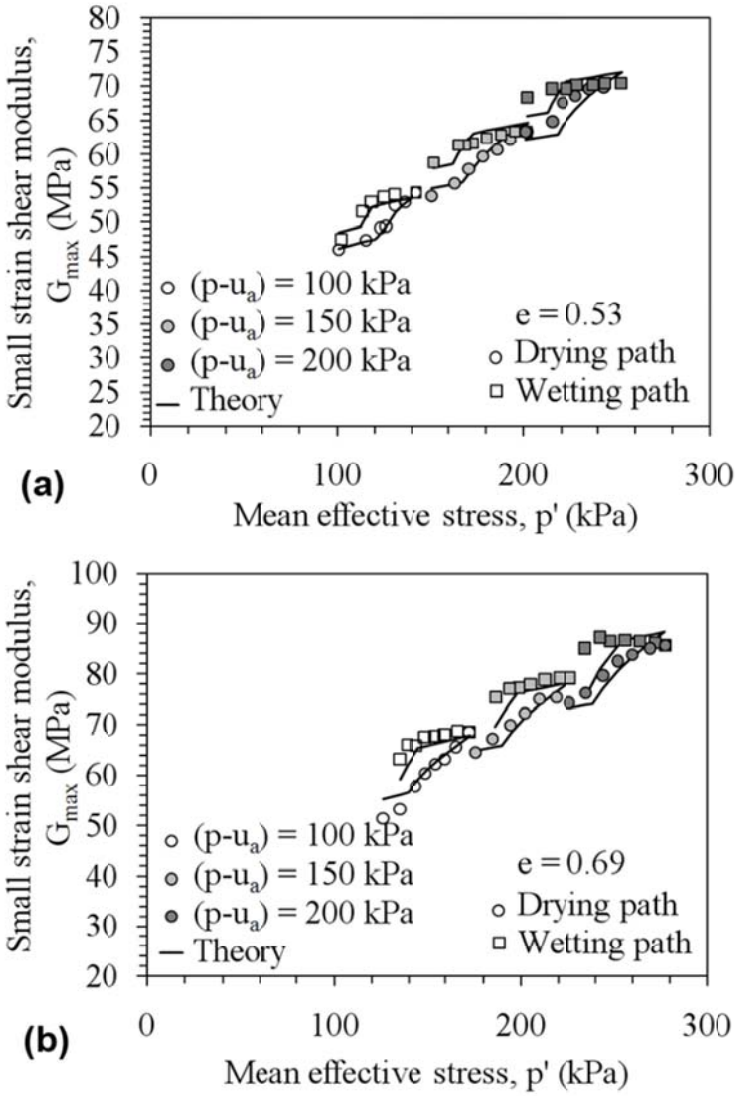

Figure 6.5: Model and experimental trends in Gmax with mean effective stress for compacted Bonny silt during hydraulic hysteresis under different net normal stress values

CHAPTER VII

Conclusion and Recommendation

7.1 Summary of Contribution

1. As a part of modeling the small strain shear modulus, the consideration of degree of saturation as the effective stress parameter in the definition of effective stress was evaluated using a multistage testing method for unsaturated soils. Based on results from the multistage drying shearing, the degree of saturation was found to be a good approximation of the effective stress parameter of unsaturated soils during the test. Results indicated differences in the SWRC of soil specimens subjected to different net confining stresses emphasizes the importance of using soil-specific tests to define the relationships between suction stress and matric suction.
2. A new framework was presented in this study to represent the impact of hydraulic hysteresis on the small strain shear modulus G_{max} of unsaturated soils. Different from previous empirical frameworks, coupling between effective stress and void ratio was incorporated using

a double-hardening constitutive relationship. The double-hardening mechanism was found to suitably model the different trends in G_{max} of unsaturated soils during wetting after a dying phase.

3. In an attempt to predict changes in G_{max} with matric suction, a rational approach was described to estimate the parameters for the framework, involving use of the compression curve, SWRC, G_{max} data for tests on saturated soils under different mean effective stress values, and empirical trends between hardening parameters and the plasticity index.
4. A new resonant column with suction-saturation control testing apparatus and experimental procedures was presented in this study to evaluate changes in the small strain shear modulus G_{max} of unsaturated soils during hydraulic hysteresis and validate the proposed approach for the G_{max} of unsaturated soils. The combination of suction control using the axis translation technique, saturation control using an automated flow pump, and volume change measurements with a proximeter was found to permit investigation of coupling between hydraulic hysteresis, volume change, and G_{max} of unsaturated soils.
5. The framework for G_{max} was then validated using experimental data reported in literature as well as data obtained from the proposed test

procedure on compacted soil tested in a fixed-free resonant column setup with suction-saturation control.

7.2 Conclusion

1. For compacted silt tested under different net confining stresses and prepared at different initial void ratios, G_{max} was found to increase during drying for the range of matric suction applied to the specimen with trends starting to flatten out for higher values of suction close to the water occlusion conditions. During wetting, a small reduction in G_{max} with decreasing ψ was observed. A greater reduction in G_{max} was noted for low suctions during wetting, where a greater amount of water was absorbed by the specimen. The hysteretic behavior in G_{max} was found to be due to drying-induced hardening that is not fully recovered during wetting, as well as due to the different distributions in water throughout the specimen during the wetting process. Net confining stress was observed to reduce the effect of matric suction on G_{max} while in specimens with higher initial void ratio, the effect of matric suction on the small strain shear modulus was more pronounced.
2. One of the aspects of the new experimental approach is the measurement of the SWRC during the application of loading. Results indicated a significant difference between the SWRCs of the soil specimens under different net confining stresses, suggesting that net confining stress has a great influence on the soil water retention curve.

Soil specimen with higher net confining stress was observed to have a better retention ability (lower desorption rate) compared to that under lower net confining stress, resulting in a shift to right in the measured SWRC. This observation may be due to a new arrangement between the particles in a smaller average pore-size distribution in the soil specimen due to a higher applied net confining stress.

3. Similar to the small strain shear modulus, a hysteretic behavior in the void ratio measurements of the specimens during the hydraulic hysteresis was observed. Changes in void ratio with matric suction during drying were observed to be higher than that during wetting. Results indicated that for the range of conditions evaluated in this study, the void ratio did not play a major role in the SWRC or the magnitude of G_{max}.

7.3 Recommendation

1. In the development of the proposed framework for the small strain shear modulus of unsaturated soils, using concepts of single variable effective stress (Bishop 1959) and double hardening for unsaturated soils, the conventional concepts of soil dynamics for saturated soils was extended for unsaturated soils. It is believed that available approaches for the strain dependent shear modulus of saturated soils may be also applicable for the prediction of shear modulus of unsaturated soils at different shear strain levels. This idea is needed to be validated by

using some dynamic tests for different ranges of shear strain. For this purpose, the Stokoe-type resonant column used in this study can be modified for performing the torsional shear tests by mounting two proximeters on top of the drive platen of the system.

2. In this study, based on results reported in literature, preliminary guidance was presented for the determination of parameters for the proposed framework for the small strain shear modulus of unsaturated soils. Although using this guidance, a good determination of the parameters for this type of soil was obtained, to have a better understanding of the parameters involving in the prediction of the small strain shear modulus of unsaturated soils, further studies on different types of soils with the consideration of different parameters (e.g. plastic limit, initial void ratio, compaction water content, …) is desired.

References

Abu-Hejleh, A.N., Znidarcic, D., and Illangasekare, T.H. (1993). "Permeability determination for unsaturated soils." *Unsaturated Soils. GSP 39.* S.L. Houston and W.K. Wray, Eds. ASCE. New York. 163-174.

Aiban, S. A., and Znidarcic, D., (1989). "Evaluation of the Flow Pump and Constant Head Techniques for Permeability Measurements," *Geotechnique* 39, No. 4, 655-666.

Bicalho, K.V. (1999). *Modeling Water Flow in an Unsaturated Compacted Soil*. Ph.D. Dissertation. University of Colorado at Boulder. Boulder, CO, USA.

Bicalho, K.V., Znidarcic, D., and Ko, H.-Y. (2000). "Air entrapment effects on hydraulic properties." *Advances in Unsaturated Geotechnics, Proceedings of Sessions of Geo-Denver 2000, GSP No. 99,* Shackelford, C.D., Houston, S.L., and Chang, N-Y. eds. ASCE, Reston, VA. 517-528.

Bishop, A.W. (1959). The Principle of Effective Stress. *Teknisk Ukeblad I Samarbeide Med Teknikk.* Oslo, Norway 106, No. 39, 859-863.

Biot, M. A. (1956) "Theory of Propagation of Elastic Waves in a Fluid Saturated Porous Solid, I. Low-Frequency Range." *Journal of the Acoustical Society of America*, Vol. 28, 168-178.

Brooks, R. and Corey, A., (1964), "Hydraulic properties of Porous media," Colorado State University, Fort Collins. Hydrology Paper No. 3.

Cabarkapa, Z., Cuccovillo, T. and Gunn, M. (1999). "Some aspects of the pre-failure behaviour of unsaturated soil." *Proceedings of the Second International Conference on Pre-failure Deformation Characteristics of Geomaterials*, Torino, Italy, Sept. 27–29.

Clayton, C. R. I., Priest, J. A., Bui , M., Zervos , A. and Kim, S. G. (2009) "The Stokoe resonant column apparatus: effects of stiffness, mass and specimen fixity*" Ge´otechnique* 59, No. 5, 429–437.

Darendeli, F.-Y. (2001). Development of a New Family of Normalized Modulus Reduction and Material Damping Crves. PhD Dissertation. Department of Civil Engineering. The University of Texas at Austin.

Fredlund D.G., Morgenstern, N.R. (1977). Stress State Variables for Unsaturated Soils. *Journal of Soil Mechanics and Foundation Division*. ASCE. **103**, 447–466.

Gallipoli, D., Gens, A., Sharma, R., and Vaunat, J. (2003). "An Elasto-Plastic Model for Unsaturated Soil Incorporating the Effects of Suction and Degree of Saturation on Mechanical Behaviour." *Géotechnique* Vol. 53, No. 1, 123–135.

Gan, K.J. and Fredlund, D.G. (1988). "Multistage Direct Shear Testing of Unsaturated Soils." ASTM Geotechnical Testing Journal. Vol. 11, No. 2, 132-138.

Gibson, R.E. and Henkel, D.J. (1954). “Influence of Duration of Tests at Constant Rate of Strain on Measured ‘Drained’ Strength.” Géotechnique. Vol. 4, No. 1, 6-15.

Hardin, B.O. and Black, W.L. (1968). “Vibration modulus of normally consolidated clay.” *Journal of the Soil Mechanics and Foundations Division*. ASCE. Vol. 94, No. SM2, 353–369.

Hardin, B.O. and Black, W.L. (1969). “Vibration modulus of normally consolidated clay; closure.” *Journal of the Soil Mechanics and Foundations Division*. ASCE. Vol. 95, No. SM6, 1531–1537.

Hardin, B.O. and Drnevich, V.P. (1972). "Shear modulus and damping in soils: measurement and parameter effects." *Journal of the Soil Mechanics and Foundations Division*. ASCE. Vol. 98, No. SM 6, 603-624.

Hardin, B.O., and Richart, F.E., Jr. (1963). “Elastic wave velocities in granular soils.” Journal of the Soil Mechanics and Foundation Division, ASCE, Vol. 98, No. SM1, 33-65.

Hardin, B.O. (1978). “The Nature of Stress Stain Behavior of Soils.” *Earthquake Engineering and Soil Dynamics*. **1**, 3–90.

Hilf, J.W. (1956). *An Investigation of Pore-Water Pressure in Compacted Cohesive Soils*. Ph.D. Dissertation. University of Colorado, Boulder, CO, USA.

Ho, D.Y.F. and Fredlund, D.G. (1982). "A Multistage Triaxial Test for Unsaturated Soils," ASTM Geotechnical Testing Journal. Vol. 5, No. 1/2, 18-25.

Hwang, C. (2002). *Determination of Material Functions for Unsaturated Flow*. Ph.D. Dissertation. University of Colorado at Boulder, CO, USA.

Inci, G., Yesiller, N., and Kagawa, T. (2003). "Experimental investigation of dynamic response of compacted clayey soils." *Geotechnical Testing Journal*. Vol. 26, No. 2, 125-141.

Iwasaki, T., Tatsuoka, F. & Yoshikazu, T. (1978). "Shear moduli of sands under cyclic torsional shear loading." *Soils and Foundations*, Vol. 18, No. 1, 39-56.

Ishihara, K. (1996) "Soil Behavior in Earthquake Geotechnics." Oxford University Press, Walton Street, Oxford, 350 pp.

Janbu, N. (1963) "Soil Compressibility as Determined by Oedometer and Triaxial Tests." *European Conference on Soil Mechanics and Foundation Engineering,* Wiesbaden, Germany, Vol. 1, 19-25.

Kawajiri, S., Kato, S., Shibuya. S., and Kawaguchi, T. (2009) Effects of Suction on Elastic Shear Modulus for Unsaturated Soil. *4th Asia Pacific Conference on Unsaturated Soils, Nov. 23-25, 2009*. Newcastle, Australia. CD-ROM.

Khalili, N., Geiser, F., and Blight, G.E. (2004). Effective Stress in Unsaturated Soils, A Review with New Evidence. *Int. Journal of Geomechanics* **4**, No. 2, 115–126.

Khalili, N. and Khabbaz, M.H. (1998). "A Unique Relationship for χ for the Determination of the Shear Strength of Unsaturated Soils," *Géotechnique*. Vol. 48, No. 5, 681-687.

Khalili, N., Zargarbashi, S. (2010). "Influence of hydraulic hysteresis on effective stress in unsaturated soils." *Géotechnique*. Vol. 60, No. 9, 729-734.

Khoury, N.N. and Zaman, M.M. (2004). "Correlation between resilient modulus, water variation, soil suction for subgrade soils," *Transportation Research Record*, No. 1874, Washington, D.C., pp. 99-107.

Khoury, C. (2010). *Influence of Hydraulic Hysteresis on the Mechanical Behavior of Unsaturated Soils and Interfaces.* Ph.D. Dissertation. University of Oklahoma, Norman, OK.

Khosravi, A. and McCartney, J.S. (2009). Impact of Stress State on the Dynamic Shear Modulus of Unsaturated, Compacted Soils. *4th Asia Pacific Conference on Unsaturated Soils,* Nov. 23-25, 2009 Newcastle, Australia. CD-ROM.

Khosravi, A., Ghayoomi, M., McCartney, J.S. and Ko, H. Y. (2010). "Impact of effective stress on the dynamic shear modulus of

unsaturated sand." *GeoFlorida 2010,* West Palm Beach, Florida, USA. Feb. 20-24. CD-ROM.

Kim, D. S., Seo, W. S. & Kim, M. J. (2003). "Deformation characteristics of soils with variations of capillary pressure and water content." *Soils and Foundations*. Vol. 43, No. 4, 71–79.

Lee, J.-Y. (2010). Personal communication.

Lee, Y. B. (2010). Deformation Behavior of Shored Mechanically Stabilized Earth (SMSE) Wall Systems. Ph.D. Dissertation. University of Colorado at Boulder.

Leong, E. C., Rahardjo, H., (1997). "Review of Soil Water Characteristic Curve Equations," *Journal of Geotechnical and Geoenvironmental Engineering*, 123(12), 1106-1117.

Lu, N. and Likos, W.J. (2006). "Suction stress characteristic curve for unsaturated soil." *Journal and Geotechnical and Geoenvironmental Engineering*. Vol. 132, No. 2, 131-142.

Lu, N (2008). Is Matric Suction a Stress Variable? *Journal of Geotechnical and Geoenvironmental Engineering*. ASCE. **134**, No. 7, 899-905.

Lu, N. Godt, J.W., and Wu, D.T. (2010). "A closed-form equation for effective stress in unsaturated soil." *Water Resources Research*. Vol. 46, 14 pg.

Mancuso, C., Vassallo, R., and d'Onofrio, A. (2002). "Small strain behavior of a silty sand in controlled-suction resonant column-torsional shear tests." *Canadian Geotechnical Journal*. CGJ. Vol. 39, No. 1, 22-31.

Marinho, E.A.M., Chandler, R.J., and Crilly, M.S. (1995). "Stiffness measurements on an unsaturated high plasticity clay using bender elements." *In Proceedings of the First International Conference on Unsaturated Soils, UNSAT '95*, Paris, France, 6– 8 September 1995. A.A. Balkema, Rotterdam, the Netherlands. Vol. 2. 535–539.

McCartney, J.S., Villar, L. and Zornberg, J.G. (2008). "Nonwoven Geotextiles as Hydraulic Barriers for Capillary Rise." *GeoAmericas*. Cancun, Mexico. March 3-5, 2008.

McCartney, J.S. and Znidarcic, D. (2010). "Test system for hydraulic properties of unsaturated nonwoven geotextiles." Geosynthetics International. Vol. 17 No. 5, 10 pp.

Mendoza, C.E., Colmenares, J.E., and Merchan, V.E. (2005). "Stiffness of an unsaturated compacted clayey soil at very small strains." *Conf. on Advanced Experimental Unsaturated Soil Mechanics*. Trento, Italy. 27-29 June. 199-204.

Morrison, K., Harrison, F., Collin, J., Dodds, A. & Arndt, B. (2006). Shored Mechanically Stabilized Earth (SMSE) Wall Systems. FHWA-CFL/TD-06-001.

Ng, C.W.W., and Pang, Y.W. (2000). "Experimental Investigations of the Soil-Water Characteristics of a Volcanic Soil." Canadian Geotechnical Journal. Vol. 37, No. 6, 1252-1264.

Ng, C.W.W., Xu, J. and Yung, S.Y. (2009). "Effects of imbibition-drainage and stress ratio on anisotropic stiffness of an unsaturated soil at very small strains." *Canadian Geotechnical Journal, Vol.* 46, No. 9, 1062-1076.

Nuth, M. and Laloui, M. (2008). Effective Stress Concept in Unsaturated Soils: Clarification and Validation of a Unified Framework. *Int. J. Numer. Anal. Meth. Geomech.* **32**, 771–801.

Oh, W.T. and Vanapalli, S.K. (2009) A Simple Model for Predicting the Shear Modulus of Unsaturated Sandy Soils. *4th Asia Pacific Conference on Unsaturated Soils, Nov. 23-25, 2009.* Newcastle, Australia. CD-ROM.

Olsen, H.W. (1966). "Darcy's law in saturated kaolinite." Water Resources Res. Vol. 2, 287-295.

Qian, X., Gray, D.H., and Woods, R.D. (1991). "Resonant column tests on partially saturated sands." *Geotechnical Testing Journal.* Vol. 14, No.3, 266–275.

Qian, X., Gray, D.H., and Woods, R.D. (1993). "Voids and granulometry: effects on shear modulus of unsaturated sands." *Journal of Geotechnical Engineering*, ASCE, Vol. 119, No. 2, 295-314.

Rahardjo, H., Lim, T., Chang, M., and Fredlund, D. (1995). "Shear-Strength Characteristic of a Residual Soil." Canadian Geotechnical Journal, Vol. 32, No. 1, 60-77

Richart, F.E., Jr., Hall, J. And Woods, R.D. (1970). *Vibrations of Soils and Foundations*. Prentice Hall, Inc.

Rowe, P. W. (1963) "Stress-Dilatancy, Earth Pressures,and Slopes" Journal of the Soil Mechanics and Foundations Division, ASCE, Vol. 89, No. SM3, May, 37-61.

Sawangsuriya, A., Edil, T.B., and Bosscher, P.J., and Wang, X. (2009). "Modulus-suction-water relationship for compacted soils in postcompaction state." *Journal of Geotechnical and Geoenvironmental Engineering ASCE*. Vol. 135, No. 10, 1390-1403.

Schuurman, E. (1966). "The compressibility of an air/water mixture." *Geotechnique*. Vol. 16, No.4, 269-281.

Saeedy, H.S. and Mollah, M.A. (1988). "Application of Multistage Triaxial Test to Kuwaiti Soils," Advanced Triaxial Testing of Soil and Rock, ASTM STP 977, Robert T. Donaghe, Ronald C. Chaney, and Marshall L. Silver, Eds., ASTM, Philadelphia. pg. 363-375.

Seed, H. B., and I. M. Idriss (1970) "Soil Moduli and Damping Factors for Dynamic Response Analyses". Earthquake Engineering Research Center, University of California at Berkeley, Report EERC-70/10.

Seed,H.B.,Wong, R.T., Idriss, I.M., and Tokimatsu,K. (1986) "Moduli and damping factors for dynamic analyses of cohesionless soils." *Journal of Geotechnical Engineering*, ASCE, 112: 1016–1032.

Skempton, A.W. (1961). "Effective Stress in Soils, Concrete, and Rocks." Pore Pressure and Suction in Soils. Butterworths. London. pg. 4-16.

Soranzo, M. (1988). "Results and Interpretation of Multistage Triaxial Compression Tests," Advanced Triaxial Testing of Soil and Rock, ASTM STP 977, Robert T. Donaghe, Ronald C. Chaney, and Marshall L. Silver, Eds., ASTM, Philadelphia. pg. 353-362.

Stokoe, K.H., III, Hwang, S.K., Lee, J.N.K, and Andrus, R.D. (1995). "Effects of various parameters on the stiffness and damping of soils at small to medium strains." Proc. Of Int. Symp. on Pre-Failure Deformation of Geomaterials. Eds. S. Shibuya, T. Mitachi, and S. Muira. Vol. 2, 785-816.

Stokoe, K.H., II, Darendeli, M.B., Andrus, R.D., Brown, L.T. (1999). Dynamic Soil Properties: Laboratory, Field and Correlation Studies. *2nd Int. Conf. on Earthquake Geotechnical Engineering.* Lisbon, Portugal. Vol. 3.

Tamagnini, R. (2004). "An extended cam-clay model for unsaturated soils with hydraulic hysteresis." *Géotechnique.* Vol. 54, No. 3, 223–228.

Tatsuoka, F., Lo Presti, D.C.F. and Kohata, Y. (1995). Deformation Characteristics of Soils and Soft Rocks Under Monotonic and Cyclic Loads and their Relationships", SOA Report, *Proc. 3rd Int. Conf. on Recent Advances in Geotechnical Earthquake Engineering and Soil Dynamics*, *St Luois* **2**, 851-879.

Terzaghi, K. (1936) "The shearing resistance of saturated soils." *Proc., 1st Int. Conf. on Soil Mechanics,* Vol. 1, Cambridge, Mass., 54–56.

van Genuchten, M.T. (1980). "A closed-form equation for predicting the hydraulic conductivity of unsaturated soils." *Soil Science Society of America Journal.* Vol. 44, No. 5, 892–898.

Vassallo R., Mancuso, C. and Vinale, F. (2007). "Effects of net stress and suction history on the small strain stiffness of a compacted clayey silt." *Canadian Geotechnical Journal*, Vol. 44, No. 4, 447-462.

Vanapalli, S.K., Fredlund, D.G., and Sillers, W.S. (1998). "The Meaning and Relevance of Residual State to Unsaturated Soils," *51st Canadian Geotechnical Conference*, Edmonton, Alberta, October 4-7, 1998.

Vucetic, M. and Dobry, R. (1991). Effect of Soil Plasticity on Cyclic Response. *Journal of Geotechnical Engineering.* ASCE. **117**, No. 1, 89-107.

Wheeler, S.J., Sharma, R.S., and Buisson, M.S.R. (2003). "Coupling of hysteresis and stress–strain behaviour in unsaturated soil." *Géotechnique.* Vol. 53, No. 1, 41–54.

Wu, S., Gray, D.H., and Richart, F.E., Jr. (1984). "Capillary effects on dynamic modulus of sands and silts." *Journal of the Geotechnical Engineering Division, ASCE,* Vol. 110, No. 9, 1188-1203.

Znidarcic, D., Illangasekare, T. and Manna, M. (1991). "Laboratory testing and parameter estimation for two-phase flow problems." *Proceedings of*

the Geotechnical Engineering Congress. Boulder, CO. McLean, Campbell and Harris, Eds. ASCE. New York. 1078-1089.

APPENDIX A

Validation of the Effective Stress Concept for Unsaturated Compacted Soils

A.1 Introduction

This Appendix summarizes an experimental methodology to define relationships between p_s and ψ using drained multistage triaxial tests on a single soil specimen under a net confining pressure. Results from this testing methodology are used to evaluate the application of the degree of saturation of the soil as the effective stress parameter χ in the definition of suction stress. This definition of χ was selected because the value of S_r is not only known at the beginning of each shearing stage, but any changes in S_r during shearing can be estimated from any changes in the measured water levels in the burettes. Multistage shearing tests have been used with some success to define the shear strength of unsaturated residual soils in triaxial tests (Ho and Fredlund 1982; Rahardjo et al. 1995) and in direct shear tests (Gan and Fredlund 1988). Triaxial tests are particularly suitable for compacted soils under unsaturated conditions

as they typically reach peak strength values before significant distortion of the specimen.

A.2 Material Properties and Sample Preparation

In order to validate the effective stress concept in compacted soils, a mix of mortar sand and Bonny silt was used to define the relationship for the effective stress of unsaturated compacted soils. Mortar sand is a commonly used sand in geotechnical testing (Morrison 2006; Lee 2010), while Bonny silt is obtained from the borrow source for the Bonny Dam on the Colorado-Kansas border. The reason for using a soil mixture in this chapter was to increase the hydraulic conductivity of the Bonny silt to expedite the validation tests. A higher hydraulic conductivity expedites the process of multistage shearing for unsaturated soils. The grain size distribution of the soil mixture used in this chapter is shown in Figure A.1.

The soil of sand and silt used classifies as SM according to the USCS classification scheme. Prior to compaction, the sand and silt were mixed at a gravimetric water content of 12% representing the optimum ater content of the soil specimen and placed in a sealed plastic bag for 24 hours to allow the water content to homogenize. Static compaction was then used to prepare 142.2 mm-tall specimens to a target dry density of 18.1 kN/m^3 (a void ratio of 0.44).

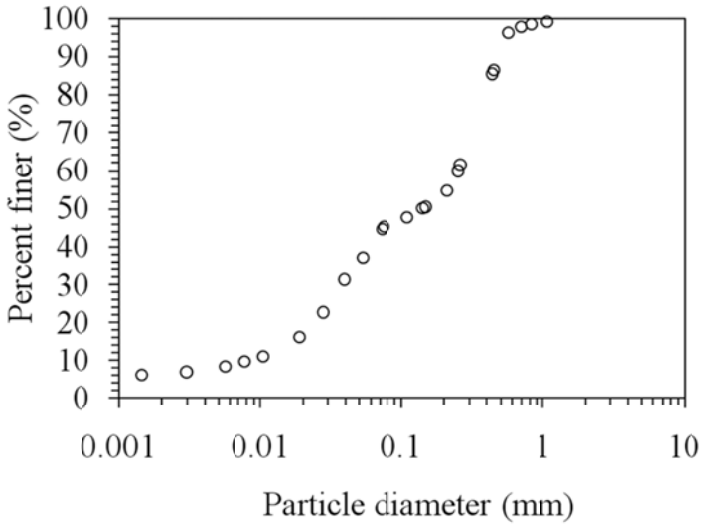

Figure A.1: Grain size distribution of the soil mixture

Specifically, a manual press was used to compress the soil within a 71.1 mm-diameter split mold in five 28 mm-thick lifts. The lifts were carefully scarified to obtain uniformly compacted specimens. Before performing multistage triaxial testing on this soil, a series of consolidated-undrained triaxial tests with pore pressure measurement were performed on saturated soil specimens under mean effective stresses of 50, 100, 150 and 200 kPa, following ASTM D4767. The stress-strain curves are shown in Figure A.2(a) and the excess pore water pressure response is shown in Figure A.2(b).

The excess pore water pressures indicate that the soils have a transition in behavior near the maximum preconsolidation stress induced by compaction. The stress paths shown in Figure A.3 indicate that the tests under different mean effective stresses converge on a single CSL.

Consistent with the excess pore water pressure response, the compacted specimens tested under lower consolidation stresses have stress paths similar to over-consolidated soils, while those under higher consolidation stresses have transitional behavior closer to that of normally consolidated soils. The slope of the CSL in this figure is M = 1.4, which corresponds to an effective friction angle of 34.7°.

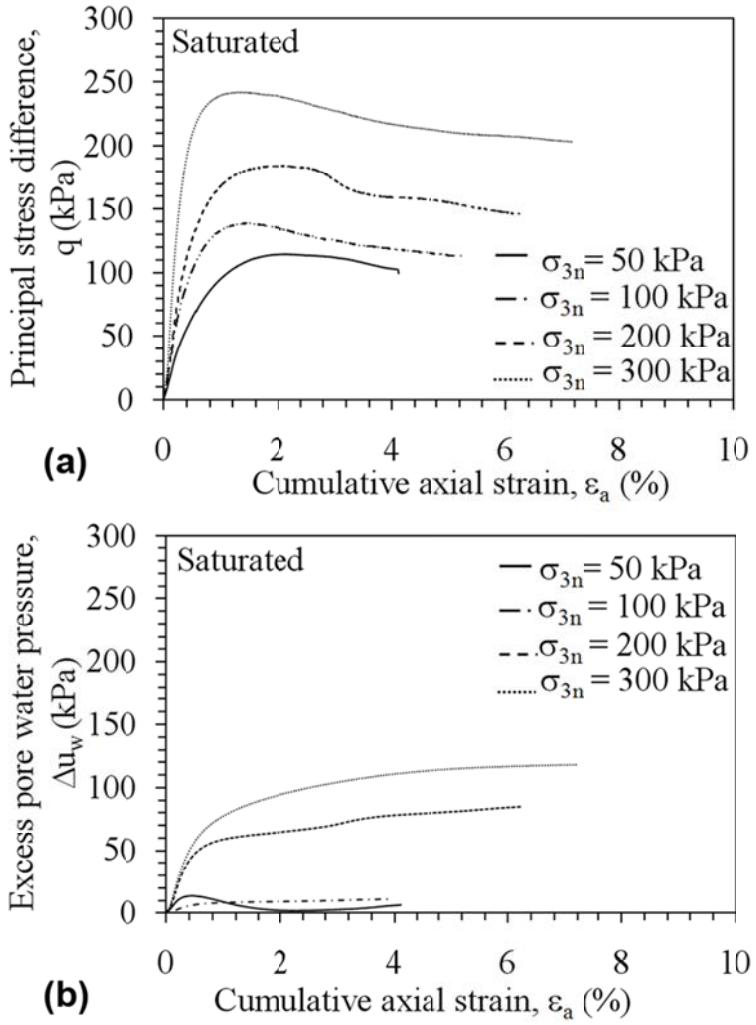

Figure A.2: Shear strength results for saturated specimens subjected to different net confining pressures: (a) Principal stress difference vs. axial strain; (b) Pore water pressure vs. axial strain

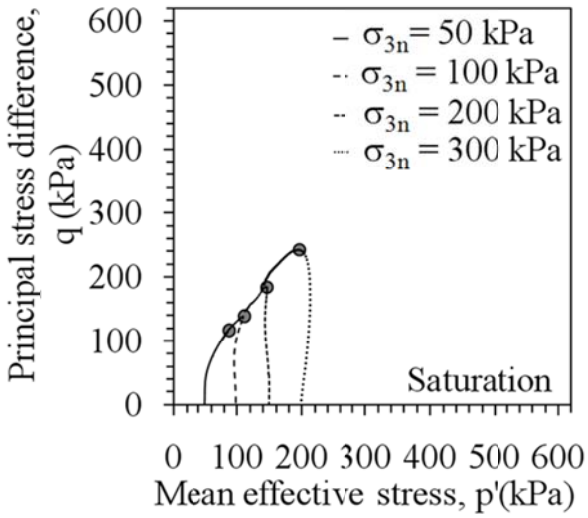

Figure A.3: Stress paths in the p´-q plane for saturated soil specimens subjected to different stress state conditions

A.3 Experimental Setup

A schematic of the triaxial cell and pressure control system used for shearing of unsaturated soils is shown in Figure A.4. The axis translation technique was used in this chapter to control suction in the specimen, which involves independently controlling the pore air and water pressures in a soil specimen through porous disks having different porosities (Hilf 1956). Specifically, air pressure is applied to the top of the specimen though a coarse porous disk and water pressure is applied to the bottom of the specimen through a ceramic disk having an air-entry suction of 100 kPa.

Ceramic disks having higher air-entry suctions were evaluated in preliminary tests, but the disk having air-entry suction of 100 kPa was found to permit the fastest rate of drainage from the soil specimen while

still having a sufficiently high air entry suction investigate the behavior of the soil specimen above and below its air entry suction. An approach was used in this study to implement the axis-translation in a conventional triaxial cell without major modification. Specifically, a bottom platen having a diameter of 76 mm, slightly greater than that of the soil specimen, was first installed in the triaxial cell. A piece of thin steel mesh having high permeability was then placed atop the platen, which was used to ensure a uniform distribution of water from the bottom platen to the overlying ceramic disk and to prevent stress concentrations near the ports in the bottom platen which may cause the overlying ceramic to crack.

Next, the high air-entry ceramic disk, also having a diameter of 76 mm, was placed atop the water distribution disk. The soil specimen having a diameter of 71.1 mm was then placed directly atop the ceramic disk. When a latex membrane was placed around the soil specimen, ceramic disk, and bottom platen, and a confining pressure was applied to the cell, a hydraulic seal was obtained between the membrane and the top of the disk. Specifically, the overlap in diameters was found to prevent air from short-circuiting past the ceramic disk during axis translation techniques. For additional security under low confining pressures, an "O"-ring was placed around the latex membrane on the ceramic disk.

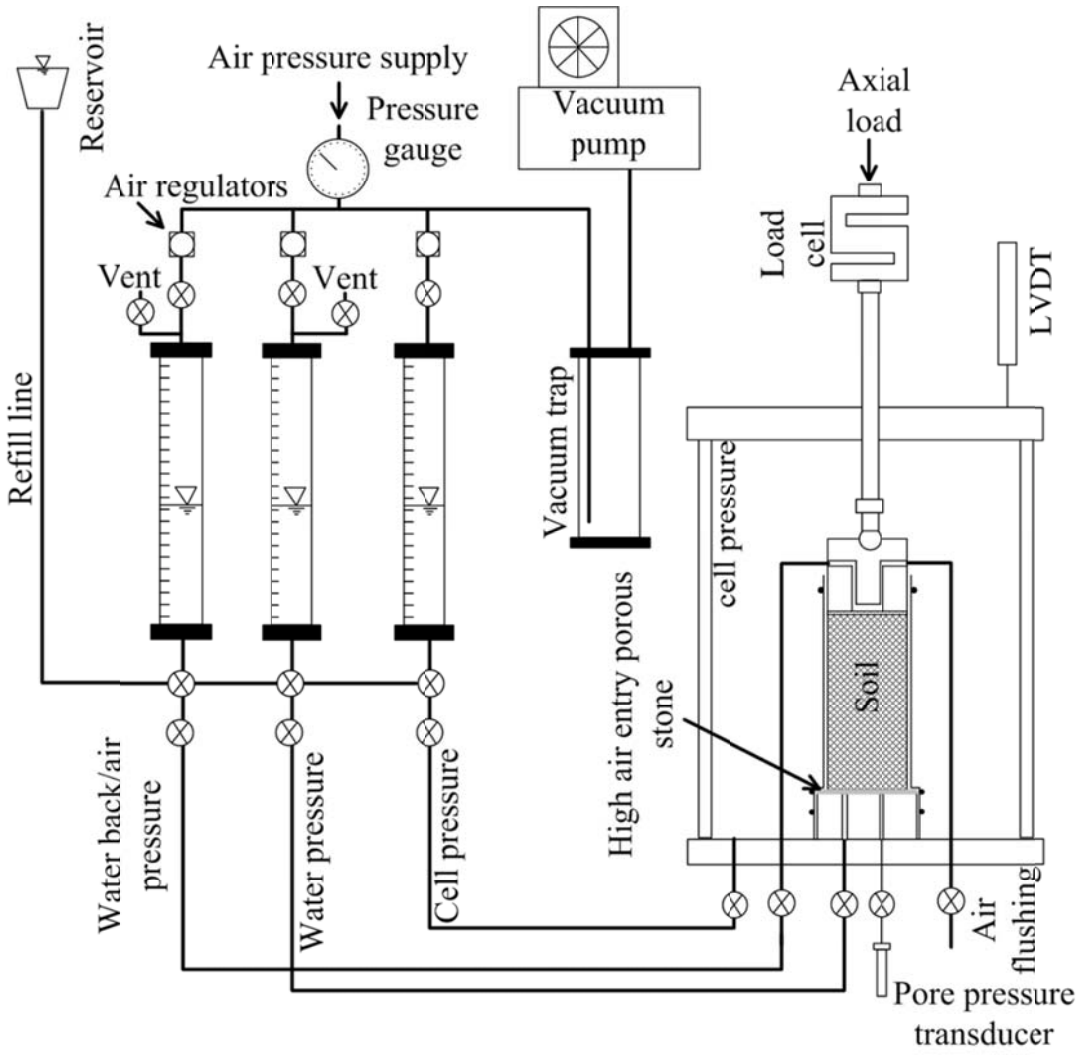

Figure A.4: Schematic of the experimental setup used for multistage testing of unsaturated soils

In this test setup, water flow from the specimen during both shearing and during application of increments of matric suction was measured using visual observation of the water level in graduated burettes connected to the water drainage lines from the specimen and cell pressure, as shown in Figure A.4. The pore water pressure in the axis translation technique needs not be zero as the suction is equal to the difference in the air and water pressure. As will be explained, the tests

were performed under backpressure saturation, which permits accurate outflow measurements using visual observations.

A Brainard-Kilman Model S-600 triaxial load frame was used to apply axial loads to the triaxial cell piston. This frame is appropriate for performing constant displacement rate test, but does not have force-displacement feedback capabilities. Although a constant displacement rate was used, the axial displacement during shearing was also measured using an LVDT and a load cell was used to record axial loads applied to the specimen during shearing. In the case of saturated shear strength tests or constant water content tests, a pore water pressure transducer connected to the bottom of the specimen was used to track changes in the water pressure of the specimen during the application of loading.

A.4 Experimental Procedure

The testing methodology in this study involves loading-unloading multistage tests on soils under successively higher suction increments (i.e., drying tests). Two values of net confining pressure σ_{3n} of 100 and 150 kPa were used to demonstrate the difference in behavior for different stress levels. After the soil specimen was prepared within the triaxial cell, a high vacuum pump was used to apply a vacuum with a magnitude of -80 kPa to the soil specimen and all plumbing lines for approximately one hour to void the specimen of air. During this time, the cell was assembled around the specimen. A cell pressure σ_3 of 20 kPa was applied

to the cell as a seating pressure. De-aired water from the backpressure reservoirs was then introduced into the bottom platen to saturate the ceramic disk, soil specimen, top platen, and all supply lines from the bottom up. During this upward flow of water, de-aired water was flushed through both chambers of the pressure transducer as well as all valves and tubes to ensure that the system is fully water-saturated. The cell pressure was then increased to 70 kPa and the backpressure was increased to 40 kPa, corresponding to an initial mean effective stress of 30 kPa. After ensuring that the volume of the specimen inferred from the water level in the burette connected to the cell remained constant, the cell pressure and backpressure were increased in stages to 520 kPa and 490 kPa, respectively, maintaining an effective stress equal to 30 kPa. Skempton's (1961) B-value parameter was checked during this process to evaluate the initial saturation of the specimen. A minimum B-value of 0.95 observed for the tests presented in this study.

After this initial saturation process, the cell pressure was increased to reach a desired initial effective confining pressure. When consolidation of the soil specimen under the desired effective confining pressure was finished, air under the same pressure as the water backpressure (490 kPa) was then flushed through the top platen and all drainage lines connected to the top of the specimen. At this point, the initial effective confining pressure is equal to the net confining pressure σ_{3n}, and this

value is held constant through the rest of the test (i.e., the cell pressure σ_3 and the pore air pressure u_a are held constant throughout all stages of the multistage test).

A series of unsaturated multistage consolidated drained (CD) tests were then conducted at different net confining pressures and matric suctions. The matric suction was then increased to a value of 7 kPa by lowering the pore water pressure u_w applied to the bottom of the specimen. Water outflow from the specimen during application of this and subsequent increments of matric suction was measured through the graduated burettes, and sufficient time was permitted to reach hydraulic equilibrium throughout the height of the specimen (i.e., when outflow from the specimen ceased). The first stage of shearing was then started by imposing a constant displacement rate of 0.005 inches per minute to the piston. This value was selected based on the value of t_{50} for this soil calculated from the outflow data from the consolidation data. Monitoring of the pore water pressure generated in the specimen during shearing indicates that this rate of strain was low enough to a constant rate of dissipation of extra pore water pressure generated during shearing (Gibson and Henkel 1954). At each stage of shearing, drainage of both air and water was permitted and volume change of the specimen was measured by recording the water outflow from the bottom of the specimen and from the cell (i.e., redundant measures).

One of the important contributions of the multistage testing methodology in this study is the criterion for stopping a shearing stage. While it is important to reach stress path tangency to ensure that each point is representative of failure, it is also undesirable to accumulate too much strain in the specimen. Most previous multistage testing programs relied primarily on observations of the maximum principal stress difference during testing. In this study, the criterion for stopping the test was the point at which the maximum principal stress difference reaches a value corresponding to an intersection between the effective stress path and the critical state line (CSL). If shearing were continued after reaching the CSL, plastic strains would accumulate during each stage, while reversing too soon would produce lower than actual strengths. Because the slope of a drained triaxial compression test is known, the only two pieces of information needed to define this intersection point are the slope of the CSL and the initial effective stress in the soil specimen. This study assumes that the CSL is unique, and is the same for both saturated and unsaturated soils, an assumption which has been well validated (Khalili et al. 2004; Khalili and Zargarbashi 2010). Although the CSL was measured for saturated specimens of the soil mixture used in this study, the slope of the CSL can also be estimated from empirical relationships based on the index properties of a soil.

The other variable needed for the stopping criterion is the value of the mean effective stress p' at the beginning of a drained triaxial compression stage. Because the degree of saturation is known at all stages in this triaxial test, it was used to estimate the effective stress parameter χ. The residual volumetric water content was not known for this soil mixture, so the approach of Lu et al. (2010) using the effective saturation could not be used, and the air-entry suction was also not known a-priori (i.e., the SWRC of the soil mixture was not known prior to the shear strength test), so the empirical equation for χ of Khalili and Khabbaz (1998) could not be used. Accordingly, by assuming that $\chi = S_r$, the maximum principal stress at which the specimen should be on the CSL can be estimated. One issue with using $\chi = S_r$ in a stopping criterion is that changes in the degree of saturation due to outflow of water will lead to a change in the degree of saturation, even though the test is in drained conditions. However, it was observed that the volume of water flowing out of the specimen during the shearing stages did not lead to a significant enough change in the degree of saturation to lead to a deviation in the stress path.

Using this criterion, the specimens were unloaded after reaching the intersection points corresponding to the CSL and the initial effective stress. During unloading, water outflow and displacement were continuously monitored. After reaching a principal stress difference of 10 kPa, unloading was stopped in order to prevent the piston from losing

contact with the specimen. After ensuring that the specimen had reached equilibrium, a higher increment of matric suction was applied to the specimen to start the next stage of loading. Through all stages of the multistage shearing tests, the volume of water withdrawn from the specimen to reach equilibrium (no flow) conditions was recorded to define changes in volumetric water content (and degree of saturation) of the soil specimen. The outflow data was also used to define points on the SWRC.

A.5 Results

The SWRC data obtained from the multistage triaxial tests on two soil specimens under net confining pressures of 100 and 150 kPa are shown in Figure A.5. The van Genuchten (1980) SWRC model was fit to each set of data, with the fitting parameters α_{vG} and N_{vG} reported in the figure. The SWRCs for different net confining pressures were observed to differ in shape, with the soil specimens subjected to a higher net confining pressure having a higher air entry suction. This observation may be due to the effect of σ_{3n} on the pore size distribution of the soil specimens subjected to higher σ_{3n}. Ng and Pang (2000) and Ng et al. (2009) observed a shift in the pore-size distribution of soils during application of higher stresses, leading to a similar change in the shape of the SWRC. Although the two specimens under σ_{3n} values of 100 and 150 kPa in this study only had a small difference in porosity, the first shearing stage in each test may have changed the pore size distribution in different ways. The

difference in the SWRCs noted in this study emphasizes the importance of soil-specific testing to evaluate relationships between p_s and ψ, as it may not be appropriate to use the SWRC obtained under a given σ_{3n} to other values of σ_{3n} when predicting the value of χ from the degree of saturation or effective saturation (Gallipoli et al. 2003; Wheeler et al. 2003; Tamagnini 2004; Nuth and Laloui 2008; Lu et al. 2010).

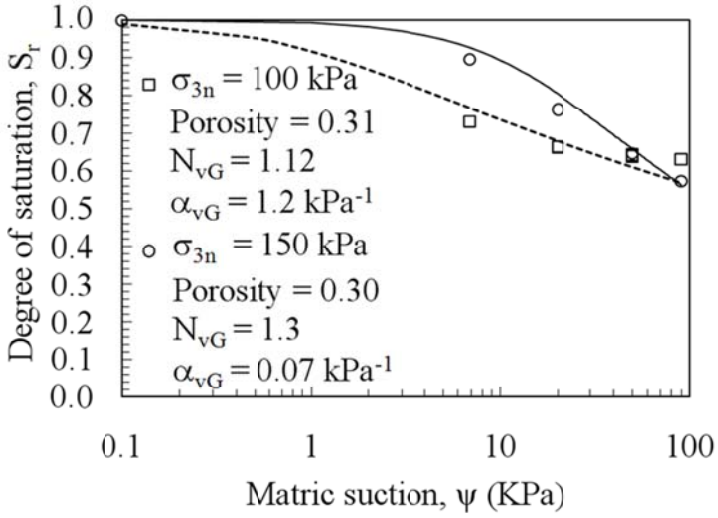

Figure A.5: SWRC of soil specimens subjected to different net confining pressures

The principal stress difference q as a function of axial strain from the drained unsaturated multistage shear tests for specimens subjected to net confining pressures of 100 and 150 kPa are shown in Figures A.6(a) and A.6(b), respectively.

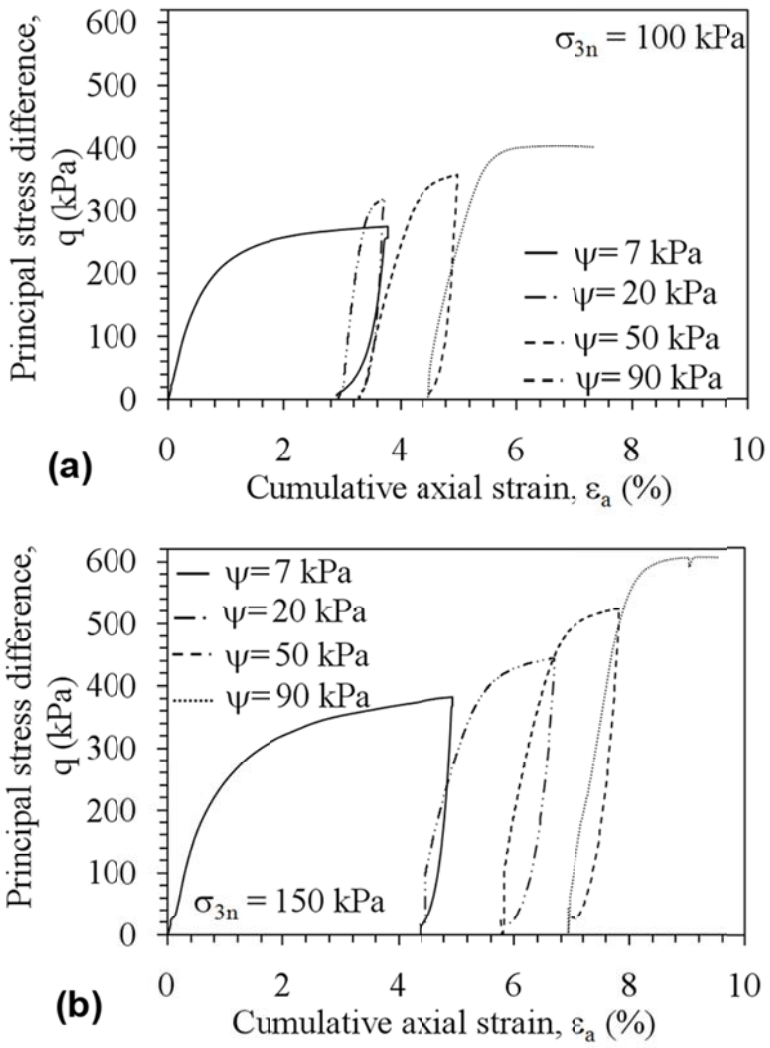

Figure A.6: Principal stress difference vs. cumulative axial strain for different conditions: (a) σ_{3n} = 100 kPa; (b) σ_{3n} = 150 kPa

Evaluation of the maximum principal stress difference data using the criterion for stopping each loading stage indicates that a clear peak value was obtained during each shearing stage. An increase in the maximum principal stress difference was observed for each successive increase in suction, and the values obtained under σ_{3n} = 150 kPa were consistently higher than those obtained under σ_{3n} = 100 kPa. The volumetric strain

measured as a function of axial strain is shown in Figures A.7(a) and 4.7(b) for the tests under net confining pressures of 100 and 150 kPa, respectively.

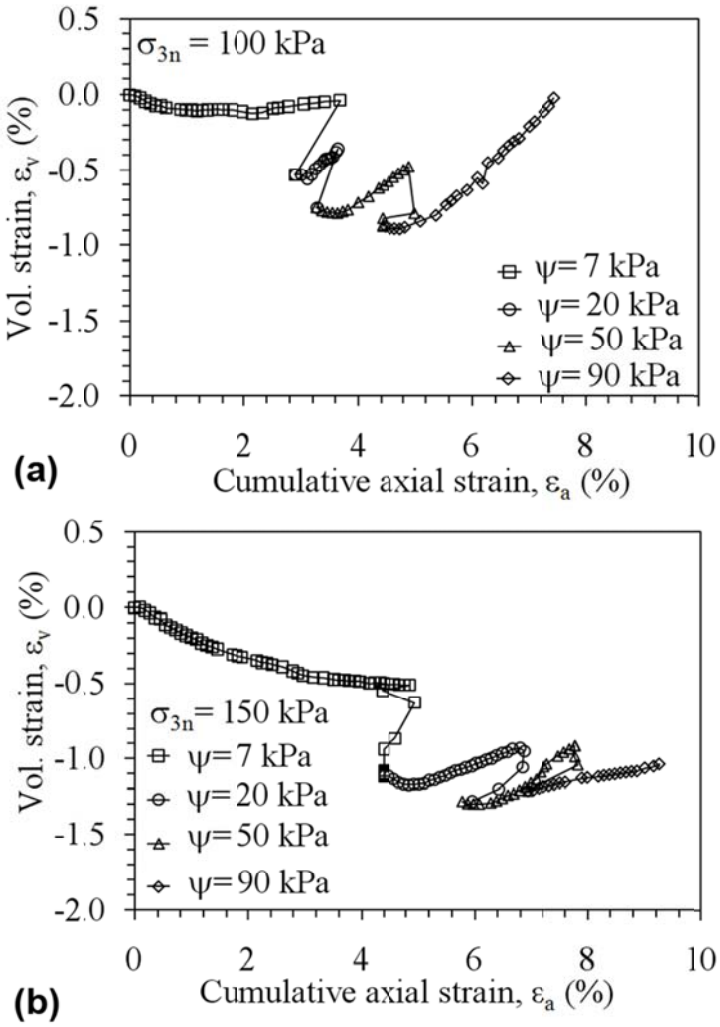

Figure A.7: Volumetric strain vs. axial strain results: (a) σ_{3n} = 100 kPa; (b) σ_{3n} = 150 kPa

The volumetric strain was measured from the burette connected to the cell pressure line. The same trend was noted in both tests for the cumulative volumetric strain, with greater volumetric strain noted for the

test under higher net confining pressure. The test performed under higher net confining pressure showed behavior more typical of dense or over-consolidated soils (greater dilation). The effect of increasing matric suction on the magnitude of volumetric strain was lower for the specimen tested under higher net confining pressure.

A.6 Analysis

The use of the multistage triaxial testing herein has enabled an evaluation of the impact of suction stress-matric suction relationship on the effective stress. The drained stress paths for the unsaturated soil specimens tested under net confining pressures of 100 and 150 kPa are shown in Figure A.8. In these figures, the mean effective stress was defined using Eq. (2.7) with a value of χ equal to S_r.

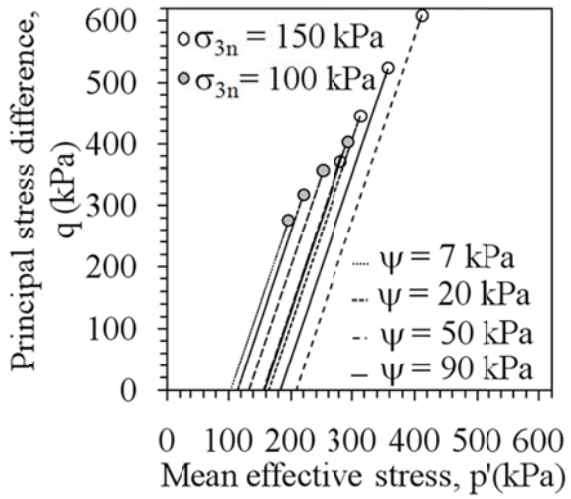

Figure A.8: Stress paths in the p´-q plane for unsaturated soil specimens subjected to different net confining pressures

A plot of the principal stress differences measured at the end of each stage of the unsaturated multistage triaxial tests versus the value of p' at failure calculated using Eq. (2.7) with $\chi = S_r$ is shown in Figure A.9, along with the points of stress-path tangency for saturated soils obtained from the saturated CU stress paths in Figure A.3.

The failure points were observed to all fall on a single CSL indicating the efficiency of the use of degree of saturation for the definition of the effective stress parameter for unsaturated soils. The slope of the CSL, M, was used to back-calculate the suction stress p_s of the soil at the different values of ψ for each stage of the test, as follows:

$$p_s = \frac{\left(1 - \frac{M}{3}\right) q - M \sigma_{3n}}{M} \qquad (A.1)$$

where q is the principal stress difference at failure and σ_{3n} is the net confining pressure defined as $\sigma_{3n} = \sigma_3 - u_a$. The relationships between p_s and ψ for the soil mixture under net confining pressures of 100 and 150 kPa are shown in Figure A.10.

Based on the value of p_s inferred from Eq. (2.7), the relationships between p_s and ψ are different for the soil under the two net confining pressures.

This observation is likely due to the difference in the shapes of the SWRC of the specimens under different net confining stresses. As mentioned before, specimens under higher net confining stress show a greater water retention, which corresponds to a greater number of water

menisci between the particles. For the same value of matric suction, a specimen with greater water retention will have greater inter-particle contact stresses.

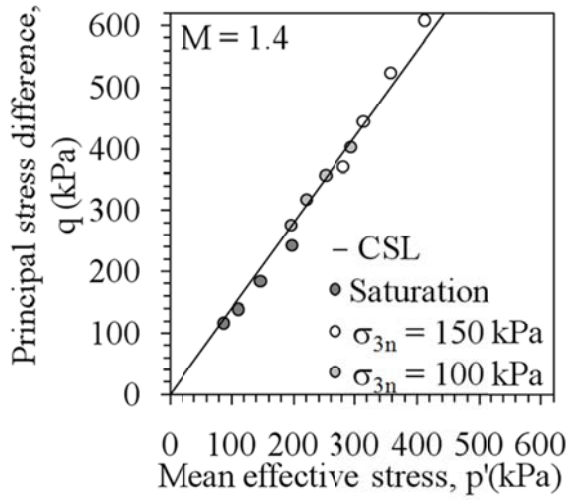

Figure A.9: Evaluation of the critical state line (CSL) for specimens under different conditions

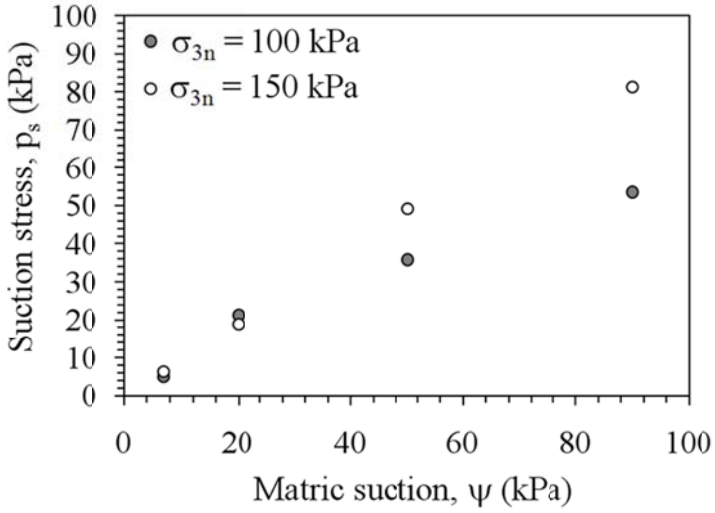

Figure A.10: Comparison of the relationships between suction stress and matric suction measured for soil specimens subjected to different net confining pressures

APPENDIX B

Calibration of the Resonant Column Test Device

B.1 Introduction

The Stokoe-type resonant column test apparatus because of its simplicity, relatively high available torque and access to the base of the specimen for ducting to allow isotropic effective stress has been found very advantageous especially for the purposes of testing stiff and hard geomaterials. In this test, the specimen is assumed to be elastic, homogeneous and isotropic with a fixed base pedestal and a drive system assumed as a lumped mass. Based on these assumptions, the shear wave velocity of the soil can be determined from the geometry of the soil specimen, measured resonant frequency and geometry of drive plate as follows (Richard et al. 1970):

$$\frac{I}{I_o} = \left(\frac{\omega_r L}{V_s}\right) tan\left(\frac{\omega_r L}{V_s}\right) \qquad (B.1)$$

where I is the mass polar moment of inertia of the specimen; I_o is the mass polar moment of inertia of the components mounted on top of the specimen (drive mechanism, accelerometer and counterweight masses and

top platen); ω_r is the circular frequency of the first torsional mode of vibration, L is the length of the specimen; and V_S is the shear wave velocity.

In Eq. (B.1), the value of I_o could be determined by measuring and weighing the various components of the drive head. However, because of the complex geometry of the drive head, it is traditionally measured using a calibration procedure by substituting a single, relatively flexible calibration bar, tested with three or four added masses for the soil specimen and measuring the resonant frequency of the system.

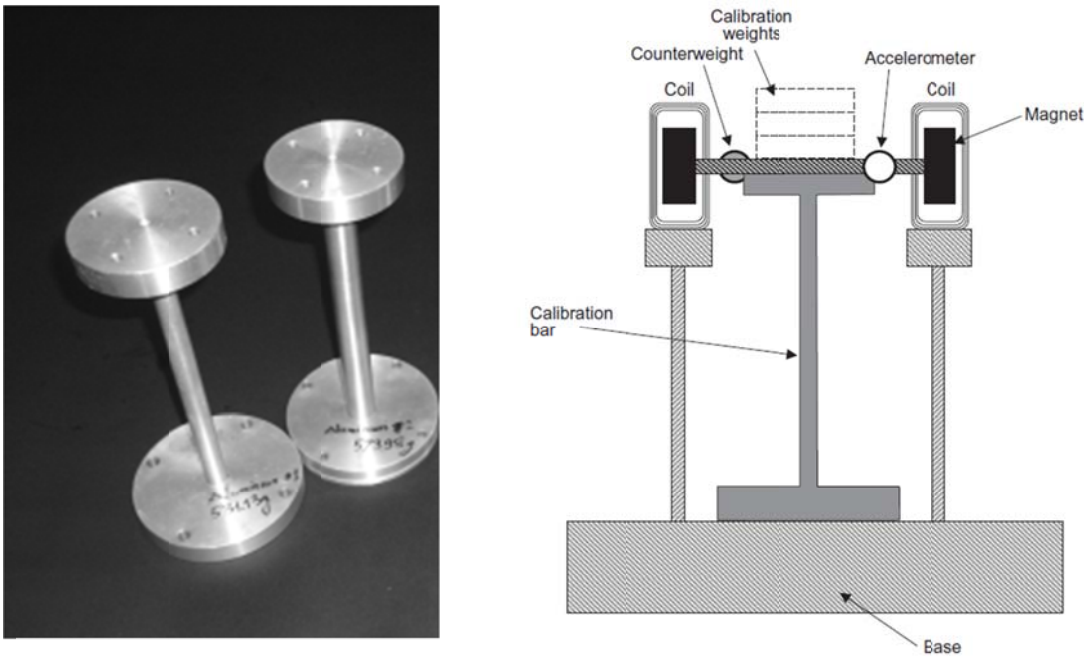

Figure B.1: The Calibration method for the determination of I_o of the drive plate in the Stokoe-type resonant column test device

In this method, the system is assumed as a torsional pendulum with a single degree of freedom, where the drive system is the pendulum mass

and the calibration bar is the torsional spring. With this assumption, the mass polar moment of inertia of the added masses is calculated as follows:

$$I = \frac{k}{\omega^2} - I_o \qquad \text{(B.2)}$$

where ω is the circular frequency of the system I is the mass polar moment of inertia of the added masses, k is the stiffness of the bar and I_o is the mass polar moment of inertia of the components mounted on top of the specimen (drive mechanism, accelerometer and counterweight masses and top platen). By plotting the values of I as a function of $\frac{1}{\omega^2}$, I_o is defined by the y axis intercept and k is represented by the gradient of the line. In this method, the polar inertia of the calibration rod stem is assumed to be negligible. As reported by Clayton et al. (2009) I_o for the calibration rods with a stem diameter less than 18 mm is almost constant.

B.2 Tests Results

In the University of Colorado at Boulder, the mass polar moment of inertia of the drive system of the Stokoe resonant column was measured using a calibration bar with the dimensions presented in Figure B.2. These dimensions have been chosen based on the observations by Clayton et al. (2009). The properties of the added masses are shown in Table B.1.

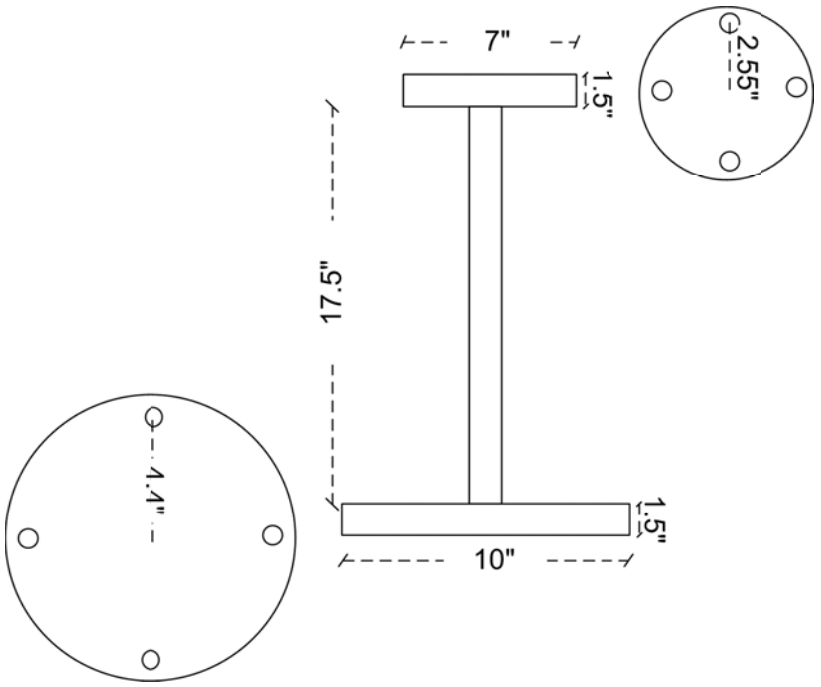

Figure B.2: Calibration bar used to measure the I_o value for the Stokoe resonant column

Table B.1: Properties of masses used to calibrate the Stokoe resonant column device.

No.	W (kg)	D (m)	H (m)	G(m)
#1	2.01287	0.05478	0.1069	7.93E+10
#2	0.36544	0.0622	0.04486	2.55E+10
#3	0.62921	0.03567	0.07125	4.47E+10

Results in this study show an I_o value of 0.00134 for the drive platen (Figure B.3) which is in the range of values reported by other researchers (Clayton et al. 2009; Pak et al. 2009) (Table B.2). There is a small difference between reported values of I_o which might be because of the

magnets used in the derive system. The drive system for the Stokoe resonant column consists of four magnets attached at the end of arms spaced equidistantly around the drive plate. These relatively heavy magnets, accounting for 75% of the mass of the drive system have important roles in measuring I_o.

Table B.2: I_o values reported by other researchers for the Stokoe resonant column drive platen.

Researcher	I_o (kg.m^2)
Clayton et al. (2009)	2.85E-03 (for the drive plate)
Pak et al. (2009)	1.83E-03 (drive plate and top cap)

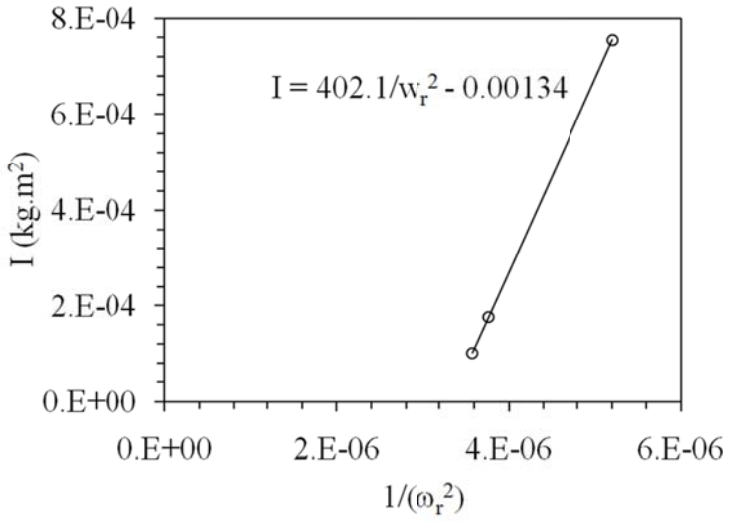

Figure B.3: Results of calibration of a Stokoe resonant column apparatus with a calibration bar of differing weights

The top cap in the RC device is a cylinder consisting of different materials. Therefore, its mass polar moment of inertia cannot be easily obtained. In this test, to measure I value of the top cap, an inverse calculation was used. Since I_o has been already obtained, the top cap is

considered as an added mass and then Eq. B.2 is used to measure the mass polar moment of inertia of the top cap (I_{tc}=2.12e-5). By defining I value for the drive plate and top cap, the mass polar moment of inertia of the drive system attached to the top of the specimen is obtained (I= I_0+I_{tc}=1.36e-3). A summary of the results are given in Table B.3.

Table B.3: Summary of calibration results for the Stokoe resonant column test device

Part	I (kg. m^2)
Drive plate	1.34E-03
top cap	2.12E-05
drive system	1.36E-03

APPENDIX C

A Predictive Relationship for the Air-Entry Suction of Unsaturated Soils

C.1 Introduction

Air entry value has been observed to play an important role in describing the behavior of unsaturated soils. The air entry value is usually selected from visual inspection of the SWRC and consequently, considerable error may occur in this process. In this part, using the methodology described by Vanapalli et al. (1998) (Figure C.1), a procedure for defining the air entry suction from the fitted van Genuchten (1980) SWRC. The procedure consists of the following steps:

Step 1. Fit the van Genuchten model (1980) to a set of experimental SWRC. The model is given by the following equation:

$$\theta = \theta_r + (\theta_s - \theta_r)(1 + (\alpha\psi)^N)^{-\left(1-\frac{1}{N}\right)} \quad \text{(C.1)}$$

In this equation, it can be assumed that $\theta_r = 0$. Therefore, the volumetric water content can be defined as:

$$\theta = \theta_s(1 + (a\Psi)^n)^{-\left(1-\frac{1}{n}\right)} \quad \text{(C.2)}$$

Since the SWRC is usually shown in a semi-logarithmic scale in the horizontal axis, Eq. (C.2) can be written in the form of:

$$\theta = \theta_s(1 + (\alpha exp(s))^N)^{-\left(1-\frac{1}{N}\right)} \quad \text{(C.3)}$$

where:

$$\psi = exp(s) \quad \text{(C.4)}$$

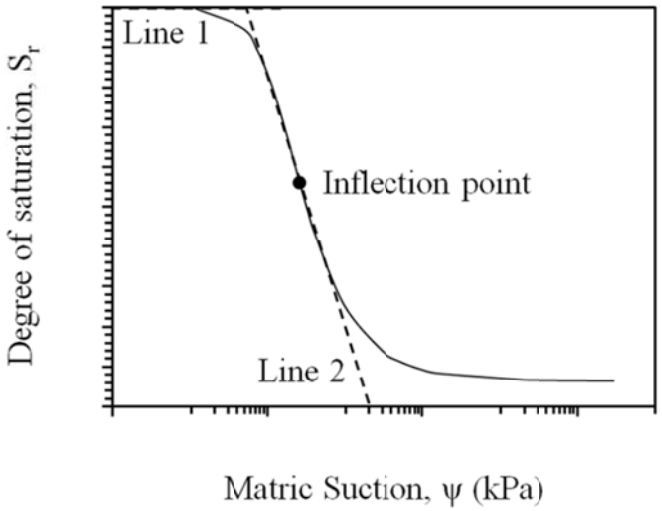

Figure C.1: An illustration of the steps to obtain the air-entry suction from the parameters of the SWRC (after Vanapalli et al. 1998)

Step 2. The equation for a line drawn tangent to the SWRC through the inflection point can be determined. The inflection point in which the slope of the SWRC has its maximum value is equal to the point at which the second derivation of Eq. (C.1) is zero.

$$\theta - \theta_{inf} = m\, ln\left(\frac{\psi}{\psi_{inf}}\right) \quad \text{(C.5)}$$

where m=dθ(s_{inf})/ds is the first derivation of Eq.(C.2) at the inflection point and θ_{inf} and ψ_{inf} are the volumetric water content and suction value at the inflection point, respectively, defined as:

$$\theta_{inf} = \frac{\theta_s}{\left(\frac{2N-1}{N-1}\right)^{1-\frac{1}{N}}} \quad \text{(C.6)}$$

$$\Psi_{inf} = exp\left(s_{inf}\right) = exp\left(-\left(\frac{N\,ln(\alpha) - ln\left(\frac{N}{N-1}\right)}{N}\right)\right) = \frac{1}{\alpha}\sqrt[N]{\frac{N}{N-1}} \quad \text{(C.7)}$$

Step 3. A horizontal line defined as Eq. (B.8) through the maximum volumetric water content can be drawn, having the equation:

$$\theta = \theta_s \quad \text{(C.8)}$$

Step 4. The intersection of the lines drawn in Steps 3 and 4 can be used as an estimate of the air-entry value.

Following these steps, an analytical expression for the air-entry suction can be defined as:

$$\psi_b = \left(\frac{1}{\alpha}\sqrt[N]{\frac{N}{N-1}}\right) exp\left(\frac{\left(\frac{2N-1}{N-1}\right)\left[\left(\frac{2N-1}{N-1}\right)^{1-\frac{1}{N}} - 1\right]}{(1-N)\sqrt[N]{\frac{N}{N-1}}}\right) \quad \text{(C.9)}$$

where α and N are the fitting parameters from the van Genuchten (1980) model.

C.2 Model Validation

Values of ψ_b, reported in the technical literature (Brooks and Corey 1964; Leong and Rahardjo 1997; and Vanapalli et al. 1998) were used to validate the predicted value of ψ_b from Eq. (C.9). Tables C.1 and C.2 summarize the van Genuchten (1980) SWRC parameters of soil specimens

and Figure C.2 shows the SWRC of different soils reported in literature data. In this figure, the van Genuchten (1980) SWRC fitting curves to data points are also presented.

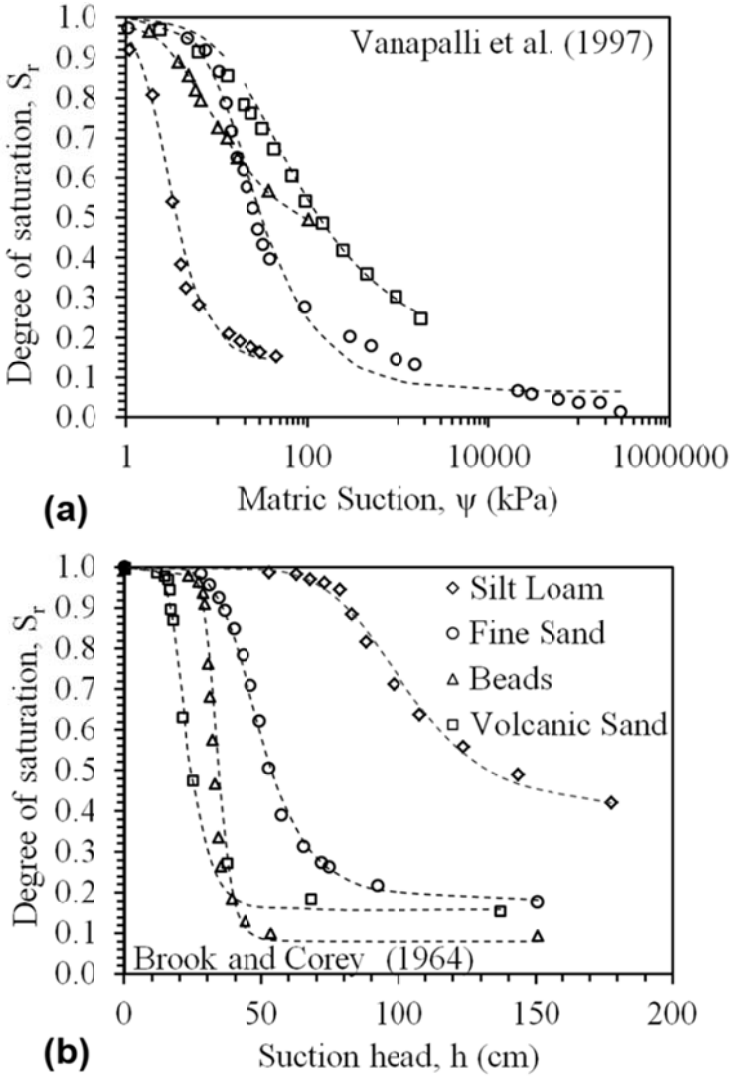

Figure C.2: SWRCs of different soils reported in literature

Table C.1: The van Genuchten (1980) SWRC parameters and a comparison between the air-entry values reported by Vanapalli et al. (1997) and Leong (1997) with those from the proposed model

Researcher	a	n	$S_{r(sat)}$	$S_{r(res)}$	$\Psi_{b\ (Exp.)}$ (kPa)	$\Psi_{b\ (Model)}$ (kPa)
Vanapalli et al.(1997)	0.42	2.70	0.37	0.14	1.08	0.99
	0.07	1.82	0.45	0.30	4.76	3.67
	0.22	1.67	0.43	0.49	1.77	1.14
	0.05	1.45	0.41	0.16	5.30	4.23
Leong et al. (1997)	0.05	4.20	0.40	0.07	10.90	11.65
	0.10	4.30	1.00	0.30	5.90	5.60

Table C.2: The van Genuchten (1980) SWRC parameters and a comparison between the air-entry values reported by Brooks and Corey (1964) and the proposed model

Researcher	a	n	$S_{r(sat)}$	$S_{r(res)}$	$h_{b(Exp.)}$ (cm)	$h_{b(Model)}$ (cm)
Brooks and Corey (1964)	0.01	6.90	1.00	0.40	75.00	72.99
	0.02	6.10	1.00	0.18	41.00	33.23
	0.03	13.00	1.00	0.08	29.00	28.38
	0.05	6.67	1.00	0.16	16.00	15.85
	0.02	9.56	1.00	0.60	54.00	51.01
	0.02	9.00	1.00	0.33	43.00	40.97
	0.04	7.08	1.00	0.30	17.20	15.84

The comparison between the predicted and measured air entry values shown in Figure C.3 follows a 1:1 relationship, indicating the validity of the proposed predictive relationship in Eq. C.9.

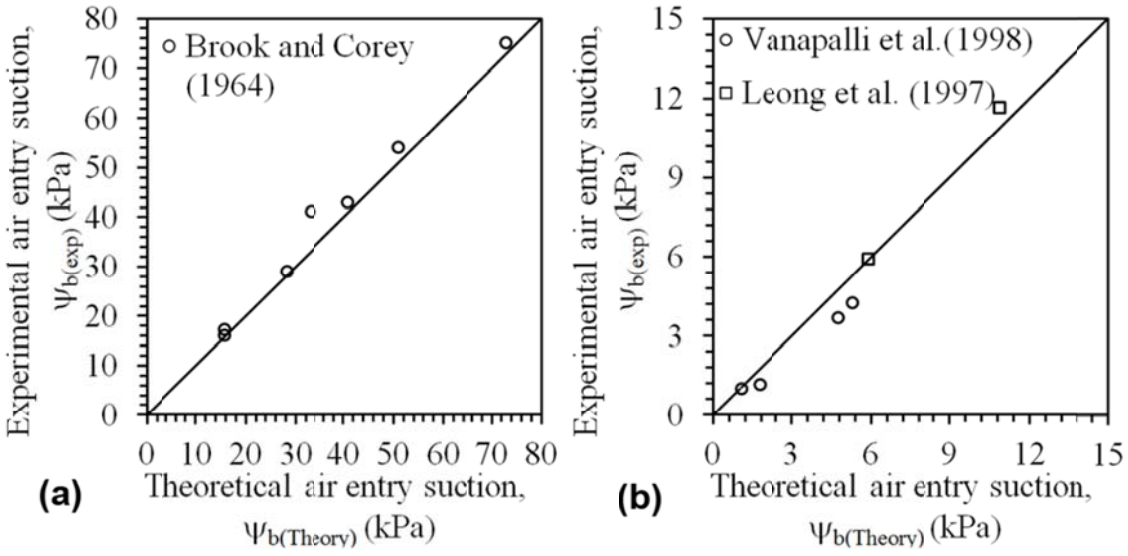

Figure C.3: Comparison between air-entry values estimated using the proposed empirical model [Eq. (C.9)] with those obtained experimentally for different USCS soil types

APPENDIX D

Raw Data

D.1 Raw data for specimen with e=0.69 and p_n=70 kPa

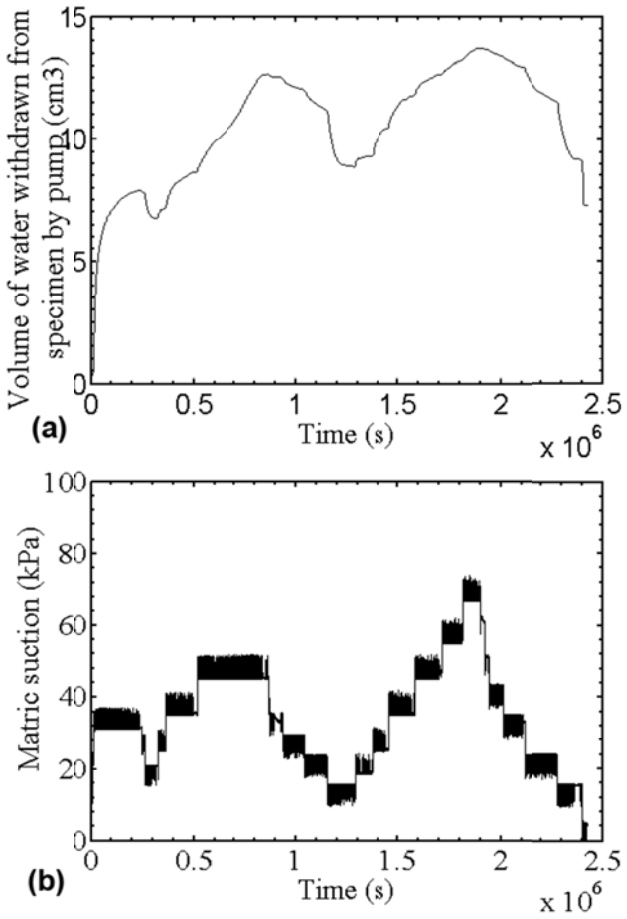

Figure D.1: (a): Variation in the volume of water extracted or injected by the flow pump during drying and wetting; and (b) Measured changes in matric suction at the outflow face of the soil specimen during wetting and drying

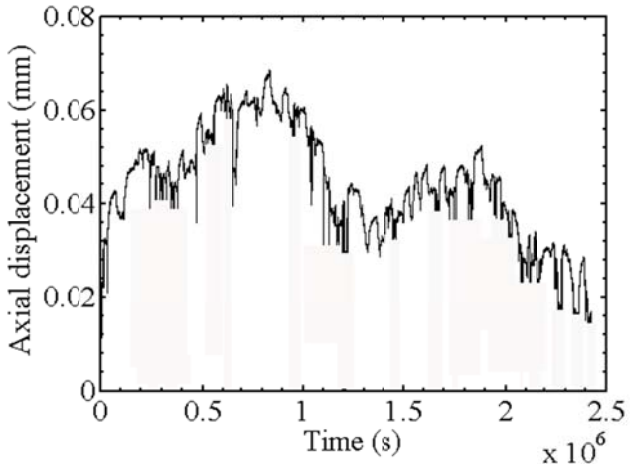

Figure D.2: Change in height during drying and wetting

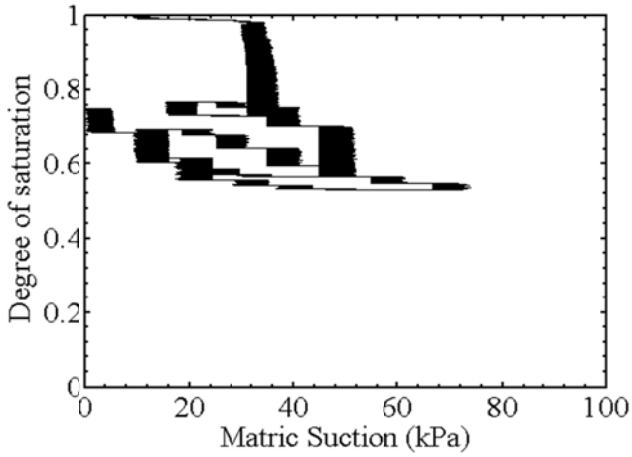

Figure D.3: The SWRC measured by the flow pump during drying and wetting

D.2 Raw data for specimen with e=0.69 and p_n=125 kPa

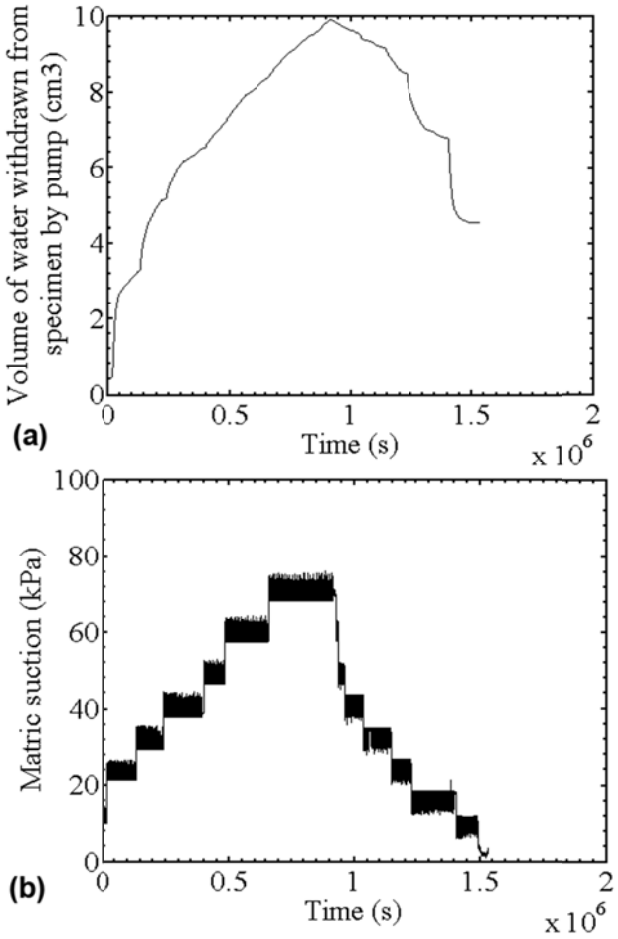

Figure D.4: (a): Variation in the volume of water extracted or injected by the flow pump during drying and wetting; and (b) Measured changes in matric suction at the outflow face of the soil specimen during wetting and drying

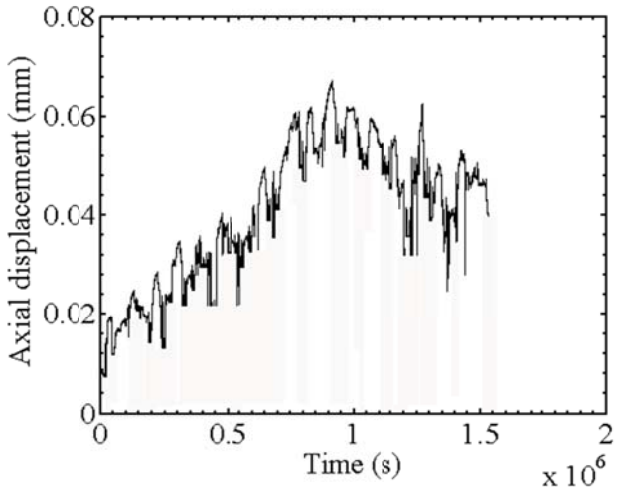

Figure D.5: Change in height during drying and wetting

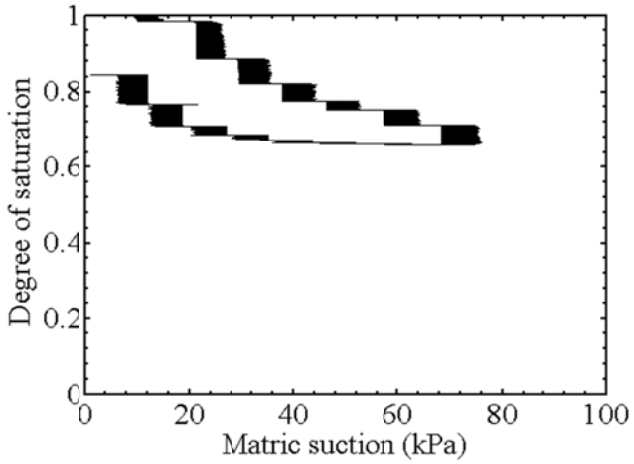

Figure D.6: SWRC measured by the flow pump during drying and wetting

D.3 Raw data for specimen with e=0.69 and p_n=175 kPa

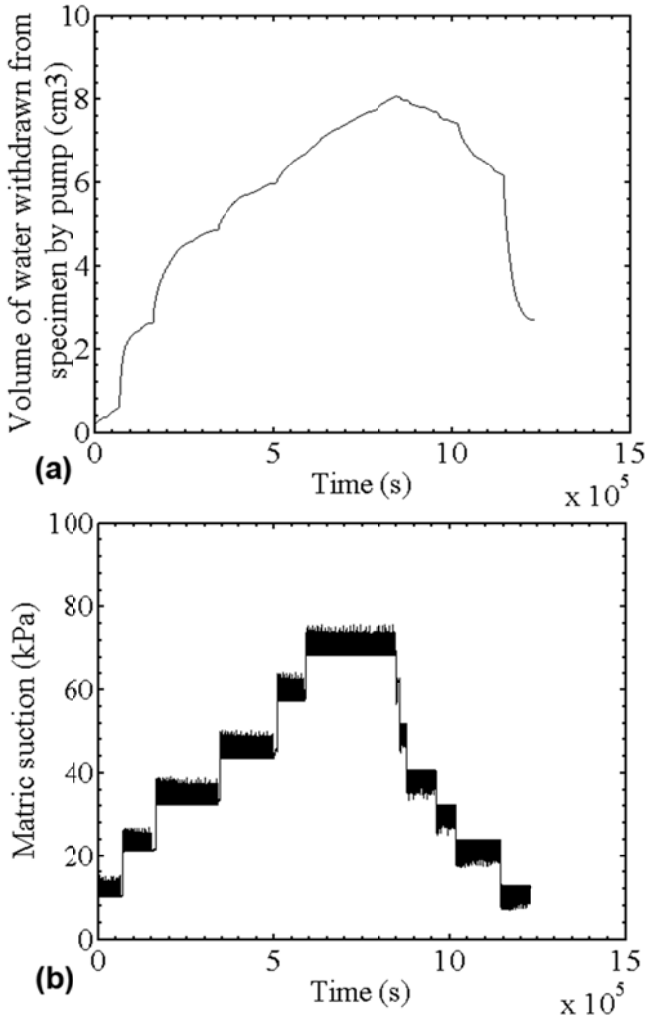

Figure D.7: (a): Variation in the volume of water extracted or injected by the flow pump during drying and wetting; and (b) Measured changes in matric suction at the outflow face of the soil specimen during wetting and drying

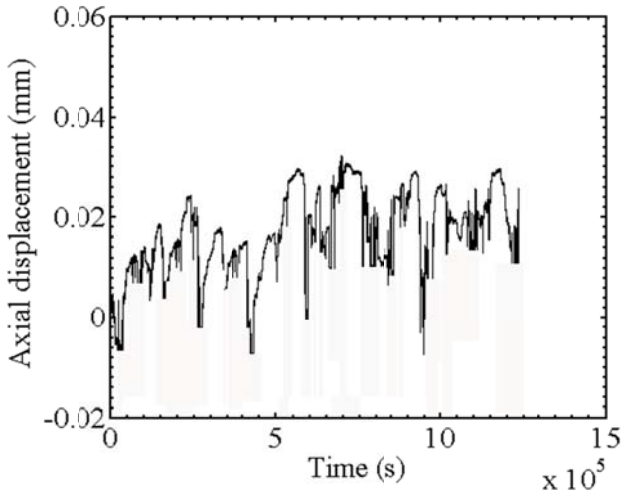

Figure D.8: Change in height during drying and wetting

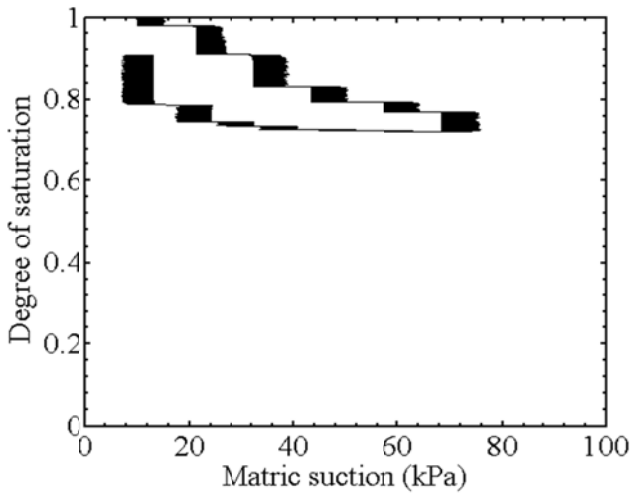

Figure D.9: SWRC measured by the flow pump during drying and wetting

D.4 Raw data for specimen with e=0.69 and p_n=225 kPa

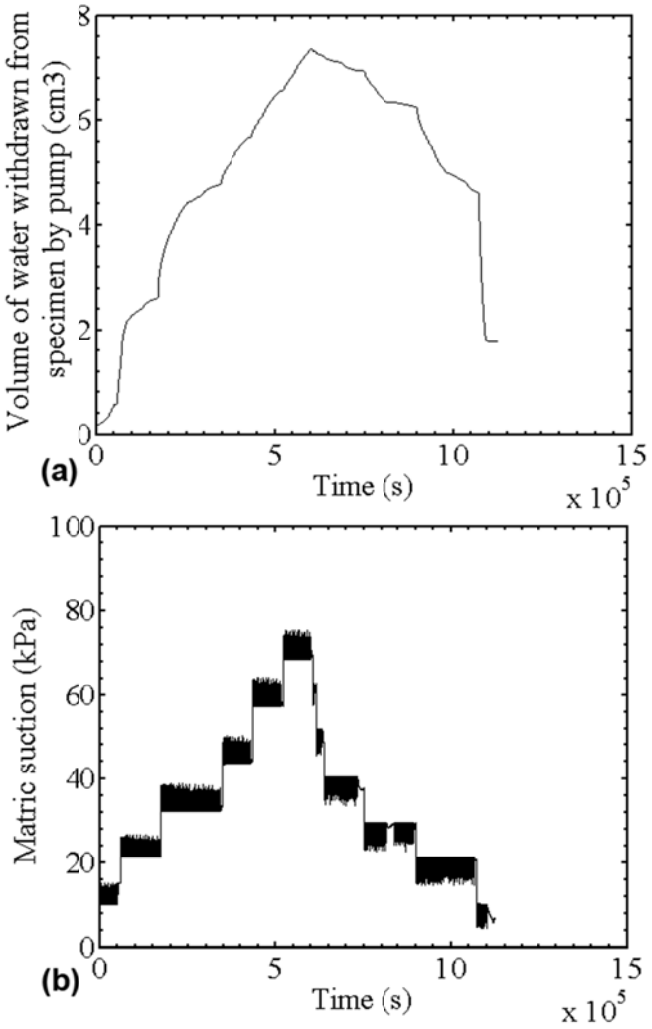

Figure D.10: (a): Variation in the volume of water extracted or injected by the flow pump during drying and wetting; and (b) Measured changes in matric suction at the outflow face of the soil specimen during wetting and drying

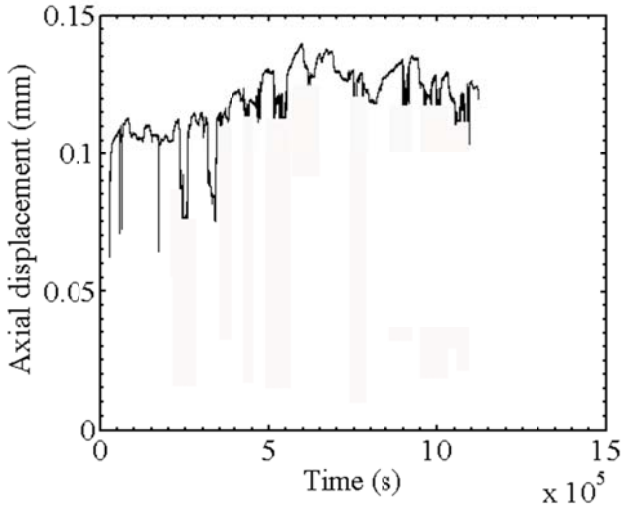

Figure D.11: Change in height during drying and wetting

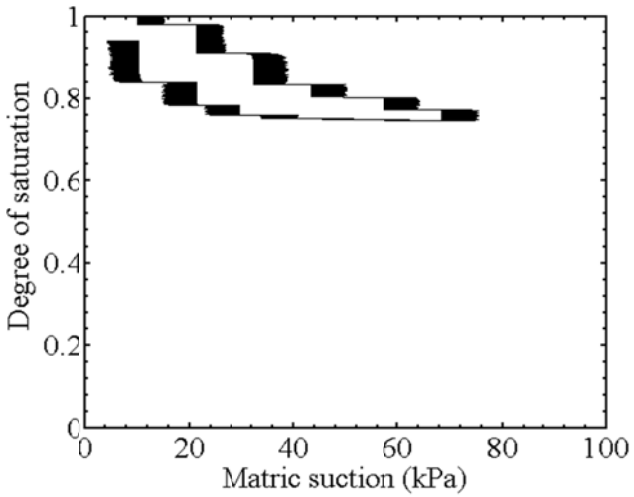

Figure D.12: SWRC measured by the flow pump during drying and wetting

D.5 Raw data for specimen with e=0.53 and p_n=150 kPa

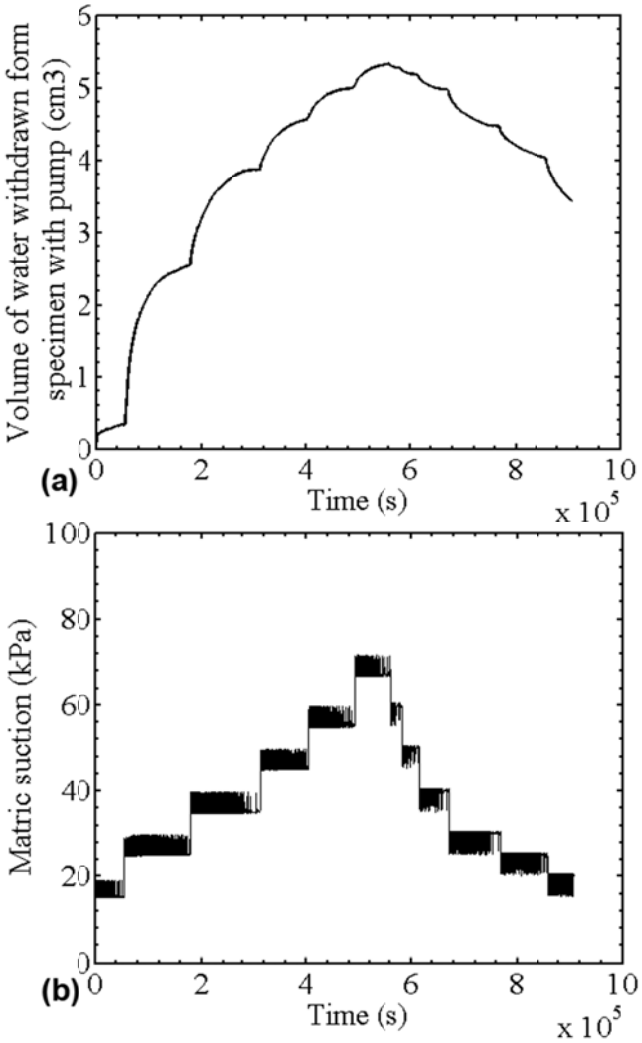

Figure D.13: (a): Variation in the volume of water extracted or injected by the flow pump during drying and wetting; and (b) Measured changes in matric suction at the outflow face of the soil specimen during wetting and drying

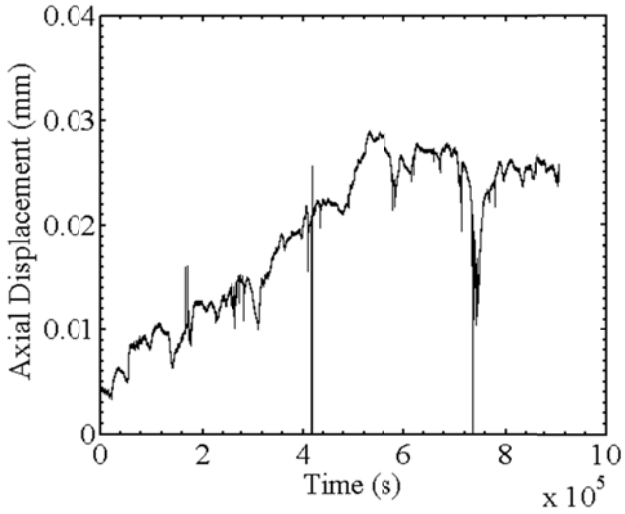

Figure D.14: Change in height during drying and wetting

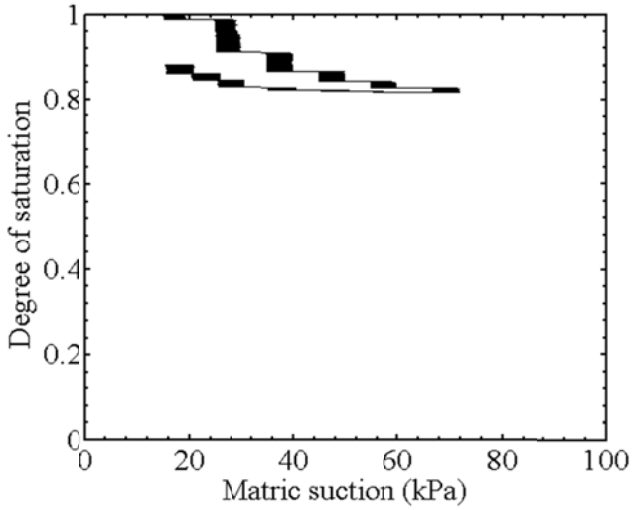

Figure D.15: SWRC measured by the flow pump during drying and wetting

D.6 Raw data for specimen with e=0.53 and p_n=200 kPa

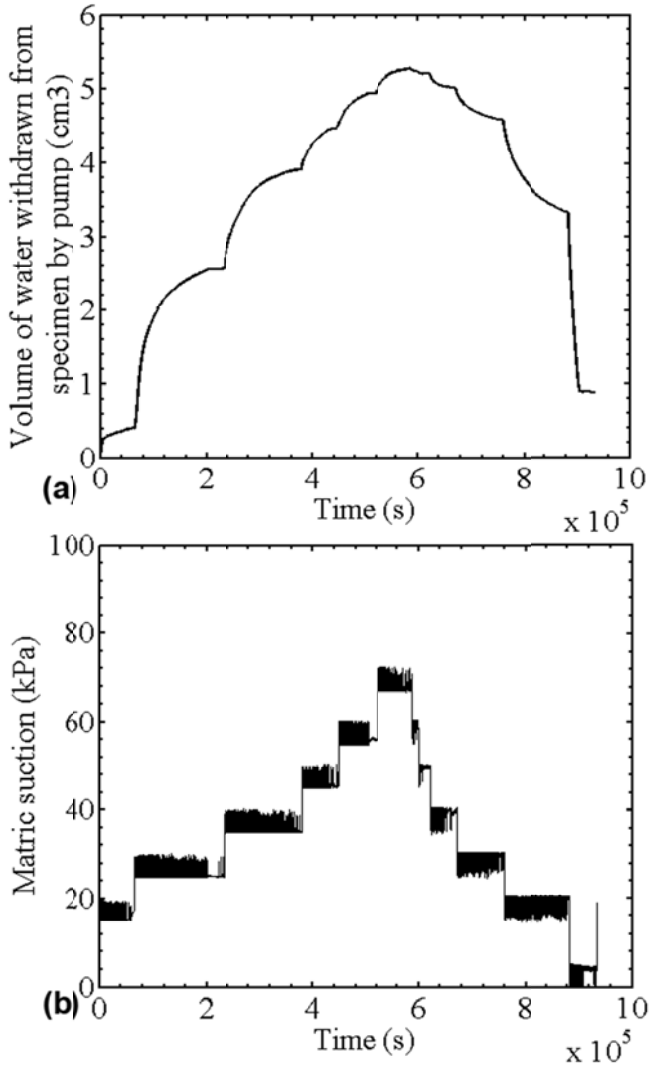

Figure D.16: (a): Variation in the volume of water extracted or injected by the flow pump during drying and wetting; and (b) Measured changes in matric suction at the outflow face of the soil specimen during wetting and drying

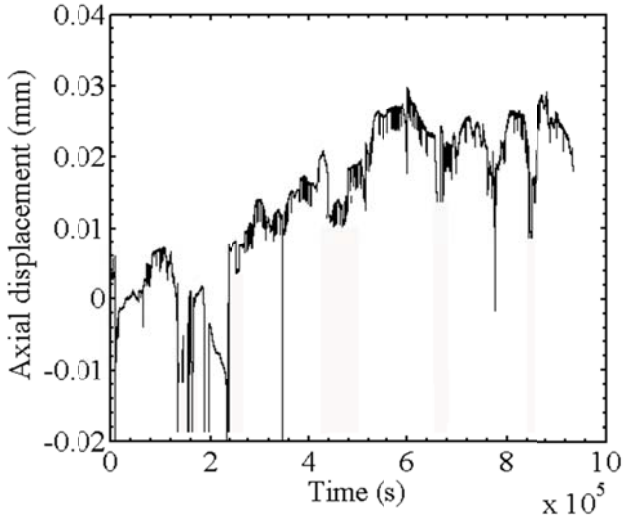

Figure D.17: Change in height during drying and wetting

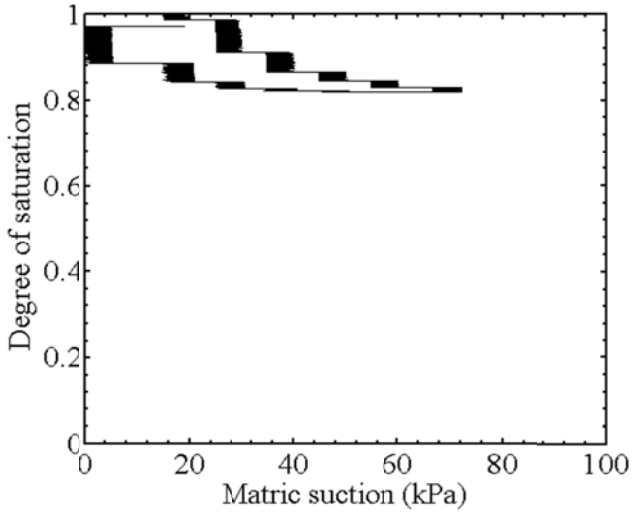

Figure D.18: SWRC measured by the flow pump during drying and wetting

APPENDIX E

MATLAB programs for data analysis

E.1 Program for the analysis of flow pump data

```
clc
clear all, close all;
[filename, pathname ] = uigetfile('*.lvm', 'Pick a data file')
fid = fopen([pathname, filename])
blank = fgetl(fid);
blank = fgetl(fid);
blank = fgetl(fid);
blank = fgetl(fid);
blank = fgetl(fid);
blank = fgetl(fid);
blank = fgetl(fid);
blank = fgetl(fid);
blank = fgetl(fid);
blank = fgetl(fid);
blank = fgetl(fid);
blank = fgetl(fid);
blank = fgetl(fid);
blank = fgetl(fid);
blank = fgetl(fid);
blank = fgetl(fid);
blank = fgetl(fid);
blank = fgetl(fid);
blank = fgetl(fid);
blank = fgetl(fid);
blank = fgetl(fid);
blank = fgetl(fid);

blank = fgetl(fid);
blank = fgetl(fid);
blank = fgetl(fid);
blank = fgetl(fid);
blank = fgetl(fid);
blank = fgetl(fid);
blank = fgetl(fid);
blank = fgetl(fid);
blank = fgetl(fid);
blank = fgetl(fid);
```

```
tempdata = fscanf(fid,'%g',[4,inf]);
tempdata=tempdata';
W= input('Enter the Weight:');
h= 2.84*2.54;
d= 1.4*2.54;
gs= 2.6;
w= .14;
V= h*3.14*d*d/4*1e3;
Ro= W/V*1e3;
e=  (gs*(1+w)/Ro)-1;
n= e/(1+e);
P0= -2.545;
Dis0= -0.0128*tempdata(1,3)*tempdata(1,3)-.2789*tempdata(1,3)+
.0085;
Dis= -0.0128*tempdata(:,3).*tempdata(:,3)-.2789*tempdata(:,3)+
.0085-Dis0;
pp0= tempdata(1,4);
PP= tempdata(:,4)-pp0;
Pdif=2.063+(tempdata(:,2)-P0)*55.56;
vp=792*(-PP)/10^9;
vd=vp-vp(1,1);
vw0=n*V/1e9;
vw=vw0-vp;
sr=vw/vw0;
teta=vw/V*10^9;
t= tempdata(:,1);
output=[Pdif sr];
figure;
plot(t,Pdif)
figure;
plot(t,Dis)
figure;
plot(t,vw)
figure;
plot(Pdif,sr)
```

E.2 Program for the analysis of flow pump data

```
clc
clc
    %-----------------------------------------------------------%
    %         input the properties of the samples               %
    %-----------------------------------------------------------%
nf=input(' the number of file to process = ');
fr=zeros(1,nf);
f1=zeros(1,nf);
f2=zeros(1,nf);
Vs=zeros(1,nf);
G=zeros(1,nf);
Ip=.00136;
% Define the output matrix
output{1,1} = 'confining pressure';
output{1,2} = 'matric sution';
output{1,3} = 'resonant frequency';
```

```
output{1,4} = 'shear velocity';
output{1,5} = 'shear modulus';
[filename, pathname ] = uigetfile('*.xlsx', ' pick a data
file');
A = xlsread(filename,'A2:F2');
figure
for kk=1:nf
    CS=A(kk,1);
    MS=A(kk,2);
    ro=A(kk,3);
    m=A(kk,4);
    di=A(kk,5);
    L=A(kk,6);
    r=di/2;
    I(1,kk)=m*r^2/2;
    Fr=I(1,kk)/Ip;
    [filename1, pathname1 ] = uigetfile('*.xlsx', ' pick a
data file');
    num = xlsread(filename1, 'A20:C3200');
    freq=num(:,1);
    freqmax=max(freq(:,1));
    g1=num(:,2);
    gmax1=max(g1);
    g2=num(:,3);
    gmax2=max(g2);
    %-------------------------------------------------------%
    %             Filtering for channel 1&2                 %
    %-------------------------------------------------------%
    xy1=g1;
    [x1,y1]=size(g1);
    x11=zeros(x1,5);
    xy2=g2;
    [x2,y2]=size(g2);
    x22=zeros(x2,5);
    %figure
    for h=1:2
        y1=fft(xy1);
        g11=fix(y1/gmax1)*gmax1;
        g12=ifft(g11);
        y11=abs(g12);
        xy1=y11;
        x11(:,h)=y11(:,1);
        y2=fft(xy2);
        g21=fix(y2/gmax2)*gmax2;
        g22=ifft(g21);
        y21=abs(g22);
        xy2=y21;
        x22(:,h)=y21(:,1);
        g=(xy2);
        plot(freq,g)
        hold on;
    end

    %-------------------------------------------------------%
    %                   Gmax calculation                    %
    %-------------------------------------------------------%
    g=(xy2);
```

```
    gmax=max(g);
    gdes=.707*gmax;
    j=1;
    while g(j)<gdes
        j=j+1;
    end
    j;
    g(j);
    gdes;
    l=1;
    while g(l)<gmax
        l=l+1;
    end
    l;
    gmax;
    g(l);
    k=l+2;
    while (g(k)>gdes)
        k=k+1;
    end
    k;
    g(k);
    gdes;
    fr(1,kk)=freq(l);
    if (g(j)==gdes)
        f1(1,kk)=freq(j);
    else
        f1(1,kk)=(freq(j)+freq(j-1))/2;
    end
    if (g(k)==gdes)
        f2(1,kk)=freq(k);
    else
        f2(1,kk)=(freq(k)+freq(k+1))/2;
    end
    wr(1,kk)=2*pi()*fr(1,kk);
    Vs=sqrt((L*wr(1,kk))^2/Fr);
    G=ro*Vs^2;
    output{kk+1,1} = CS;
    output{kk+1,2} = MS;
    output{kk+1,3} = wr(1,kk);
    output{kk+1,4} = Vs;
    output{kk+1,5} = G;
    x=[0:.000001:gmax];
    plot(freq,g)
    hold on;
end
fr=fr;
f1=f1;
f2=f2;
wr=wr;
xlswrite( [ 'Summary Data', '.xls' ], output )
```